


12-2018

ROLE OF P300 ZZ DOMAIN IN CHROMATIN ASSOCIATION AND HISTONE ACETYLATION

Yongming Xue

Follow this and additional works at: https://digitalcommons.library.tmc.edu/utgsbs_dissertations

 Part of the [Biochemistry Commons](#), [Cancer Biology Commons](#), [Molecular Biology Commons](#), and the [Structural Biology Commons](#)

Recommended Citation

Xue, Yongming, "ROLE OF P300 ZZ DOMAIN IN CHROMATIN ASSOCIATION AND HISTONE ACETYLATION" (2018). *UT GSBS Dissertations and Theses (Open Access)*. 907.
https://digitalcommons.library.tmc.edu/utgsbs_dissertations/907

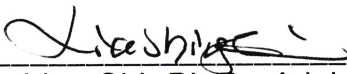
This Dissertation (PhD) is brought to you for free and open access by the Graduate School of Biomedical Sciences at DigitalCommons@TMC. It has been accepted for inclusion in UT GSBS Dissertations and Theses (Open Access) by an authorized administrator of DigitalCommons@TMC. For more information, please contact laurel.sanders@library.tmc.edu.

**ROLE OF P300 ZZ DOMAIN IN CHROMATIN ASSOCIATION AND HISTONE
ACETYLATION**


By

Yongming Xue, B.S.


APPROVED:




Xiaobing Shi, Ph.D., Advisory Professor



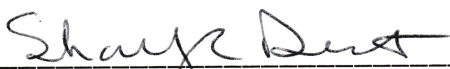
Michelle C. Barton, Ph.D.



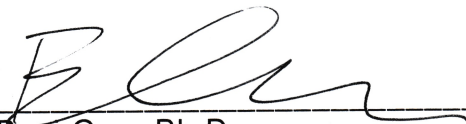
Mark T. Bedford, Ph.D.



Lauren A. Byers, M.D.



Sharon Y.R. Dent, Ph.D.



Boyi Gan, Ph.D.

APPROVED:

Dean, The University of Texas
MD Anderson Cancer Center UTHealth Graduate School of Biomedical
Sciences

**ROLE OF P300 ZZ DOMAIN IN CHROMATIN ASSOCIATION AND HISTONE
ACETYLATION**

A

DISSERTATION

Presented to the Faculty of

The University of Texas

MD Anderson Cancer Center UTHealth

Graduate School of Biomedical Sciences

in Partial Fulfillment

of the Requirements

for the Degree of

DOCTOR OF PHILOSOPHY

By

Yongming Xue, B.S.

Houston, Texas, December 2018

Dedication

This thesis is dedicated to

My parents Bin Xue, Ying Xu,

My grandmother Sufeng Yang

And my Fiancée Lulu Wang,

For their understanding, love and support

Acknowledgement

Ph.D. defense is one of the most important milestones in one's life. It would have been impossible for me to stand in front of this milestone without the support and help from many people.

First of all, I would like to express my sincerest gratitude to my advisory mentor, Dr. Xiaobing Shi, for offering me the opportunity to work in his lab. He is a great mentor spending numerous hours training my bench work and critical thinking, providing the guidance and supports for my project and scholarship application and inspiring us with his humor. Under his mentorship, I have not only gained multiple research skills, but also developed very good habits and rigorous attitude towards science. He is also a friend who cares for my life and provides a lot of help. I will regard Dr. Shi as my role model if I am fortunate enough to be a mentor in the future.

I would also like to thank Dr. Michelle Barton for being my onsite advisor after Shi lab moved this spring. I have received a warm welcome from her and all Barton lab members. Dr. Barton was also the mentor of my 1st rotation. In addition to the research training, she also provided helpful suggestions to help me to quickly adapt to graduate school life. I am also grateful for other members of my advisory committee, Drs. Sharon Dent, Mark Bedford, Boyi Gan and Lauren Byers, for providing precious guidance and sharing cell lines/reagents, which is of tremendous help to my project. I also want to acknowledge Dr. Jonathan Kurie who offered me the rotation position and introduced me to the new world of lung cancer biology.

In addition, I would also like to thank the help and encouragement from all Shi lab members. Dr. Hong Wen taught me many experimental skills and provided very helpful scientific advices. Everything is in perfect order under her management, which greatly increases my efficiency in performing experiments. Xiaolu Wang and Danni Peng also contributed a lot to keeping the lab running. I also greatly appreciated the discussion and collaboration with Drs. Wenyi Mi and Dan Su, two postdocs in our lab in p300-related projects.

I am also grateful to my excellent collaborators, Dr. Yi Zhang from Kutateladze lab and Dr. Jiejun Shi from Dr. Wei Li's lab. Their impressive intelligence and diligence ensured the completion of my project. Additionally, I highly appreciate the warm and selfless help from our neighbors Sabrina Stratton, Kendra Allton, Dr. Abhinav Jain and Robert Cardnell from Byers lab. I also want to acknowledge Elisabeth Lindheim and other members of Genes and Development Program community, for their help, support and friendship during the last four years.

Last but not least, I want to express my deep appreciation to my families and friends for their understanding and unconditional care and love. I will love them forever.

ROLE OF P300 ZZ DOMAIN IN CHROMATIN ASSOCIATION AND HISTONE ACETYLATION

Yongming Xue, B.S.

Advisory Professor: Xiaobing Shi, Ph.D.

Transcription is strictly regulated by numerous factors including transcription coactivators. The p300 protein and its close paralogue CREB-binding protein (CREBBP, aka CBP) are well-known transcriptional coactivators that have intrinsic lysine acetyltransferase activity. The functions of p300/CBP largely rely on their capabilities to bind to chromatin and to acetylate the histone substrates. However, the molecular mechanisms underlying the regulation of these processes are not fully understood.

Through combination of various biochemical, biophysical and molecular approaches, we show that the ZZ-type zinc finger (ZZ) domain of p300 functions as a histone reader that specifically binds the N-terminal tail of histone H3. Crystal structure of p300 ZZ in complex with the H3 peptide reveals that the ZZ domain adopts a negatively charged cavity to anchor Ala1 and Arg2 of H3. The ZZ-H3 interaction is not sensitive to common post-translational modifications, such as methylation or acetylation, on the H3 tail. Both *in vitro* and cell-based assays reveal that p300 ZZ domain, together with bromodomain (BRD), is important in recruiting p300 to chromatin. As a module adjacent to the histone acetyltransferase (HAT) domain, ZZ domain is also required for efficient histone

acetylation by HAT. The recognition of histone H3 by the ZZ domain selectively promotes p300-dependent acetylation specifically on histone H3K27 and H3K18, whereas the acetyllysine binding activity of BRD is required for acetylation of virtually all lysine residues in H3 and H4 tails.

p300/CBP are frequently mutated or dysregulated in many human diseases including cancer. We found that p300 is overexpressed in small cell lung cancer (SCLC), the most aggressive subtype of lung cancer. By CRISPR/Cas9-mediated gene manipulation, we found that p300 depletion impedes proliferation of human and mouse SCLC cells whereas CBP depletion has little or no effect. Depletion of p300 reduces the expression of critical oncogenes such as the *MYC* family genes, indicating that p300 promotes SCLC cell growth by sustaining oncogene expression.

In summary, we identified the ZZ domain of p300 as a novel histone H3 reader that is critical for the chromatin association and enzymatic activity of p300. Recognition of H3 by ZZ domain is important to the functions of p300 in human cancer.

Table of Contents

Approval Sheet	i
Title Page.....	ii
Dedication	iii
Acknowledgement.....	iv
Abstract.....	vi
Table of Contents.....	viii
List of Figures	xi
List of Tables	xiv
Chapter 1. Introduction	1
1.1 Transcriptional coactivators CBP/p300.....	1
1.2 Intramolecular regulation mechanisms of CBP/p300.....	6
1.3 Intermolecular regulation mechanisms of CBP/p300.....	10
1.4 Physiological roles of CBP/p300.....	16
1.5 ZZ-type zinc finger (ZZ) domain.....	21
1.6 Small cell lung cancer (SCLC).....	24
Chapter 2. Materials and Methods	31
2.1 Plasmids and molecular cloning.	31
2.2 Primers	35

2.3 Antibodies	38
2.4 Cell lines	39
2.5 Protein expression and purification.....	40
2.6 Peptide microarray and pull-down assays	40
2.7 Calf thymus histone pull-down assay.....	41
2.8 <i>In vitro</i> histone acetyltransferase (HAT) assays.....	41
2.9 Western blot.....	42
2.10 Transfection and lentiviral infection.....	43
2.11 Salt fractionation	43
2.12 Chromatin immunoprecipitation (ChIP) and ChIP-seq	45
2.13 ChIP-western blot	46
2.14 RNA extraction, reverse transcription (RT), and RT-qPCR.....	46
2.15 Cell proliferation assay	47
2.16 Statistical analyses	47
 Chapter 3. The ZZ Domain of p300 Recognizes Histone H3 to Regulate Chromatin Association and Histone Acetylation	
3.1 p300 ZZ domain is a reader for histone H3	49
3.2 The structural basis of H3 recognition by p300 ZZ domain.....	53
3.3 Recognition of H3 by the ZZ domain is required for p300-chromatin association.....	58

3.4 Recognition of H3 by the ZZ domain facilitates the acetylation of H3K18 and H3K27 by the HAT domain	63
3.5 Recognition of H3 by the ZZ domain is required for genome-wide p300 occupancy and p300-dependent deposition of H3K18ac and H3K27ac.....	79
3.6 Conclusions	88
3.7 Discussion	89
Chapter 4. p300 Is Required for Maintenance of SCLC Cell Growth	95
4.1 Depletion of p300 impedes SCLC cell proliferation.....	95
4.2 Depletion of p300 attenuates oncogene activation in SCLC cells.....	107
4.3 Conclusions	112
4.4 Discussion	113
Chapter 5. Future Directions	115
5.1 Determining the physiological importance of p300 ZZ domain	115
5.2 Determining the role of p300 in SCLC maintenance.....	119
Chapter 6. References.....	121
Vita.....	158

List of Figures

Figure 1. The regulation of CBP/p300 acetyltransferase activity by AIL, RING domain and BRD.....	4
Figure 2. Summary of intramolecular and intermolecular mechanisms regulating CBP/p300.	15
Figure 3. Mutation diagrams of human <i>CREBBP</i> and <i>EP300</i> genes based on 215 cancer genomic studies.	20
Figure 4. Phylogenetic tree and sequence alignment of ZZ domains in human proteins.	22
Figure 5. Genetic alterations in small cell lung cancer.	28
Figure 6. The map of LentiCRISPR v2 Puro vector.	32
Figure 7. The workflow for salt fractionation assay.	44
Figure 8. The expression, purification and peptide microarray analysis of p300 ZZ domain.	48
Figure 9. The ZZ domain of p300 binds to histone H3 tail.	51
Figure 10. Recognition of H3 by p300 ZZ domain is not sensitive to methylation or acetylation on H3.	52
Figure 11. Structure of the p300 ZZ-H3 complex.	55
Figure 12. Key residues required for ZZ-H3 binding.	57

Figure 13. Both ZZ domain and BRD are required by p300 for chromatin association.....	61
Figure 14. Both the H3-recognition ability of ZZ domain and the acetyllysine binding activity of BRD are required by p300 for chromatin association.	62
Figure 15. The p300 fragments used in <i>in vitro</i> HAT assays.	65
Figure 16. Deletion of ZZ domain specifically attenuated the acetylation of H3K27 and H3K18.....	68
Figure 17. H3 binding by ZZ domain facilitates p300 HAT activity on H3K18 and H3K27.....	71
Figure 18. The first two residues of H3 are required for the acetylation of H3K18 and H3K27.....	73
Figure 19. H3 recognition by ZZ domain is critical to p300-mediated H3K18 and H3K27 acetylation in cells.....	77
Figure 20. H3 recognition by ZZ domain is required by full-length p300 to acetylate H3K18 and H3K27 in cells.....	78
Figure 21. The ZZ domain is necessary to p300's chromatin binding and acetylation activity on H3K18 and H3K27 in cells.	83
Figure 22. Box plots comparing FLAG, H3K18ac and H3K27ac occupancies in different samples at FLAG-p300 _{BRPHZT} binding peaks.....	84
Figure 23. Representative genome-browser views of ChIP-seq data.	85

Figure 24. ChIP-qPCR in H1299 cells stably expressing wild type FLAG-p300 _{BRPHZT} or the ZZ mutants.	86
Figure 25. ChIP-qPCR in H1299 cells stably expressing wild type FLAG-p300 _{BRPHZT} or the BRD mutant.....	87
Figure 26. The proposed functions of ZZ domain-mediated p300 chromatin recruitment.....	93
Figure 27. The structural basis of ZZ-mediated HAT specificity toward the distal lysine sites in H3.....	94
Figure 28. p300 is overexpressed in murine SCLC cell lines.....	97
Figure 29. The depletion of p300 impedes murine SCLC cells proliferation.	99
Figure 30. p300 and CBP are overexpressed in human SCLC cell lines.....	102
Figure 31. The depletion of p300 impedes human SCLC cells proliferation.	105
Figure 32. The depletion of p300 does not affect the proliferation of human NSCLC cells and normal lung epithelial cell.	106
Figure 33. Expression activation of the dominant <i>MYC</i> family gene is dependent on p300.....	110
Figure 34. Histone acetylation at <i>MYC</i> super-enhancer regions requires p300.	111
Figure 35. Mutations of p300 ZZ domain occurring in cancers.	118

List of Tables

Table 1. Plasmids used in this study.....	33
Table 2. Oligos used in this study.....	35
Table 3. Antibodies used in this study.....	38
Table 4. Cell lines used in this study.....	39
Table 5. The mutation status of <i>EP300</i> and <i>CREBBP</i> genes in lung cancer cell lines used in this study.....	101
Table 6. Mutations in p300 ZZ domain occurring in cancers.....	117

Chapter 1. Introduction

Copyright information:

Contents of Chapter 1.1-1.3 are based on my review article: Xue Y*, Wen H, Shi X*. 2018. CBP/p300: intramolecular and intermolecular regulations. *Front Biol.* 13: 168-179. (*: Corresponding authors). I am the primary author of this review. Permission to reuse the whole article for thesis was obtained from www.copyright.com with license number: 4456690546571.

1.1 Transcriptional coactivators CBP/p300

Transcription is critical for deciphering the commands encrypted in DNA for the completion of various important biological processes. Regulation of this molecular event in eukaryotes is complex, but strictly controlled by a vast network of regulatory factors. Two of these factors are cAMP response element-binding protein (CREB)-binding protein (CREBBP, aka CBP or lysine acetyltransferase 3A, KAT3A) and its close paralogue p300 (aka KAT3B) (1, 2). CBP and p300 were initially identified as interacting proteins of CREB and adenoviral protein early region 1A (E1A), respectively (3-7). Both proteins contain intrinsic histone lysine acetyltransferase (HAT) activity (8, 9) and constitute the KAT3 family of acetyltransferase in mammals. The encoding genes of CBP and p300 in human genome are *CREBBP* and *EP300*, respectively.

Acetylation on histone lysine residues neutralizes positive charge on their

side chain, weakens not only the interaction between histones and negatively charged DNA but also that between neighboring nucleosomes, creating an open chromatin structure that facilitates transcription (10). CBP and p300 have promiscuous acetyltransferase activity. *In vitro* they are able to acetylate multiple sites of histones H2A, H2B, H3 and H4 in the context of free histone (8) or nucleosome (8, 9, 11). However, depletion (12-14) or inhibition (14, 15) of both CBP and p300 in cells greatly reduces the global level of histone H3K18 and K27 acetylation without dramatically affecting acetylation at other sites, indicating that they are mainly required for H3K18 and K27 acetylation *in vivo*. In response to DNA damage, CBP/p300 acetylate H3K56 on free histones (16, 17), which is required for chromatin reassembly after DNA repair (18). In addition to their histone substrates, CBP/p300 can also acetylate many other proteins including transcription factors (19). By interacting with hundreds of proteins, CBP and p300 work as scaffolds to assemble transcriptional activation complexes, or serve as bridges linking the activator complexes to the RNA polymerase II (Pol II) transcription machinery (20-22). Consistent with their roles in transcriptional activation, CBP/p300 are mainly localized at regulatory DNA elements, especially enhancers (23, 24). In fact, the genomic occupancy of CBP/p300 has been used as a predictive marker for active enhancers (25).

CBP and p300 proteins are composed of multiple conserved domains, which, from N- to C-terminus, include a nuclear receptor-interacting domain (NRID), a transcriptional adapter zinc-binding (TAZ1) domain, a kinase-inducible domain interacting (KIX) domain, a bromodomain (BRD), a combined Really

Interesting New Gene (RING) domain and plant homeodomain (PHD), a HAT domain that contains an autoinhibitory loop (AIL), a ZZ-type zinc finger (ZZ) domain, another TAZ domain (TAZ2) and an interferon binding domain (IBiD) (19). Of note, the TAZ1, RING/PHD and ZZ/TAZ2 domains each forms a cysteine/histidine-rich region (CH), named as CH1, CH2 and CH3, respectively. BRD, CH2, HAT domain and CH3 form the catalytic core of CBP/p300 (26). Other domains and regions are linked to the catalytic core by long stretches of unstructured regions (Figure 1A).

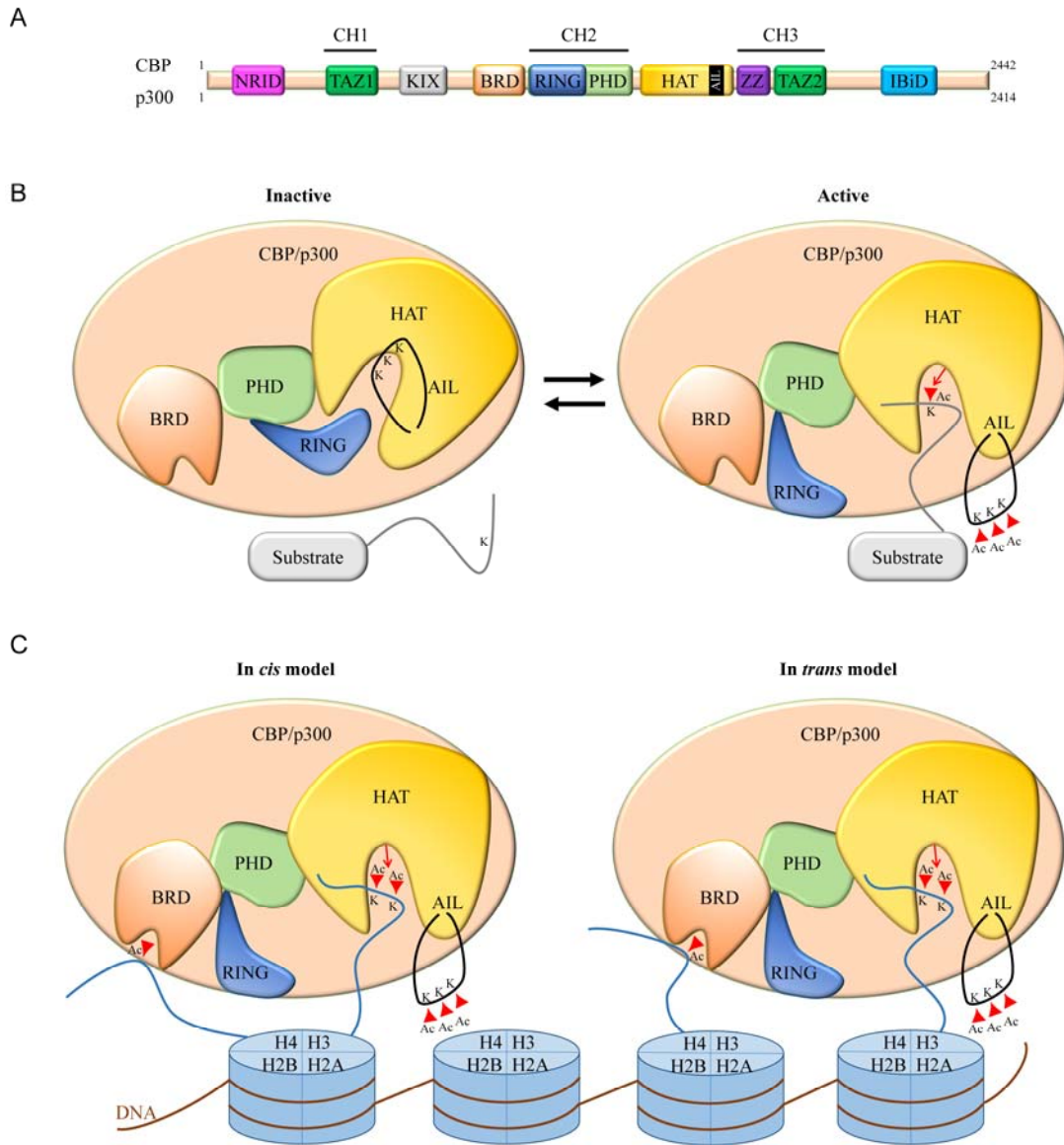


Figure 1. The regulation of CBP/p300 acetyltransferase activity by AIL, RING domain and BRD.

(A) Schematic representation of human CBP/p300 domain architecture. The numbers of amino acid residues of CBP and p300 are labeled. (B) When the HAT domain is in its inactive state, the hypoacetylated AIL occupies the substrate-binding groove along with the RING domain packed in close proximity

to the HAT catalytic site. Upon autoacetylation of the AIL, it is displaced from the catalytic site along with the RING domain, making the HAT domain accessible to its substrates. (C) The BRD recognizes acetylated histones, preferentially acetylated histone H4. Binding of acetylated histone tail by BRD facilitates the recruitment of CBP/p300 to chromatin and also increases the access of HAT domain to the histone substrate such as the H3 tail. Such an enhancement may occur either *in cis* on the same nucleosome or *in trans* on adjacent nucleosomes.

1.2 Intramolecular regulation mechanisms of CBP/p300

The functions of CBP/p300, especially their acetyltransferase activity and chromatin association, are regulated both intramolecularly by their AIL, BRD, and PHD-RING region and intermolecularly by their interacting partners and post-translational modifications (PTM).

The AIL (aka autoregulatory loop or activation loop) is a lysine-rich loop region adopting a disordered structure within the HAT domain (26, 27) (Figure 1A). It encompasses amino acid residues (AA) 1520-1581 and 1556-1618 of human p300 and CBP, respectively. The AIL was discovered by the Philip Cole laboratory when they studied how autoacetylation regulates the HAT activity of p300 (28). Up to 17 lysine residues in the AIL and nearby regions of p300 can be autoacetylated through an intermolecular mechanism (29, 30). When AIL is hypoacetylated, it occupies the catalytic site of HAT domain with its lysine residues interacting with the acidic residues in the substrate-binding groove of HAT domain. This interaction prevents the positively-charged substrates such as lysine-rich histone tails from entering the catalytic site, thus inhibiting the acetyltransferase activity of p300 (30, 31). Acetylation on the AIL lysine residues disrupts their binding to the substrate-binding groove of HAT domain (30), displacing the AIL from the catalytic site. As a result, the catalytic site of HAT domain becomes more accessible to its substrates and the acetyltransferase activity is thus activated (Figure 1B). In addition to the modulation of HAT activity, the AIL also plays a role in regulating CBP/p300 chromatin association. In an *in vitro* system, autoacetylation of the AIL induces the dissociation of p300 from the

preinitiation complex (PIC) containing GAL4-VP14 and Mediator at the chromatin, which enhances both TFIID binding and transcription initiation (32).

The CH2 region, located between the BRD and HAT domains, is comprised of a RING domain and a PHD. Crystal structure of the p300 catalytic core encompassing the BRD, CH2 and HAT domains reveals that CH2 region serves as a bridge to connect the BRD and HAT domains (27). The RING domain is packed in close proximity to the HAT domain and restricts the access of HAT active site to the AIL and other substrates (27, 30). Deletion of the RING domain or the mutations in RING that impairs either its structural integrity or its interaction with HAT enhances p300 autoacetylation (on K1499) and acetylation of p53 substrate (on K382) (27, 30, 33), suggesting RING negatively regulates the acetyltransferase activity of p300. Likewise, the RING domain of CBP shows a similar regulatory role in both CBP autoacetylation and p53 acetylation (26). However, in contrast to the enhanced autoacetylation and p53 acetylation, acetylation on histone H3K9 and H3K14 is reduced by the deletion of p300 RING domain (33), whereas in the case of CBP, RING deletion has no dramatic effect on histone acetylation (26). These results suggest that the regulatory role of RING in CBP/p300 acetyltransferase activity may be substrate-specific.

The PHD of p300 is discontinuous as it is interrupted by the RING domain (27). Distinct from the mutations in RING, the mutations either within PHD or at PHD-HAT interfaces do not strongly affect p300 autoacetylation or p53 substrate acetylation (27). In addition, the PHD is not directly involved in the regulation of p300/CBP chromatin binding, because unlike the canonical PHDs that function

as readers recognizing modified or unmodified histones (34, 35), the CBP/p300 PHD does not recognize histones due to the lack of conserved residues critical for histone binding (27, 36). To date, the actual function of the PHD in CBP/p300 remains unknown.

Acetylated histone lysine can be recognized by specific reader proteins, which facilitates the recruitment or retention of transcription co-activators at acetylated chromatin loci. BRD is the first discovered reader of histone acetylation (Dhalluin et al., 1999). The BRD in CBP/p300 has histone- and nucleosome-binding capability (Manning et al., 2001; Ragvin et al., 2004). It recognizes multiple acetylated histone peptides *in vitro*, preferentially di- and tri-acetylated histone H4 and H2B (27, 36). Substitution of Asn1132 (N1132), a conserved residue within the hydrophobic acetyllysine-binding pocket of p300 BRD, to alanine abolishes its binding to all acetylated histone peptides (27). Furthermore, deletion of BRD prevents p300 from forming stable and direct interaction with nucleosomes (Manning et al., 2001); and treatment of CBP30, a small-molecule inhibitor targeting CBP/p300 BRD, in cells displaces CBP/p300 from chromatin (37, 38), suggesting that a functional BRD is required for p300-chromatin association.

Although CBP/p300 BRD is not adjacent to the HAT domain, it is crucial to CBP/p300-mediated histone acetylation. Deletion of BRD greatly impairs the ability of p300 to acetylate histones in the contexts of nucleosome (39), native chromatin (40) and recombinant chromatin (41) *in vitro*. In cells, the increase of global histone H3K9ac and H3K14ac levels caused by ectopic p300 expression

can be diminished by BRD deletion or mutations in its acetyllysine-binding pocket (33). Interestingly, in contrast to its critical role in histone substrate acetylation, loss of BRD does not significantly affect p300 autoacetylation or the acetylation of non-histone substrate such as p53, indicating that BRD is not required for the intrinsic acetyltransferase activity of p300 (27, 40, 41). Considering its nature as a histone acetylation reader, BRD may function as a “hand” that grabs acetylated histone tails, thus increasing the accessibility of nucleosome substrates to the catalytic HAT domain of CBP/p300 (Figure 1C). This model is supported by the recent finding that preexisting histone H4 acetylation in nucleosomes enhances wild-type p300-catalyzed H3K18 acetylation while this enhancement is not observed in p300 with BRD deletion or mutations (39). However, it remains unclear whether the recognition of acetylated histone H4 by BRD facilitates acetylation of the histone H3 within the same nucleosome (in *cis* model) or in the adjacent nucleosomes (in *trans* model) (Figure 1C).

The critical role of CBP/p300 BRD in chromatin binding and histone acetylation explains the requirement of BRD in CBP/p300-mediated transcription enhancement (40) and gene activation (42). Consistently, CBP30 treatment in cells, dramatically reduces H3K18ac and H3K27ac level at multiple CBP/p300 target loci and deactivates transcription of target genes in cells (38, 43). Thus, the cooperation between BRD and HAT ensures efficient transcription activation by p300/CBP on chromatin.

1.3 Intermolecular regulation mechanisms of CBP/p300

In addition to the intramolecular regulation mechanisms described, CBP/p300 are also subject to intermolecular regulation by numerous external molecules, which is critical for the functions of CBP/p300 in response to various cell signaling pathways (44, 45). Upon the perception of intra- or extracellular signals, cells initiate a series of molecular events of signal transduction, leading to activation of a group of genes and deactivation of others. CBP/p300 play indispensable roles in activating gene expression in response to almost all signaling pathways. CBP/p300 receive and execute commands from upstream signals through signal-induced protein-protein interactions and PTMs, which modulates the dynamics of chromatin association and HAT activity of CBP/p300.

To date, more than 400 proteins have been reported to interact with CBP/p300 (19), including transcription factors, coactivators, mediators and basal transcription machinery components. These protein-protein interactions allow CBP/p300 to integrate the assembly of transcription activation complexes, to be connected with the basal transcription machinery, and to gain access to a subset of these proteins for acetylation (19, 46). CBP/p300 contain a number of domains that interact with binding partners, including NRID, TAZ1, KIX, TAZ2, IBiD, and to a less extent, BRD and HAT domains (46). Notably, a single protein may interact with multiple domains or regions of CBP/p300 simultaneously.

As CBP/p300 do not contain specific DNA-binding domains, recruitment of CBP/p300 to specific chromatin regions, such as enhancers or promoters, is achieved by interacting with transcription factors that bind to specific DNA

sequences. A well-studied example is CREB, a transcription factor that recognizes the DNA sequence known as cAMP-response elements (CREs). Following the activation of G protein-coupled receptors (GPCRs), accumulated cAMP promotes the catalytic subunit of protein kinase A (PKA) to dissociate from its regulatory domain, diffuse into nucleus, and phosphorylate the kinase-inducible domain (KID) of CREB (47). Phosphorylation of KID (at Serine 133) greatly increases its binding to the KIX domain of CBP. The CREB-CBP interaction mediated by KID-KIX binding thus recruits CBP to CREs, leading to the activation of cAMP-responsive genes (7, 48). The hydrogen bond formed between phosphorylated Ser133 of CREB KID and Tyr658 of CBP KIX domain plays an indispensable role in the interaction between these two domains (49). Upon interaction with KIX, the unstructured KID undergoes a coil-to-helix transition, forming two helices, with one helix interacting with the hydrophobic groove of KIX to stabilize KID-KIX interaction (49).

Intermolecular protein-protein interactions also directly regulate the HAT activity of CBP/p300. P300 was originally discovered as one of the proteins that bind E1A, an adenoviral oncoprotein (3, 4). Small E1A protein, the shorter isoform of E1A, contains three conserved regions (CR1-3), with CR1 and CR2 interacting with CBP/p300 and retinoblastoma (RB) proteins, respectively (50). Binding of small E1A to the TAZ2 domain of CBP/p300 inhibits their HAT activity on histones *in vitro*, thus repressing CBP/p300-dependent transcription (51-53). Infection of cells with adenovirus Type 5 (Ad5) *dl1500* that expresses only small E1A markedly reduces global H3K18 acetylation level, which mimics the

phenotype when both CBP and p300 are depleted (13). Interestingly, small E1A can be acetylated at K239 by CBP/p300, implying that as a substrate of CBP/p300, small E1A may inhibit HAT activity by directly competing with histones for the catalytic site of CBP/p300 (54).

In contrast to small E1A that inhibits CBP/p300 HAT activity, Mastermind like 1 (MAML1), another protein that binds to p300 TAZ2 domain, activates its HAT activity both *in vitro* (55) and *in vivo* (56), probably through potentiating p300 autoacetylation (56). MAML1 also helps to recruit p300 to the genomic loci of Notch pathway genes (57), suggesting that MAML1 regulates both HAT activity and chromatin association of p300. Additionally, dimerization of transcription factors that interact with p300 (IRF3, STAT1 etc.) can engage two p300 molecules, which increases the likelihood of p300 AIL autoacetylation *in trans*, thus enhancing its HAT activity (30).

In addition to protein interactors, CBP also directly binds to RNAs (58). Interestingly, CBP-bound RNAs arise from the chromatin regions with high CBP occupancy and a large fraction of them are enhancer RNAs (eRNAs). eRNAs are non-coding RNAs transcribed from enhancers (59). Those CBP-bound eRNAs directly bind to AIL and displace it from the HAT catalytic site, thus stimulating HAT activity *in vitro*. Consistently, depletion of a certain eRNA in cells greatly reduces the H3K18 and H3K27 acetylation level at the same enhancer where this eRNA is originated and its associated promoter without affecting CBP occupancy (58). This study suggests that when CBP is recruited to active enhancers where eRNAs are produced and locally enriched, these eRNAs can

bind to the AIL of CBP to stimulate its HAT activity, leading to a local increase of CBP-dependent histone acetylation at the same enhancer and associated promoters. This finding also indicates that in addition to AIL autoacetylation, cells may employ multiple mechanisms to ensure AIL is displaced from the HAT active site, safeguarding histone acetylation and gene activation.

While CBP/p300 catalyze lysine acetylation on histones and non-histone proteins, they themselves are also subject to PTMs, such as phosphorylation, methylation and SUMOylation, which in turn affects the functionality and homeostasis of CBP/p300.

CBP/p300 can be phosphorylated at various sites. For example, AKT phosphorylates p300 at S1834 (60), ERK1/2 phosphorylate p300 at S2279, S2315 and S2366 (61), and mTORC1 phosphorylates p300 at S2271, S2279, S2291 and S2315 (62). All these phosphorylation events stimulate HAT activity. In contrast, PKC-catalyzed p300 phosphorylation at S89 inhibits the catalytic activity of p300 (63). The mechanisms by which phosphorylation at the N- or C-terminal distal regions regulate the HAT domain that is located in the central region of p300 have remained elusive. However, Wan et al. recently showed that mTORC-catalyzed p300 phosphorylation in the C-terminal region abrogates the interaction between p300 HAT and RING domain, thus releasing the HAT catalytic site from the RING domain-mediated inhibition (62). This finding indicates the existence of crosstalk between inter- and intramolecular regulation mechanisms of CBP/p300. Phosphorylation can also regulate CBP/p300 homeostasis. For instance, phosphorylation of p300 S106 by ATM contributes to

p300 stabilization in response to double-strand breaks (DSBs) (64) while MAPK/AKT-catalyzed p300 S1834 phosphorylation induces p300 degradation during nucleotide excision repair (NER) (65).

In addition to phosphorylation, other PTMs also contribute to CBP/p300 regulation. Coactivator-associated arginine methyltransferase 1 (CARM1) interacts with and methylates CBP/p300 at multiple arginine residues (66-68). Methylation of arginine residues at different regions has distinct regulatory outcomes. For example, methylation of the arginine residues within the KIX domain of disrupts CBP/p300-CREB interaction, thus reducing the recruitment of CBP/p300 to the chromatin of CREB target loci (67) whereas methylation of the arginine residues located downstream of KIX increases the recruitment of CBP to estrogen receptor (ER)-responsive target genes and enhances CBP HAT activity (68, 69). Additionally, SUMOylation of CBP/p300 on the lysine residues upstream of BRD negatively regulates CBP/p300-mediated transcription, probably through the recruitment of transcriptional corepressor Daxx (70, 71).

A summary of both intramolecular and intermolecular mechanisms regulating p300/CBP is depicted in Figure 2. In the future, a deeper understanding of how all the regulatory regions coordinate with each other in the context of the complete CBP/p300 proteins will be required.

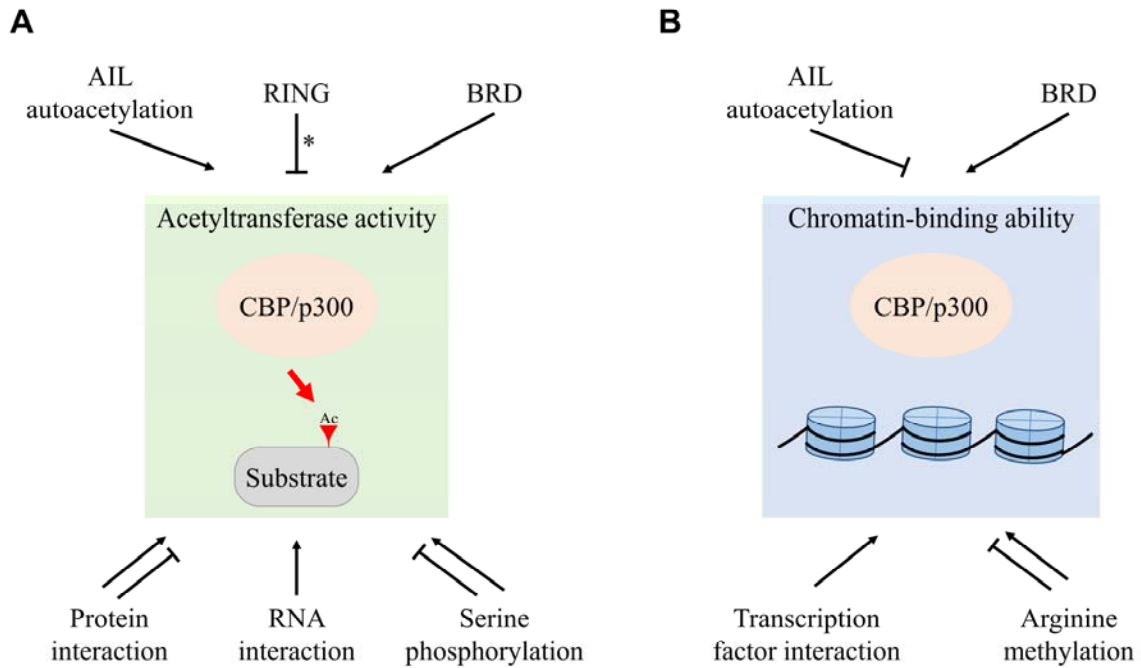


Figure 2. Summary of intramolecular and intermolecular mechanisms regulating CBP/p300.

The mechanisms regulating CBP/p300 acetyltransferase activity (A) and chromatin association (B) are shown. Lines with arrows indicate positive regulation whereas blunt-ended lines indicate negative regulation. *: the negative regulatory role of the RING domain in CBP/p300 acetyltransferase activity is only observed on non-histone substrates.

1.4 Physiological roles of CBP/p300

CBP/p300 are essential for various cellular processes such as cell proliferation, differentiation and apoptosis (45). They play critical roles in mammal development, memory consolidation and pathogenesis.

Mice homozygous null for either CBP (*Crebbp*^{-/-}) or p300 (*Ep300*^{-/-}) are embryonic lethal (72-74). *Crebbp*^{-/-} mice die around embryonic day 10.5~12.5 (E10.5~E12.5) (72) while *Ep300*^{-/-} die around E9.0~E11.5 (73). Embryos from both mutants display severe defects in growth and neural tube closure (73). In addition, *Crebbp*^{+/-} *Ep300*^{+/-} double heterozygotes are also embryonic lethal and single heterozygotes show reduced viability and multiple developmental defects (73, 75, 76). These studies indicate that CBP and p300 exert overlapping functions and that there may be a significant dosage requirement for both genes during embryonic development.

Heterozygous mutations/deletions of *CREBBP* or, less commonly, *EP300*, cause Rubinstein–Taybi syndrome (RTS) (77, 78), a human genetic disorder characterized by mental retardation, broad thumbs and toes, craniofacial defects and cardiac abnormalities (79). Consistently, monoallelic loss (75, 76) or truncation of *Crebbp* (80) in mice also causes phenotypes reminiscent of RTS.

In addition, both CBP (75) and p300 (81) are crucial for hematopoiesis. However, they seem to play distinct roles in this process. CBP, but not p300, is critical to hematopoietic stem cell self-renewal while p300 plays more important roles in hematopoietic differentiation (82). Furthermore, CBP is also required for long-term memory consolidation in mice brain (83-85). The expression of

deactivated or truncated CBP in mice causes defects in long-term memory formation and synaptic plasticity through a dominant-negative mechanism (86).

CBP/p300 are involved in a number of human cancers. Somatic mutations of *CREBBP* and *EP300* frequently occur in multiple types of malignancies (87), such as colorectal cancer (88, 89), lung cancer (88, 90), breast cancer (88), skin cancer (91) and lymphoma (92-94). Most of these mutations are missense mutations clustering within HAT domain or its adjacent regions as well as frameshifts and nonsense mutations resulting in protein truncations (Figure 3) (92, 93, 95), implying that inactivation of CBP/p300 acetyltransferase activity may contribute to tumorigenesis. In addition, *CREBBP*, and less commonly, *EP300*, are targets of chromosome translocations. *MLL-CREBBP* (96, 97), *MLL-EP300* (98), *MOZ-CREBBP* (99) and *MOZ-EP300* (100) translocations have been implicated in acute myeloid leukemia (AML) and myelodysplastic syndrome.

The precise roles of CBP/p300 in cancers are complicated. They function as tumor suppressors in certain types of cancers, such as colon cancer (101, 102) and B-cell lymphoma (103). Recently, the elegant work from four labs clearly demonstrate the function and mechanism of CBP in B-cell lymphoma (103-106). Follicular lymphoma (FL) and diffuse large B-cell lymphoma (DLBCL) are the two most common types of non-Hodgkin lymphomas derived from germinal center (GC) B cells. The mutation rates of *CREBBP* in DLBCL and FL are around 30% and 60%, respectively (92, 93, 107). In comparison, *EP300* is less frequently mutated in FL and DLBCL. Although GC B cells-specific knockout of *Crebbp* alone is not sufficient to drive oncogenic transformation in mice, it

cooperates with *Bcl2* overexpression, an event that frequently co-occurs with *Crebbp* mutations in human FL and DLBCL, to promote lymphomagenesis (104, 106), indicating *Crebbp* is a tumor suppressor gene. Mechanistically, CBP directly binds to the promoter and enhancers of a large number of genes involved in B cell signaling and GC exit (104) in GC B cells. Loss of CBP represses the expression of these target genes by reducing the histone H3K27 acetylation level at their enhancers (103, 104). As most CBP target genes are also occupied by the BCL6-containing transcription repressor complex (103, 104), the function of this repressor complex may become more dominant on these genes when CBP is depleted, which contributes to the silencing of these genes and lymphomagenesis (103). Interestingly, the timing of CBP mutation matters in lymphoma because loss of *Crebbp* in early stages of lymphopoiesis is advantageous for lymphoid transformation whereas *Crebbp* loss after lymphoid fate commitment does not show an obvious phenotype (105).

CBP/p300 are also reported to play roles in promoting oncogenesis or disease maintenance in other types of cancers. For example, high expression of CBP/p300 was correlated with poor prognosis in prostate cancer (108), hepatocellular carcinomas (109) and lung cancers (110, 111). In addition, p300 is required for androgen receptor (AR) expression and prostate tumorigenesis in a *PTEN*-deficient mouse model (112). CBP/p300 also work as the coactivators of AR to support the androgen-induced gene expression in prostate cancer (113). Consistently, small-molecule inhibitors targeting the CBP/p300 HAT domain efficiently reduces prostate cancer cell viability and represses tumor growth (15,

114). Furthermore, CBP/p300 also facilitate the induction and maintenance of AML both *in vitro* and *in vivo* (115), which may partially be dependent on their interaction with c-Myb (116, 117). The oncogenic roles of CBP/p300 in AML suggest that they may be promising therapeutic targets (115, 118).

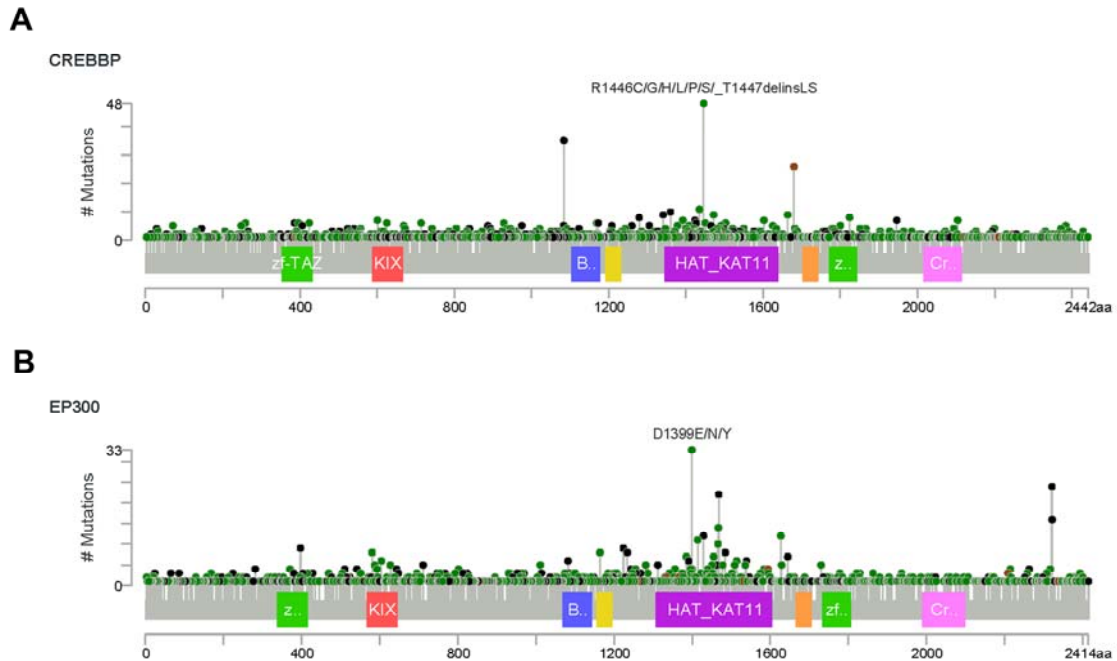


Figure 3. Mutation diagrams of human *CREBBP* and *EP300* genes based on 215 cancer genomic studies.

The mutation diagrams of human *CREBBP* (A) and *EP300* (B) genes were obtained from cBio Cancer Genomics Portal (<http://cbioportal.org>) (119, 120) on 4/27/2018. Mutation types and corresponding color codes are as follows:

Green: missense mutations. Black: truncating mutations (nonsense, nonstop, frameshift deletion or insertion, splice site variant). Brown: in-frame deletion, in-frame insertion. Purple: all other types of mutations.

1.5 ZZ-type zinc finger (ZZ) domain

The ZZ domain is a small (~45 AA) motif with a cross-braced zinc finger topology. It uses 4 cysteine residues and 2 histidine residues to coordinate 2 Zn²⁺ ions (121). This domain was named ZZ for its capacity to bind two Zn²⁺ ions (122). The ZZ domain was originally identified in dystrophin, a cohesive protein critical to muscle fiber integrity, and its related proteins (122). Dystrophin is a vital subunit of the dystrophin-associated protein complex that connects the actin cytoskeleton of muscle fibers to the surrounding extracellular matrix (123). The ZZ domain of dystrophin is located within its C-terminal cysteine-rich domain and is required for its interaction with the transmembrane adhesion receptor β -dystroglycan (124), which is crucial to dystrophin function.

ZZ domain has been identified in approximately 20 human proteins with various functions including chromatin modification, RNA processing, cytoskeletal scaffolding, ubiquitin binding or conjugating, and autophagy (121). The phylogenetic tree and sequence alignment of the ZZ domains from multiple proteins are shown in Figure 4. The function of the ZZ domain has been poorly studied. A few ZZ domains were reported to be involved in protein-protein interaction. For example, p62 ZZ domain interacts with RIP1 in NF- κ B pathway (125) and the ZZ domains of the E3 ligase HERC2 (126) and CBP (127) bind Small Ubiquitin-like Modifier 1 (SUMO1). However, a more comprehensive understanding of ZZ domains' functions is in need.

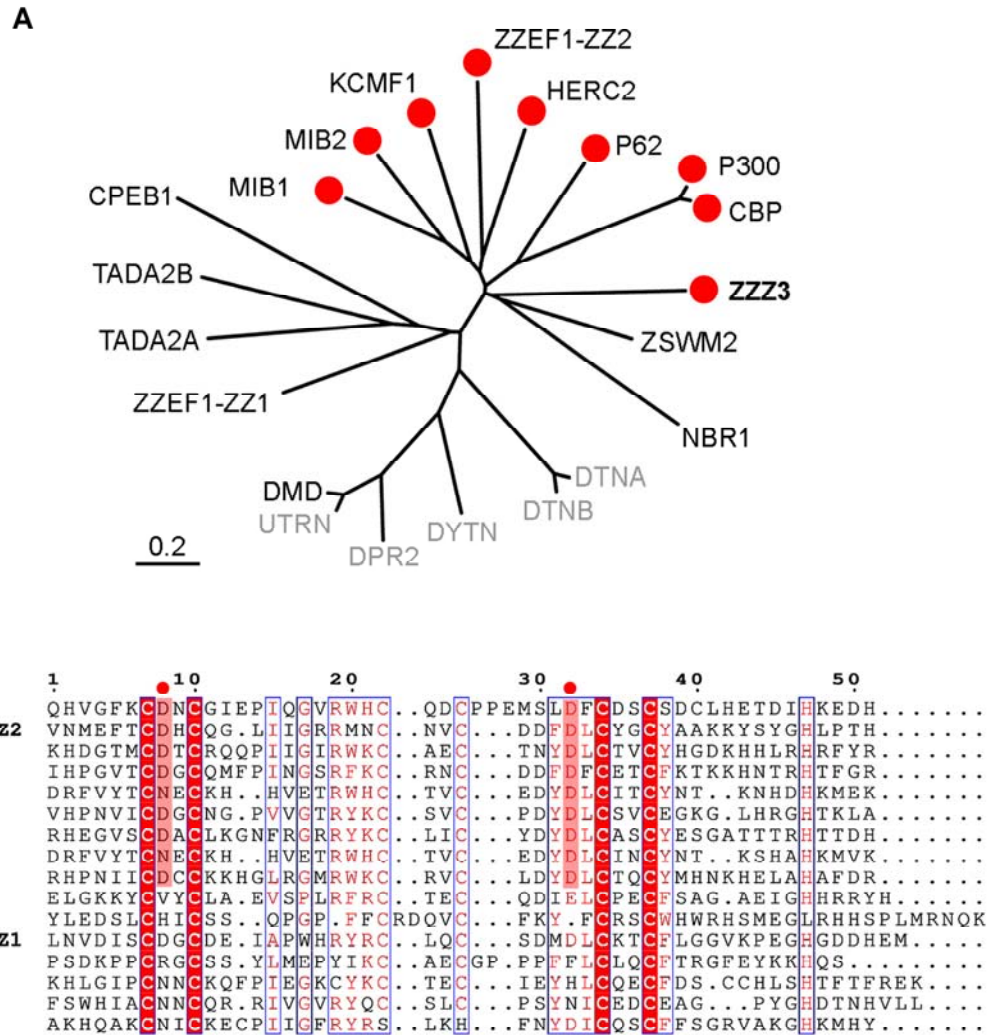


Figure 4. Phylogenetic tree and sequence alignment of ZZ domains in human proteins.

(A) Phylogenetic tree presentation of ZZ domains in human proteins. (B) Sequence alignment of human ZZ domains. Identical residues are in white text shaded in red. Conserved residues are in red text and framed by blue line.

Figure 4 is adapted from Mi W, Zhang Y, Lyu J, Wang X, Tong Q, Peng D, Xue Y, Tencer AH, Wen H, Li W, Kutateladze TG and Shi X. 2018. The ZZ-type zinc finger of ZZZ3 modulates the ATAC complex-mediated histone acetylation and

gene activation. Nat Comm. 9:3759. Permission to reuse these figures for thesis was obtained from www.copyright.com with license number 4456700921676.

1.6 Small cell lung cancer (SCLC)

Lung cancer is divided into three main subtypes (Figure 5A): non-small cell lung cancer (NSCLC), small cell lung cancer (SCLC) and lung carcinoid tumor (<http://www.cancer.org/cancer/lungcancer/index>). SCLC, the most aggressive subtype, accounts for 10~15% of all lung cancer cases and is tightly associated with heavy smoking behavior in patients (128). This disease is characterized by rapid tumor expansion, frequent relapse and early metastasis (129). SCLC cells are small, poorly differentiated, and likely originated from neuroendocrine cells within the pulmonary epithelium (130, 131).

SCLC is commonly divided into limited stage and extensive stage. Limited stage SCLC is confined to a single radiation field in one side of the chest while extensive stage SCLC has distant metastases (132). Approximately two-thirds of SCLC patients are diagnosed with extensive stage (133). In general, limited-stage patients are treated concurrently with chemotherapy in combination with radiation therapy, whereas extensive-stage patients are treated with chemotherapy alone (134). Despite the initial good response to frontline therapies in most SCLC patients, the disease will soon relapse with resistance to second-line and subsequent therapies. Numerous clinical trials since the 1970s have failed and there are still no approved targeted drugs for this disease. The 5-year survival rate of SCLC patients remains lower than 7% (128, 134).

The mutation rate of SCLC is among the highest, which can be explained by its link to tobacco exposure (135). Genomic studies have revealed multiple recurrent genetic alterations in SCLC (Figure 5B, C). For example, loss-of-

function mutations in *TP53* and *RB1* are present in almost all SCLC samples (95, 136, 137). Amplified *SOX2* (137) and *MYC* family genes (138, 139), activated phosphatidylinositol 3 kinase (PI3K) pathway and inactivated NOTCH signaling pathway are also common (95, 136, 140, 141).

In addition to the genetic alterations, dysregulated epigenetic mechanisms also contribute to SCLC onset and progression. For example, Enhancer of zeste homolog 2 (EZH2), a core subunit of the polycomb repressive complex 2 (PRC2) and a histone H3K27-specific methyltransferase, is highly expressed in SCLC compared to normal lung tissues and other cancer types (142-145). This might be the result of E2 promoter binding factors (E2Fs) upregulation, which is caused by the universal *RB1* loss or frequent *E2Fs* amplification in SCLC (143).

Overexpressed EZH2 directly silences *TGFBR2*, the gene encoding transforming growth factor- β (TGF- β) type II receptor (T β RII), by catalyzing histone H3K27 trimethylation at its promoter, which suppresses TGF- β pathway, enabling SCLC cells to escape apoptosis (146). EZH2 also directly silences Schlafen family member 11 (*SLFN11*), a gene critical to DNA damage response, to promote the resistance to chemotherapy in SCLC (147). Inhibiting EZH2 with small molecules such as EPZ reduces SCLC xenograft tumor growth (145) and prevents the acquisition of chemoresistance in SCLC (147).

While anti-tumor genes are silenced, oncogenes such as *MYC*, *MYCN*, *NFIB*, *SOX2*, *NEUROD1* and *ASCL1*, are expressed at very high levels in SCLC (148-153). Recently it has been reported that these highly-expressed oncogenes are associated with large and clustered enhancer elements containing

extraordinarily high level of H3K27ac (153, 154), namely super-enhancers (155). Many factors involved in transcription activation, such as BET proteins, mediator components and p300/CBP, are enriched at super-enhancers to maintain the activation of those oncogenes (154). Inhibition of the BET family member BRD4 by JQ1 (156, 157) or the cyclin-dependent kinase CDK7 by THZ1 (153) in SCLC suppresses the expression of super-enhancer-associated oncogenes and cell growth.

EP300 and *CREBBP* are also frequently mutated in SCLC (90, 95, 136, 137, 158) with mutation frequencies of 13% and 15%, respectively (136). Alterations in *EP300* and *CREBBP* are mutually exclusive (95). Except for the inactivating translocations, mutations of *EP300* and *CREBBP* are clustered within the HAT domain and its adjacent regions (95, 136). However, only a few of mutations in HAT domain have been confirmed to reduce HAT activity (95), whereas the functional consequences of most mutations are still elusive. SCLC patient survival analysis has not revealed any significant differences between individuals with and without *EP300/CREBBP* mutations (136). Interestingly, high p300/CBP expression levels have been reported to be associated with poor overall survival for resected SCLC patients (111). Direct evidence clearly revealing the roles of p300/CBP in SCLC initiation and progression is still lacking.

The pathogenesis of SCLC is a complex, multi-step process. Understanding the genetic and epigenetic basis of SCLC will contribute to the development of novel therapies. In the future, more multidisciplinary and

comprehensive studies will be required for translating these biological findings into clinical practice.

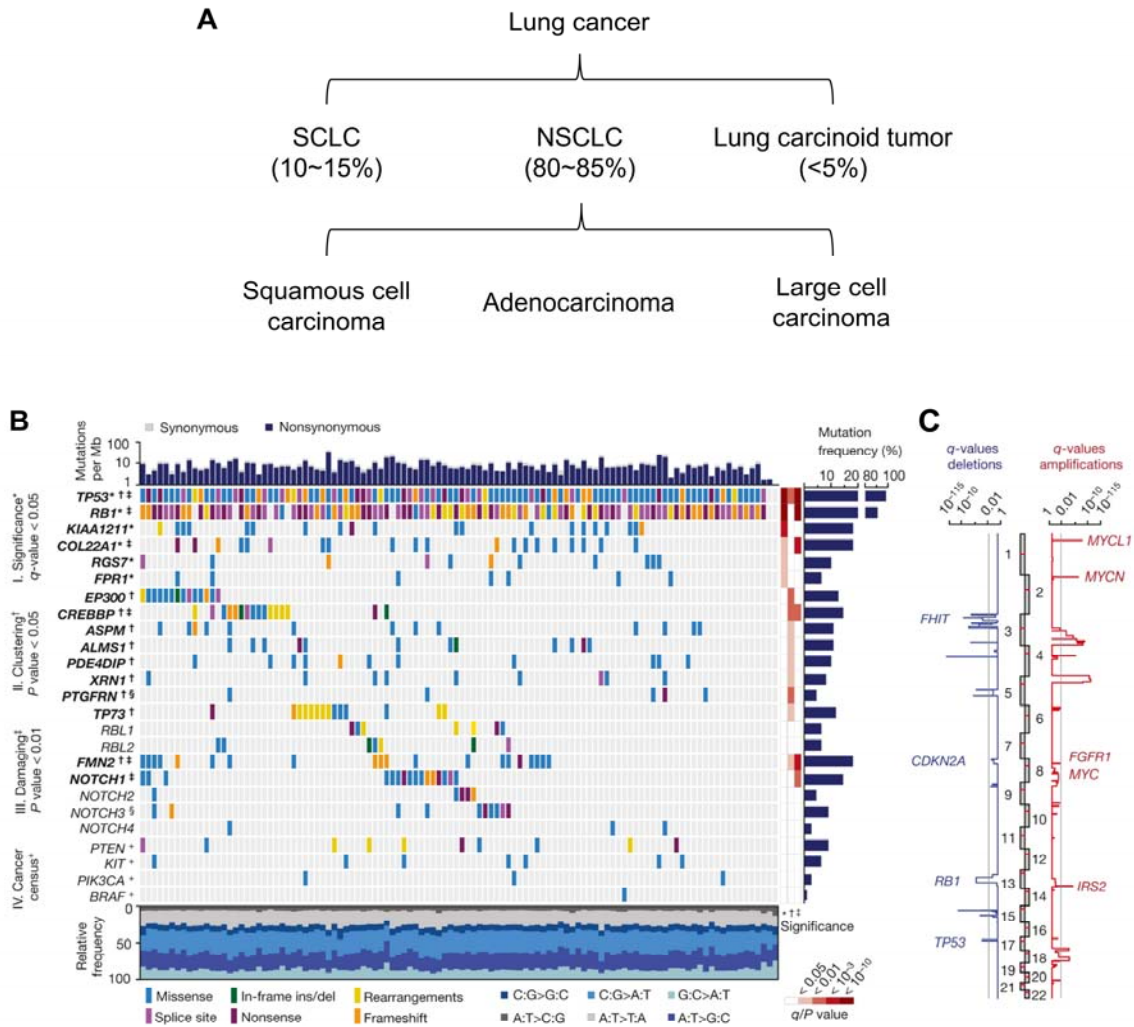


Figure 5. Genetic alterations in small cell lung cancer.

(A) The classification of lung cancers. (B) The somatic mutations of candidate genes in SCLC tumor samples. Tumor samples are arranged from left to right. Alterations of SCLC candidate genes are annotated for each sample according to the color panel below the image. The somatic mutation frequencies for each candidate gene are plotted on the right panel. Mutation rates and type of base-pair substitution are displayed in the top and bottom panel, respectively. Significant candidate genes are highlighted in bold (*corrected q-values < 0.05,

†P < 0.05, ‡P < 0.01). The respective level of significance is displayed as a heatmap on the right panel. Genes that are also mutated in murine SCLC tumors are denoted with a § symbol. Mutated cancer census genes of therapeutic relevance are denoted with a + symbol. (C) Somatic copy number alterations determined for 142 human SCLC tumors by single nucleotide polymorphism (SNP) arrays. Significant amplifications (red) and deletions (blue) were determined for the chromosomal regions and are plotted as q-values (significance < 0.05).

Figure 5B and 5C are adapted from George, J., J. S. Lim, S. J. Jang, Y. Cun, L. Ozretic, G. Kong, F. Leenders, X. Lu, L. Fernandez-Cuesta, G. Bosco, C. Muller, I. Dahmen, N. S. Jahchan, K. S. Park, D. Yang, A. N. Karnezis, D. Vaka, A. Torres, M. S. Wang, J. O. Korbel, R. Menon, S. M. Chun, D. Kim, M. Wilkerson, N. Hayes, D. Engelmann, B. Putzer, M. Bos, S. Michels, I. Vlastic, D. Seidel, B. Pinther, P. Schaub, C. Becker, J. Altmuller, J. Yokota, T. Kohno, R. Iwakawa, K. Tsuta, M. Noguchi, T. Muley, H. Hoffmann, P. A. Schnabel, I. Petersen, Y. Chen, A. Soltermann, V. Tischler, C. M. Choi, Y. H. Kim, P. P. Massion, Y. Zou, D. Jovanovic, M. Kontic, G. M. Wright, P. A. Russell, B. Solomon, I. Koch, M. Lindner, L. A. Muscarella, A. la Torre, J. K. Field, M. Jakopovic, J. Knezevic, E. Castanos-Velez, L. Roz, U. Pastorino, O. T. Brustugun, M. Lund-Iversen, E. Thunnissen, J. Kohler, M. Schuler, J. Botling, M. Sandelin, M. Sanchez-Céspedes, H. B. Salvesen, V. Achter, U. Lang, M. Bogus, P. M. Schneider, T. Zander, S. Ansen, M. Hallek, J. Wolf, M. Vingron, Y. Yatabe, W. D. Travis, P. Nurnberg, C. Reinhardt, S. Perner, L. Heukamp, R. Buttner, S. A. Haas, E.

Brambilla, M. Peifer, J. Sage, and R. K. Thomas. 2015. Comprehensive genomic profiles of small cell lung cancer. *Nature* 524: 47-53. Permission to reuse these figures for thesis was obtained from www.copyright.com with license number: 4324930807544.

Chapter 2. Materials and Methods

2.1 Plasmids and molecular cloning.

The coding DNA sequences (CDS) encoding human full-length p300 protein and various p300 fragments were amplified from pcDNA3.1-p300 vector (#23252) purchased from Addgene. The CDS of full-length p300 and p300 BD-RING-PHD-HAT-ZZ-TAZ2 region (BRPHZ, amino acids 1035-1830) and cloned into pENTR3C vector and subsequently cloned into p3FLAG and pCDH-3FLAG destination vectors using Gateway techniques (Invitrogen). The CDS encoding the human p300 BD-RING-PHD-HAT-ZZ region (BRPHZ, amino acids 1035-1720) and ZZ domain (amino acids 1650-1720) were cloned into the pGEX-6P-1 vector (GE Healthcare). Point mutations and deletions were generated using a site-directed mutagenesis kit (Stratagene) and verified by Sanger sequencing.

Clustered Regularly Interspaced Short Palindromic Repeats (CRISPR) guide RNAs (gRNAs) were designed by the online CRISPR design tool of Feng Zhang's lab (<http://crispr.mit.edu/>) for human and mouse *EP300/CREBBP* genes. Two gRNAs targeting the 5' region of each gene's CDS and one non-target control gRNA were used in this study. The oligos encoding those gRNAs were annealed and then cloned into lentiCRISPRv2 puro vector (#98290, Figure 6) purchased from Addgene.

The detailed information of all the vectors and oligos are included in Table 1 and 2, respectively.

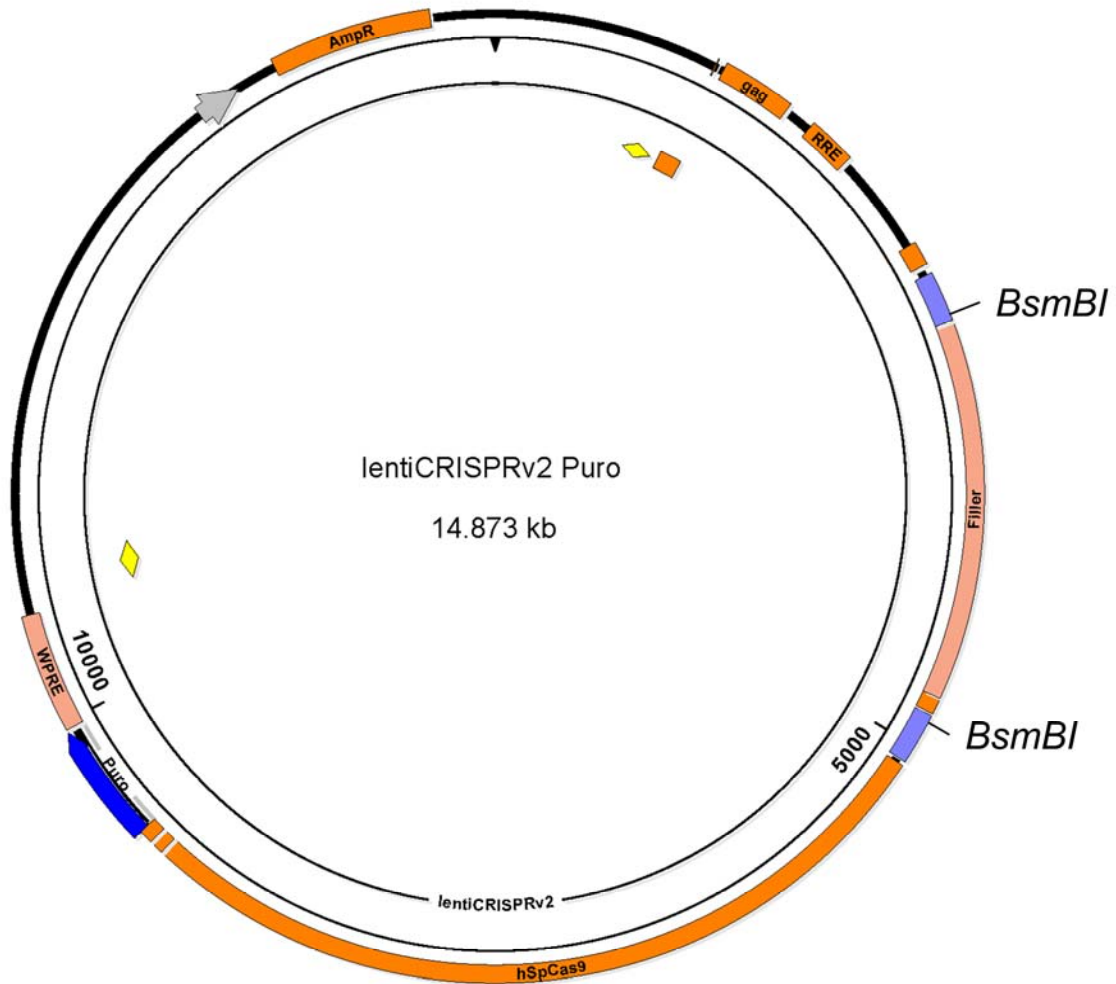


Figure 6. The map of LentiCRISPR v2 Puro vector.

The vector was linearized by *BsmI* digestion. The DNAs encoding gRNAs were inserted between two *BsmI* restriction sites. This figure is made using DNASTAR SeqBuilder Pro.

Name	Region cloned	Application
pGEX-p300-ZZ	p300 AA1650-1720	Prokaryotic expression
pGEX-p300-ZZ D1664A	p300 AA1650-1720	Prokaryotic expression
pGEX-p300-ZZ F1666A	p300 AA1650-1720	Prokaryotic expression
pGEX-p300-ZZ Y1668A	p300 AA1650-1720	Prokaryotic expression
pGEX-p300-ZZ N1671A	p300 AA1650-1720	Prokaryotic expression
pGEX-p300-ZZ R1680C	p300 AA1650-1720	Prokaryotic expression
pGEX-p300-ZZ W1681A	p300 AA1650-1720	Prokaryotic expression
pGEX-p300-ZZ D1688K	p300 AA1650-1720	Prokaryotic expression
pGEX-p300-ZZ D1690A	p300 AA1650-1720	Prokaryotic expression
pGEX-p300-BRPHZ	p300 AA1035-1720	Prokaryotic expression
pGEX-p300-BRPHZ ΔAIL	p300 AA1035-1720 (1520-1581 del)	Prokaryotic expression
pGEX-p300-BRPH	p300 AA1035-1669	Prokaryotic expression
pGEX-p300-BRPHZ N1132A	p300 AA1035-1720	Prokaryotic expression
pGEX-p300-BRPHZ D1399A	p300 AA1035-1720	Prokaryotic expression
pGEX-p300-BRPHZ N1671A	p300 AA1035-1720	Prokaryotic expression
pGEX-p300-BRPHZ D1690A	p300 AA1035-1720	Prokaryotic expression
pGEX-p300-BRPHZ N1132A D1690A	p300 AA1035-1720	Prokaryotic expression
pENTR3C-p300-BRPHZT	p300 AA1035-1830	Gateway cloning
pENTR3C-p300-BRPHZT ΔZZ	p300 AA1035-1830 (1664-1705 del)	Gateway cloning
pENTR3C-p300-BRPHZT ΔBRD	p300 AA1162-1830	Gateway cloning
pENTR3C-p300-BRPHZT ΔZZ&BRD	p300 AA1162-1830 (1664-1705 del)	Gateway cloning
pENTR3C-p300-BRPHZT ΔAIL	p300 AA1035-1830 (1520-1581 del)	Gateway cloning
pENTR3C-p300-BRPHZT N1132A	p300 AA1035-1830	Gateway cloning
pENTR3C-p300-BRPHZT D1399A	p300 AA1035-1830	Gateway cloning
pENTR3C-p300-BRPHZT N1671A	p300 AA1035-1830	Gateway cloning
pENTR3C-p300-BRPHZT D1690A	p300 AA1035-1830	Gateway cloning
pENTR3C-p300-BRPHZT N1132A D1690A	p300 AA1035-1830	Gateway cloning
pENTR3C-p300FL	p300 full-length CDS	Gateway cloning
pENTR3C-p300FL N1671A	p300 full-length CDS	Gateway cloning
pENTR3C-p300FL D1690A	p300 full-length CDS	Gateway cloning

Table 1. Plasmids used in this study.

Name	Region cloned	Application
pCDH-3FLAG-p300-BRPHZT	p300 AA1035-1830	Lentiviral expression
pCDH-3FLAG-p300-BRPHZT ΔZZ	p300 AA1035-1830 (1664-1705 del)	Lentiviral expression
pCDH-3FLAG-p300-BRPHZT ΔBRD	p300 AA1162-1830	Lentiviral expression
pCDH-3FLAG-p300-BRPHZT ΔZZ&BRD	p300 AA1162-1830 (1664-1705 del)	Lentiviral expression
pCDH-3FLAG-p300-BRPHZT ΔAIL	p300 AA1035-1830 (1520-1581 del)	Lentiviral expression
pCDH-3FLAG-p300-BRPHZT N1132A	p300 AA1035-1830	Lentiviral expression
pCDH-3FLAG-p300-BRPHZT D1399A	p300 AA1035-1830	Lentiviral expression
pCDH-3FLAG-p300-BRPHZT N1671A	p300 AA1035-1830	Lentiviral expression
pCDH-3FLAG-p300-BRPHZT D1690A	p300 AA1035-1830	Lentiviral expression
pCDH-3FLAG-p300-BRPHZT N1132A D1690A	p300 AA1035-1830	Lentiviral expression
pCDH-3FLAG-p300FL	p300 full-length CDS	Lentiviral expression
pCDH-3FLAG-p300FL N1671A	p300 full-length CDS	Lentiviral expression
pCDH-3FLAG-p300FL D1690A	p300 full-length CDS	Lentiviral expression
p3FLAG-p300FL	p300 full-length CDS	Transfection
p3FLAG-p300FL N1671A	p300 full-length CDS	Transfection
p3FLAG-p300FL D1690A	p300 full-length CDS	Transfection
Human CBP gRNA5-LentiCRISPRv2	NA	Gene depletion
Human CBP gRNA6-LentiCRISPRv2	NA	Gene depletion
Human p300 gRNA1-LentiCRISPRv2	NA	Gene depletion
Human p300 gRNA6-LentiCRISPRv2	NA	Gene depletion
Mouse CBP gRNA3-LentiCRISPRv2	NA	Gene depletion
Mouse CBP gRNA6-LentiCRISPRv2	NA	Gene depletion
Mouse p300 gRNA2-LentiCRISPRv2	NA	Gene depletion
Mouse p300 gRNA5-LentiCRISPRv2	NA	Gene depletion

Table 1 (continue). Plasmids used in this study.

2.2 Primers

The sequences and usages of all primers/oligos used in this study are described in Table 2.

Oligo name	Sequence (5'-3')	Application
p300-fl-KpnI-F	GGGGTACCATGGCCGAGAATGTG	Cloning
p300-fl-XhoI-R	GCGCCTCGAGCTAGTGTATGTCTAG	Cloning
p300-BRD-EcoRI-F	CGGAATTCACCCAGTCATCTCC	Cloning
p300-PHD-EcoRI-F	CGGAATTCTACTGTTGTGGCAGA	Cloning
p300-HAT-XhoI-R	GCGCCTCGAGTTAGGTGTAGACAAAGCG	Cloning
p300-ZZ-XhoI-R	GCGCCTCGAGTTACTGCTGGTTGTTGC	Cloning
p300-TAZ2-XhoI-R	GCGCCTCGAGTTACCTGCGAAGCATTG	Cloning
p300-dAIL-F	GAAAGCATTAAAGGAACAGAACTATATGCC	Deletion
p300-dAIL-R	GGCATATAGTTTCTGTTCTTAATGCTTTC	Deletion
p300-dZZ-F	CACACGCAGAGCCAGGAGAACTAGGCCTT	Deletion
p300-dZZ-R	AAGGCCTAGTTTCTCCTGGCTCTGCGTGTG	Deletion
p300-ZZ-D1664A-F	CACACGCAGAGCCAGGCCCGCTTTGTCTACACC	Mutagenesis
p300-ZZ-D1664A-R	GGTGTAGACAAAGCGGGCCTGGCTCTGCGTGTG	Mutagenesis
p300-ZZ-F1666A-F	CAGAGCCAGGACCGCGCTGTCTACACCTGCAAT	Mutagenesis
p300-ZZ-F1666A-R	ATTGCAGGTGTAGACAGCGCGGTCTGGCTCTG	Mutagenesis
p300-ZZ-Y1668A-F	CAGGACCGCTTTGTGCCACCTGCAATGAATGC	Mutagenesis
p300-ZZ-Y1668A-R	GCATTCATTGCAGGTGGCGACAAAGCGGTCTG	Mutagenesis
p300-ZZ-N1671A-F	TTTGTCTACACCTGCGCTGAATGCAAGCACCAT	Mutagenesis
p300-ZZ-N1671A-R	ATGGTGCTTGCATTAGCGCAGGTGTAGACAAA	Mutagenesis
p300-ZZ-R1680C-F	CACCATGTGGAGACATGCTGGCACTGTACTGTC	Mutagenesis
p300-ZZ-R1680C-R	GACAGTACAGTGCCAGCATGTCTCCACATGGTG	Mutagenesis
p300-ZZ-W1681A-F	CATGTGGAGACACGCGCGCACTGTACTGTCTGT	Mutagenesis
p300-ZZ-W1681A-R	ACAGACAGTACAGTGCGCGCGTGTCTCCACATG	Mutagenesis
p300-ZZ-D1688K-F	TGTA CTGTCTGTGAGAAGTATGACTTGTGTATC	Mutagenesis
p300-ZZ-D1688K-R	GATACACAAGTCATACTTCTCACAGACAGTACA	Mutagenesis
p300-ZZ-D1690A-F	GTCTGTGAGGATTATGCCTTGTGTATCACCTGC	Mutagenesis
p300-ZZ-D1690A-R	GCAGGTGATACACAAGGCATAATCCTCACAGAC	Mutagenesis
p300-HAT-D1399A-F	TACATATCTTACCTCGCTAGTGTTCAATTTCTTC	Mutagenesis
p300-HAT-D1399A-R	GAAGAAATGAACACTAGCGAGGTAAGATATGTA	Mutagenesis
p300-BRD-N1132A-F	AATGCCTGGTTATATGCCCGGAAAACATCACGG	Mutagenesis
p300-BRD-N1132A-R	CCGTGATGTTTTCCGGGCATATAACCAGGCATT	Mutagenesis

Table 2. Oligos used in this study.

Oligo name	Sequence (5'-3')	Application
NBPF1-46k-F	TCAAGAGCCCAGCCAACAC	ChIP-qPCR
NBPF1-46k-R	CAGCCCTACAGAAGTGCCTTTT	ChIP-qPCR
NOTCH2NL-d4k-F	AGCCCTTCGGGACACATG	ChIP-qPCR
NOTCH2NL-d4k-R	GGGCTTCCACTCTTCCAAAGT	ChIP-qPCR
DMPK-1k-F	CACCCAGAAGAACCCAAAGTTG	ChIP-qPCR
DMPK-1k-R	GGAGAACCAGCTTTGCAGACA	ChIP-qPCR
PDE4DIP-U10k-F	TCTCGTGCCATCCACTCTATCTC	ChIP-qPCR
PDE4DIP-U10k-R	GCCTGGATGTGCTGGACAA	ChIP-qPCR
INSM1-D8k-F	CCCAGTTGTTGCCCCAGTAA	ChIP-qPCR
INSM1-D8k-R	TGGTGCCCAAGCCATCA	ChIP-qPCR
ASCL1-P-F	GCACGCACTGCAACAACAA	ChIP-qPCR
ASCL1-P-R	CTCCCGCTCCTTGCAAAC	ChIP-qPCR
ASCL1-D5k-F	GAGTTTGAGACTAGCCTGGGAAAG	ChIP-qPCR
ASCL1-D5k-R	CCAGCACCTTCAGCTAATTTTTG	ChIP-qPCR
Myc-ChIP-P1k-F	CAGCCCGAGACTGTTGCA	ChIP-qPCR
Myc-ChIP-P1k-R	TTTCAGAAGAGACAAATCCCCTTT	ChIP-qPCR
Myc-ChIP-P0.1k-F	CCCGGGTTCCCAAAGC	ChIP-qPCR
Myc-ChIP-P0.1k-R	CCAGACCCTCGCATTATAAAGG	ChIP-qPCR
mMyc-RTq-F	GTCTTTCCCTACCCGCTCAAC	RT-qPCR
mMyc-RTq-R	GTGGAATCGGACGAGGTACAG	RT-qPCR
mMyc1-RTq-F	GGCAACAGCAACTGCAAAAAG	RT-qPCR
mMyc1-RTq-R	CAGGCGTTCTGGTCGGTTAG	RT-qPCR
mMycn-RTq-F	TGCCCGCGAGAAGCTAGA	RT-qPCR
mMycn-RTq-R	CGTGGCCGTGCTGTAGTTT	RT-qPCR
mAscl1-RTq-F	TCCTGTGCCCCACCATCT	RT-qPCR
mAscl1-RTq-R	AGAACCCGCCATAGAGTTCAAG	RT-qPCR
mNfib-RTq-F	CCCGTGCTGTGTCTTATCCA	RT-qPCR
mNfib-RTq-R	AGGCAGTCGATCCTCCTAATCTT	RT-qPCR
MYC-RTq-F	CGTCTCCACACATCAGCACAA	RT-qPCR
MYC-RTq-R	CACTGTCCAACCTTGACCCTCTTG	RT-qPCR
MYCL1-RTq-F	GGAGCGGACATGGACTACGA	RT-qPCR
MYCL1-RTq-R	GCCGTGGAGCGGTAGAAAT	RT-qPCR
MYCN-RTq-F	AATTGAACACGCTCGGACTTG	RT-qPCR
MYCN-RTq-R	AATGTGCAAAGTGGCAGTGA	RT-qPCR
ASCL1-RTq-F	GAGCAACTGGGACCTGAGTCA	RT-qPCR
ASCL1-RTq-R	CCCACTGCTTTTGCACACAA	RT-qPCR
NEUROD1-RTq-F	AAGGTGGTGCCTTGCTATTCTAA	RT-qPCR
NEUROD1-RTq-R	CCAAGCGCAGAGTCTCGATT	RT-qPCR

Table 2 (continue). Oligos used in this study.

Oligo name	Sequence (5'-3')	Application
CBP-gRNA5-5'	CACCGCGCGGGACTGAACACCGCAC	CRISPR gRNA
CBP-gRNA5-3'	AAACGTGCGGTGTTTCAGTCCCGCGC	CRISPR gRNA
CBP-gRNA6-5'	CACCGGCAGCCGAACAGTGCTAACA	CRISPR gRNA
CBP-gRNA6-3'	AAACTGTTAGCACTGTTCTGGCTGCC	CRISPR gRNA
EP300-gRNA1-5'	CACCGGTTCAATTGGAGCAGGCCGA	CRISPR gRNA
EP300-gRNA1-3'	AAACTCGGCCTGCTCCAATTGAACC	CRISPR gRNA
EP300-gRNA6-5'	CACCGGAATTGGGACTAACCAATGG	CRISPR gRNA
EP300-gRNA6-3'	AAACCCATTGGTTAGTCCCAATTCC	CRISPR gRNA
mCBP-gRNA3-5'	CACCGGGCCTTCTCAATAGTAACTC	CRISPR gRNA
mCBP-gRNA3-3'	AAACGAGTTACTATTGAGAAGGCC	CRISPR gRNA
mCBP-gRNA6-5'	CACCGAGCGGCTCTAGCATCAACCC	CRISPR gRNA
mCBP-gRNA6-3'	AAACGGGTTGATGCTAGAGCCGCTC	CRISPR gRNA
mEP300-gRNA2-5'	CACCGATGAACGGTTCATTGGAGC	CRISPR gRNA
mEP300-gRNA2-3'	AAACGCTCCAATGGAACCGTTCATC	CRISPR gRNA
mEP300-gRNA5-5'	CACCGGGCCACCGACTCCCATGTTG	CRISPR gRNA
mEP300-gRNA5-3'	AAACCAACATGGGAGTCGGTGGCCC	CRISPR gRNA
NT-gRNA2-5'	CACCGGGATACTTCTTCGAACGTTT	CRISPR gRNA
NT-gRNA2-3'	AAACAAACGTTCTGAAGAAGTATCCC	CRISPR gRNA

Table 2 (continue). Oligos used in this study.

2.3 Antibodies

The information of all the primary and secondary antibodies used in this study is included in Table 3.

Antibody	Vendor	Catalog #	Application
Anti-H3	Abcam	Ab1791	WB, ChIP
Anti-H3K4ac	Abcam	Ab176799	WB
Anti-H3K9ac	Abcam	Ab32129	WB
Anti-H3K9ac	Active Motif	61251	WB
Anti-H3K18ac	Active Motif	39755	WB, ChIP
Anti-H3K27ac	Abcam	Ab4729	WB, ChIP
Anti-acetyl-Histone H4	Millipore	06-598	WB
Anti-GST	Santa Cruz	Sc-459	WB
Anti-FLAG	Sigma	F1804	WB, ChIP
Anti-p300	Santa Cruz	Sc-585	WB
Anti-CBP	Santa Cruz	Sc-369	WB
Anti- β -Tubulin	Sigma	T8328	WB
IRDye® 800CW Goat anti-Rabbit IgG	LI-COR	926-32211	WB (secondary)
IRDye® 680LT Goat anti-Mouse IgG	LI-COR	926-68020	WB (secondary)
Peroxidase-conjugated Donkey anti-Mouse IgG	Jackson Immuno Research	715-035-150	WB (secondary)
Peroxidase-conjugated Donkey anti-Rabbit IgG	Jackson Immuno Research	711-035-152	WB (secondary)

Table 3. Antibodies used in this study.

2.4 Cell lines

The information of all cell lines used was described in Table 4. They were mycoplasma-negative and tested for authentication by short tandem repeat (STR) profiling by the MDACC Characterized Cell Line Core.

Cell line	Species	Cancer type	Medium	Source
HEK293T	Human	Kidney cancer	DMEM*	ATCC
HBEC	Human	Lung epithelial control cell	KSFM**	Dr. John Heymach
A549	Human	NSCLC	RPMI	Dr. John Heymach
H1299	Human	NSCLC	RPMI	Dr. John Heymach
H1048	Human	SCLC	HITES***	Dr. Lauren Byers
H1836	Human	SCLC	HITES	Dr. Lauren Byers
H209	Human	SCLC	RPMI****	Dr. Lauren Byers
H2171	Human	SCLC	HITES	Dr. Lauren Byers
H524	Human	SCLC	RPMI	Dr. Lauren Byers
H69	Human	SCLC	RPMI	Dr. Lauren Byers
H82	Human	SCLC	RPMI	Dr. Lauren Byers
ID43	Mouse	Pre-SCLC	RPMI	Dr. Kwon-Sik Park
Kp1	Mouse	SCLC	RPMI	Dr. Julien Sage
Kp3	Mouse	SCLC	RPMI	Dr. Julien Sage
Kp3 _{+GFP+Luc}	Mouse	SCLC	RPMI	Dr. Julien Sage
Kp12	Mouse	SCLC	RPMI	Dr. Julien Sage
259-2	Mouse	SCLC	RPMI	Dr. Julien Sage

Table 4. Cell lines used in this study.

*DMEM: Dulbecco's Modified Eagle Medium (Cellgro) supplemented with 10% fetal bovine serum (FBS) (Sigma). **KSFM: Keratinocyte serum-free medium.

HITES: DMEM/F12 Medium (Cellgro) supplemented with ITS mixture (Lonza, containing 0.005 mg/ml Insulin, 0.01 mg/ml Transferrin and 30nM Sodium selenite), 10 nM Hydrocortisone (Sigma), 10 nM β -estradiol (Sigma), 4.5 mM L-glutamine (Cellgro) and 5% FBS (Sigma). * RPMI: Roswell Park Memorial Institute 1640 medium (Cellgro) supplemented with 10% FBS (Sigma).

2.5 Protein expression and purification

The CDS of p300_{BRPHZ} or p300_{ZZ} cloned in the pGEX-6P-1 vector were expressed in BL21 Rosetta 2 cells. Protein production was induced with 0.2 mM IPTG and cultured overnight at 16 °C in Luria broth (LB) medium supplemented with 0.05 mM ZnCl₂. The glutathione S-transferase (GST)-tagged proteins were purified on glutathione Sepharose 4B beads (Amersham) in binding buffer (50 mM Tris-HCl pH 7.5, 150 mM NaCl, 0.05% NP-40, 1 mM PMSF plus protease inhibitors (Roche)) at 4 °C for 4 hours and eluted by 100 mM Tris pH 8.0 containing 15 mg/mL Reduced Glutathione (Sigma) at 4 °C for overnight. Eluted proteins were supplemented with 25% glycerol before frozen at -80 °C. All proteins harboring mutations or deletions were expressed and purified as WT proteins.

2.6 Peptide microarray and pull-down assays

Biotinylated histone peptides bearing different modifications were synthesized at CPC, LLC. For peptide microarray, biotinylated histone peptides were printed in triplicate onto a streptavidin-coated slide (PolyAn) using a VersArray Compact Microarrayer (Bio-Rad). After a short blocking with biotin (Sigma), the slides were incubated with the glutathione S-transferase (GST)-tagged p300 ZZ domain in binding buffer (50 mM Tris-HCl, pH 7.5, 250 mM NaCl, 0.1% NP-40, 1 mM PMSF, 20% FBS) overnight at 4 °C with gentle shake. After washed with the same buffer, the slides were probed with an anti-GST primary antibody and then a fluorescein-conjugated secondary antibody and

visualized using a GenePix 4000 scanner (Molecular Devices). For peptide pull-down, 1 µg of each biotinylated histone peptide was incubated with 1-2 µg of GST-fused p300 ZZ domain in binding buffer (50 mM Tris-HCl pH 7.5, 250 mM NaCl, 0.1% NP-40, 1 mM PMSF) for overnight with rotation at 4 °C. Streptavidin beads (Amersham) were added to the mixture, and the mixture was incubated for 1 hour with rotation at 4 °C. The beads were then washed three times and the bound proteins were analyzed using SDS-PAGE and Western blotting.

2.7 Calf thymus histone pull-down assay

2 µg GST-tagged p300_{zz} domain were incubated with 10 µg of calf thymus total histones (Worthington) in binding buffer (50 mM Tris-HCl pH 7.5, 1M NaCl, 1% NP-40) at 4 °C for overnight with rotation. Glutathione Sepharose 4B beads (Amersham) were added to the solution and incubate for 1 h. The beads were then washed six times using binding buffer and the bound histones were detected using SDS-PAGE and Western blotting.

2.8 *In vitro* histone acetyltransferase (HAT) assays

For HAT assays on recombinant nucleosomes containing full-length histone H3.1, purified wild type or mutated p300_{BRPHZ} (300 nM) was incubated with recombinant mononucleosome (100 nM) in HAT reaction buffer (50 mM Tris pH 8.0, 0.1 mM EDTA, 10% glycerol, 1 mM PMSF and 1mM DTT) in a total volume of 50 µL. After pre-warming at 37 °C for 5 minutes, reactions were initiated with the addition of acetyl-CoA (Sigma) to a final concentration of 0.1

mM and incubated for 10~80 minutes at 37 °C. For assays comparing the HAT activities on recombinant nucleosomes containing full-length histone H3.1 and N-terminally truncated H3.1, wild type p300^{BRPHZ} fragment (50 nM) and mononucleosome (500 nM) were incubated under the same condition for 1 to 6 hours. Reactions were quenched by flash-freezing in liquid nitrogen and then analyzed by SDS-PAGE and Western blot analysis. Western blot results were quantified by LI-COR Odyssey and normalized to a common standard sample.

2.9 Western blot

Cells were lysed in RIPA buffer (50 mM TrisHCl pH7.4, 150 mM NaCl, 2 mM EDTA, 1% NP-40, 0.1% SDS) and sonicated for 20s at 15% intensity. Generally, 15~30 µg protein lysate was loaded into various percentages of SDS-polyacrylamide gels for electrophoresis in PAGE running buffer (25 mM Tris, 192 mM glycine, 0.1% SDS, pH8.3). Then proteins were transferred to 0.2 or 0.45 µm PVDF membrane in transfer buffer (25 mM Tris, 192 mM glycine, 0.1% SDS, 20% methanol). The membranes were blocked by TBST buffer (150 mM NaCl, 10 mM Tris pH8.0, 0.1% Tween20) supplemented with 5% non-fat milk for 1 hour at room temperature and then blotted with primary antibodies overnight at 4°C on an orbital shaker. After three times of wash by TBST, membranes were incubated with secondary antibodies for 1 hour at room temperature and washed again by TBST for 3 times. The membranes were then either used for film-developing in darkroom after incubating with ECL Western Blotting Detection Reagent (GE Healthcare) for 5 min or directly scanned by LI-COR Odyssey.

2.10 Transfection and lentiviral infection

Transient transfection was performed using X-tremeGENE DNA transfection reagent (Roche). 48 h after transfection, cells were collected for Western blot analysis. For packaging lentivirus, 293T cells were co-transfected with pMD2.G, pPAX2 (Addgene) and pCDH (or LentiCRISPRv2) constructs using X-tremeGENE DNA transfection reagent (Roche). For infections, cells were incubated with viral supernatants in the presence of 8 mg/ml polybrene; after 48 hours, the infected cells were selected with blasticidin (10 µg/ml) or puromycin (2 µg/ml) for 4-6 days before experiments.

2.11 Salt fractionation

The method of salt fractionation was modified from Tjian lab protocol (159). In short, cells were swollen with hypotonic buffer (10 mM HEPES pH 7.9, 1.5 mM MgCl₂, 10mM KCl) and lysed by gentle disruption to isolate nuclei. The nuclei were incubated with wash buffer (20 mM HEPES pH 7.9, 1.5 mM MgCl₂, 0.2mM EDTA, 25% glycerol) containing 75 mM NaCl for 30 min at 4 °C and then pelleted and the supernatant fraction was collected. The nuclei were then similarly washed by wash buffer containing 150mM, 300mM and 600mM NaCl and the supernatant fraction of each step was collected (Figure 7). After the final wash step, the pellet was resuspended and sonicated before collection. All fractions collected were analyzed by SDS-PAGE and Western blotting.

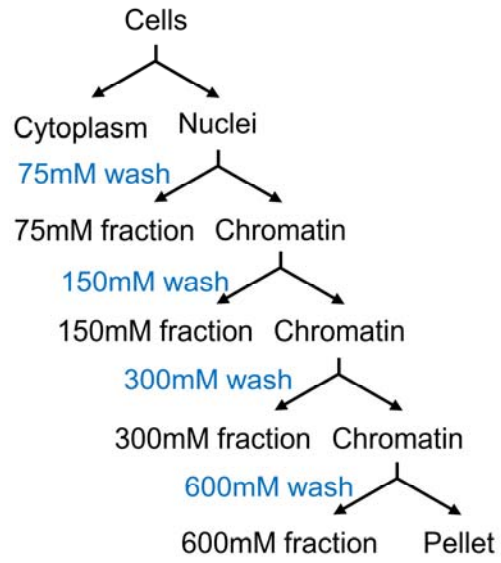


Figure 7. The workflow for salt fractionation assay.

2.12 Chromatin immunoprecipitation (ChIP) and ChIP-seq

ChIP analysis was performed as described in our previous papers (160, 161). In brief, cells were cross-linked with 1% formaldehyde for 10 min and stopped by adding 125 mM glycine. The isolated nuclei were resuspended in nuclei lysis buffer (50 mM Tris pH 8.0, 10 mM EDTA, 1% SDS) and sonicated using a Bioruptor Sonicator (Diagenode) for two cycles. The samples were immunoprecipitated with 2–4 μ g of the appropriate antibodies overnight at 4 °C. Protein A/G beads (Millipore) were added and incubated for 1 hour, and the immunoprecipitates were washed twice, each with low-salt (20 mM Tris pH 8.0, 150 mM NaCl, 2 mM EDTA, 1% Triton X-100 and 0.1% SDS), high-salt (20 mM Tris pH 8.0, 500 mM NaCl, 2 mM EDTA, 1% Triton X-100 and 0.1% SDS) and LiCl buffer (20 mM Tris pH 8.0, 250 mM LiCl, 1 mM EDTA, 1% NP-40 and 1% SDS). DNA was eluted from the beads using elution buffer (50 mM NaHCO₃, 1% SDS) and then reverse-crosslinked, purified using PCR purification kit (Qiagen). The purified DNA was analyzed by quantitative real-time PCR on the ABI 7500-FAST System using the Power SYBR Green PCR Master Mix (Applied Biosystems). The primer sequences for ChIP-qPCR are listed in Table 2.

For ChIP-seq, the purified DNA was sequenced using the Illumina Solexa HiSeq 3000. The raw reads were mapped to human reference genome NCBI 37 (hg19) or the *Drosophila melanogaster* genome (dm3) by bowtie v1.1.0, allowing up to 1 mismatch. Only uniquely mapped reads were retained for peak calling. But before that, we use spike-in normalization for sample size correction as previously described (162). For simplicity, the reads were downsampled to keep

same spike-in reads count in different samples. Then the ChIP-seq peaks were called by MACS v1.4.2 with a cutoff of $p \leq 1e-8$, and clonal reads were automatically removed by MACS. The ChIP-seq reads density was determined by deepTools v2.3.4, and then the average binding profile and heatmap were visualized using R v3.2.3.

2.13 ChIP-western blot

The ChIP-western blot (ChIP-WB) assay was largely similar to ChIP assay. Briefly, cells were cross-linked with 1% formaldehyde for 10 min and stopped by adding 125 mM glycine. The isolated nuclei were resuspended in nuclei lysis buffer (50 mM Tris pH 8.0, 10 mM EDTA, 1% SDS) and sonicated using a Bioruptor Sonicator (Diagenode). Anti-FLAG M2-conjugated agarose beads (Sigma) were incubated with sonicated lysates overnight at 4 °C. The beads were washed twice, each with low-salt (20 mM Tris pH 8.0, 150 mM NaCl, 2 mM EDTA, 1% Triton X-100 and 0.1% SDS), high-salt (20 mM Tris pH 8.0, 500 mM NaCl, 2 mM EDTA, 1% Triton X-100 and 0.1% SDS) and LiCl buffer (20 mM Tris pH 8.0, 250 mM LiCl, 1 mM EDTA, 1% NP-40 and 1% SDS), and the bound proteins were analyzed by SDS-PAGE and Western blot.

2.14 RNA extraction, reverse transcription (RT), and RT-qPCR

Total RNA was extracted using an RNeasy plus kit (QIAGEN) and reverse-transcribed using an iScript reverse transcription kit (Bio-Rad). Quantitative real-time PCR (qPCR) analyses were performed using Power SYBR

Green PCR Master Mix and the ABI 7500-FAST Sequence Detection System (Applied Biosystems). Gene expressions were calculated following normalization to *GADPH* levels using the comparative Ct (cycle threshold) method. The primer sequences for RT-qPCR are listed in Table 2.

2.15 Cell proliferation assay

Cells were seeded into a 96-well plate for 200~500 cells in 100 μ L medium per well in triplicate for each time point and their proliferation was measured every one or two days depending on the growth rate of those cells. There is a tight linear relationship between cell number and the concentration of ATP measured in cell lysate. The bioluminescence-based reagents such as CellTiter-Glo (Promega) can detect ATP, which provides a sensitive readout of cell proliferation. For proliferation measurement, directly add 25 μ L CellTiter-Glo into each well and gently rock the plate for 2 minutes on an orbit shaker to induce cell lysis. Then incubate the plate at room temperature for 10 minutes to stabilize luminescent signal before reading it using Fluostar Omega plate reader.

2.16 Statistical analyses

Data were presented as mean \pm s.e.m. unless stated otherwise. Statistical significance was calculated by two-tailed unpaired *t*-test on two experimental conditions with $P < 0.05$ considered statistically significant unless stated otherwise. Statistical significance levels are denoted as follows: * $P < 0.05$; ** $P < 0.01$. No statistical methods were used to predetermine sample size.

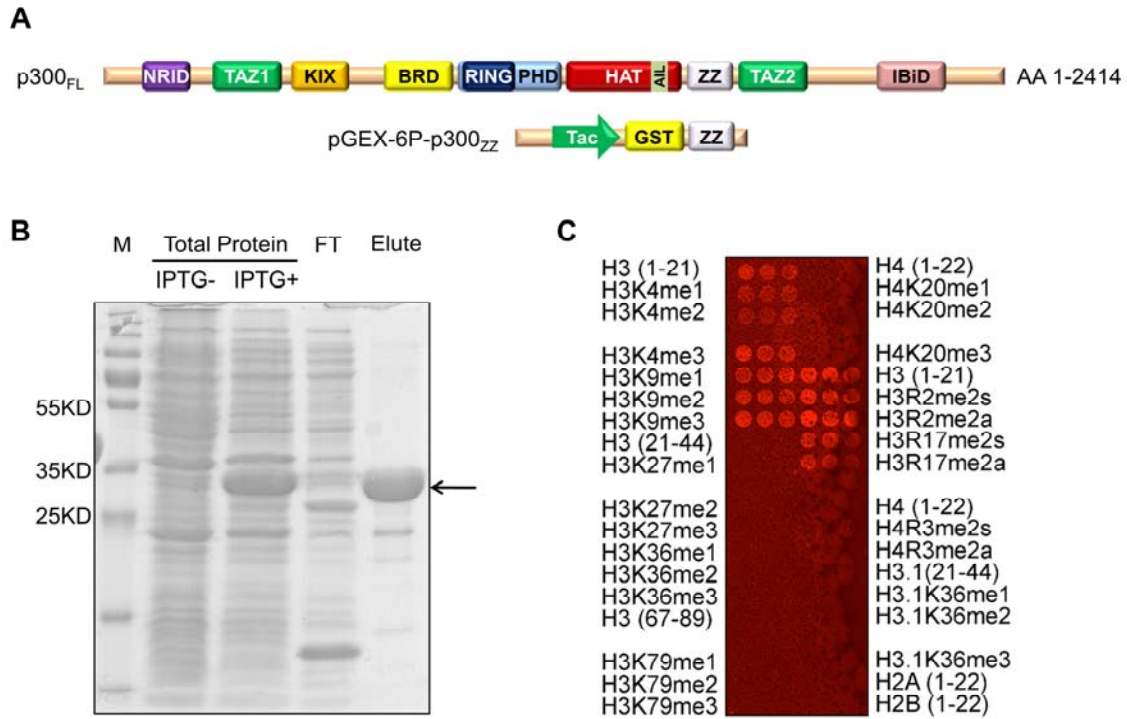


Figure 8. The expression, purification and peptide microarray analysis of p300 ZZ domain.

(A) Schematic representation of full-length p300 protein and the prokaryotic expression vector of p300 ZZ domain. (B) SDS-PAGE analysis of GST-tagged p300 ZZ domain before and after purification. The arrow points out the band for GST-p300_{ZZ}. IPTG: isopropyl β-D-1-thiogalactopyranoside. FT: flow-through. (C) The histone peptide microarray probed with GST-tagged p300 ZZ domain. Histone peptides were printed in triplicate with their names labeled on the left or right.

Chapter 3. The ZZ Domain of p300 Recognizes Histone H3 to Regulate Chromatin Association and Histone Acetylation

Copyright information:

Contents of Chapter 3.1-3.5 are based on Zhang Y*, Xue Y*, Shi J, Ahn JW, Mi W, Ali M, Wang X, Klein BJ, Wen H, Li W, Shi X and Kutateladze TG. 2018. The ZZ domain of p300 mediates specificity of the adjacent HAT domain for histone H3. *Nat Struct Mol Biol.* 25: 841-849. (*: Co-first authors). According to this journal, authors retain the rights “*to reproduce the contribution in whole or in part in any printed volume (book or thesis) of which they are the author(s)*”.

3.1 p300 ZZ domain is a reader for histone H3

To determine the function of p300 ZZ domain in histone binding, we performed histone peptide microarray using the GST-tagged p300 ZZ domain. GST-p300 ZZ showed a molecular weight ~32 kDa on SDS-PAGE (Figure 8A, 8B). On the histone peptide microarray, p300 ZZ bound to the unmodified H3₁₋₂₁ peptide and the H3₁₋₂₁ peptides containing mo-, di-, or tri-methylation on H3K4 or H3K9, or symmetric (me₂S) or asymmetric dimethylation (me₂A) on H3R2 or H3R17 (Figure 8C), suggesting that the ZZ domain is able to recognize H3 N-terminal tail independent of methylation on these residues.

To determine whether p300 ZZ domain specifically binds to histone H3 but not other histones, we performed calf thymus histone pull-down assays using GST-tagged p300 ZZ domain (Figure 9A). A known histone H3 reader, RBP2

PHD1 domain (163), was used as a positive control. The GST protein was used as a negative control. Western blots using specific histone antibodies revealed that similar to RBP2 PHD1, p300 ZZ specifically pulled down H3, but not other histones. Under the same condition, GST alone did not bind to any histone. These results demonstrate that p300 ZZ domain is a histone H3-specific reader.

To identify the minimal region of H3 tail required for p300 ZZ binding, we performed histone peptide pull-down using various fragments of histone H3 (Figure 9B). Consistent with the microarray data, p300 ZZ domain bound strongly to the H3₁₋₂₂ peptide. The H3₁₋₈ peptide retained sufficient binding to p300 ZZ. However, deletion of the first 4 amino acids from the N-terminus of H3 abolished its binding to p300 ZZ. As expected, other H3 regions did not bind to p300 ZZ.

A number of residues on the histone H3 tail can be post-translationally modified, more frequently with methylation and acetylation. To determine whether methylation or acetylation on histone H3 affects p300 ZZ binding, we performed histone peptide pull-down using histone peptides bearing methylation or acetylation on various residues (Figure 10A). Consistent with the microarray data, methylation or acetylation did not affect the binding of p300 ZZ domain to the H3 tail. Furthermore, p300 ZZ did not bind to other regions of histone H3 or H4, regardless of PTMs. Tryptophan fluorescence measurements revealed a K_d value of 8.8 μ M of p300 ZZ domain for unmodified H3₁₋₁₂ peptide, and 7.7 μ M or 7.6 μ M for the H3K4me3 or H3K4ac peptide, respectively (Figure 10B). All together, these results demonstrate that the ZZ domain of p300 is a H3-specific reader that is insensitive to histone modifications.

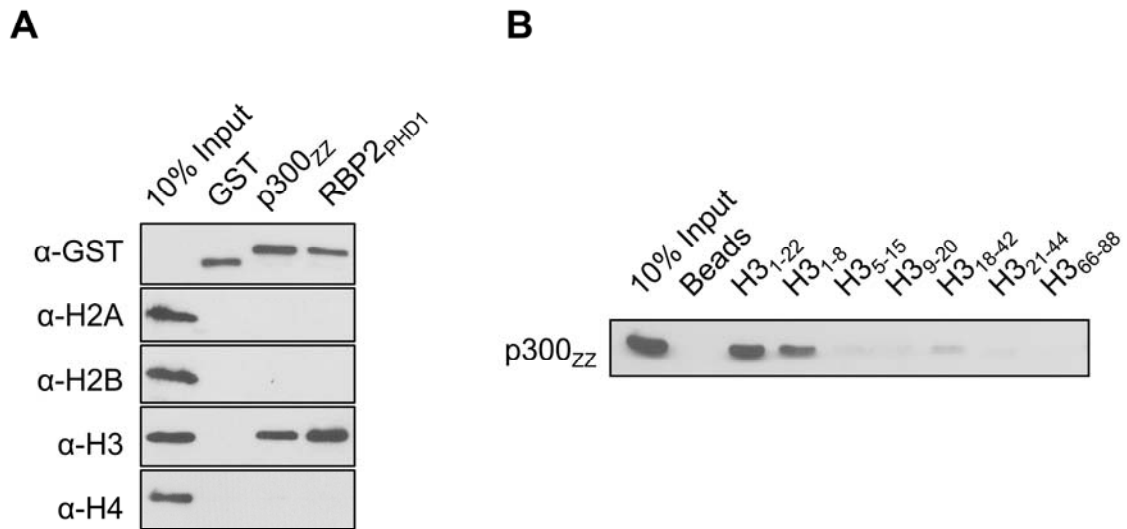
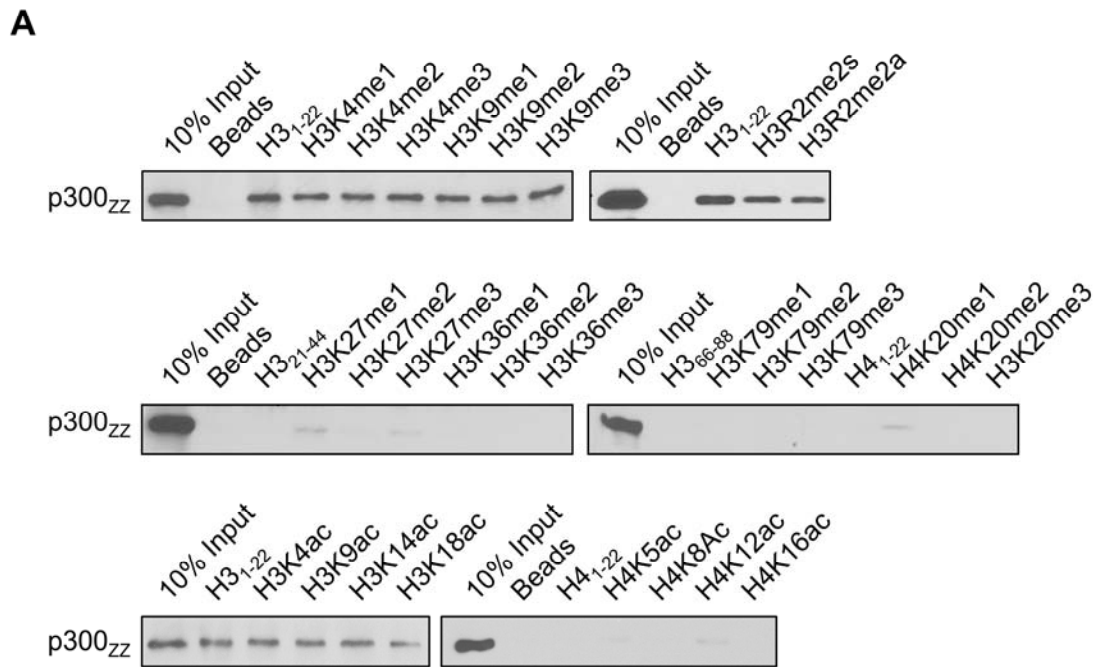


Figure 9. The ZZ domain of p300 binds to histone H3 tail.

(A) Calf thymus histone pull-down assays of p300 ZZ domain. RBP2 PHD1 or GST was used as a positive or negative control, respectively. (B) Peptide pull-down assays of p300 ZZ domain using the indicated histone H3 peptides.



B Binding affinities of p300 ZZ

H3 ₁₋₁₂ peptide	K _d (μM)
H3	8.8 ± 2.1
H3K4me1	8.3 ± 0.6
H3K4me3	7.7 ± 1.4
H3K4ac	7.6 ± 3.4

Figure 10. Recognition of H3 by p300 ZZ domain is not sensitive to methylation or acetylation on H3.

(A) Peptide pull-down assays of the p300 ZZ domain with the indicated histone peptides. (B) Binding affinities of p300 ZZ domain for the indicated histone peptides measured by tryptophan fluorescence. The experiments were carried out in triplicate for H3 and H3K4ac and in duplicate for methylated H3 by Yi Zhang from the Kutateladze lab at University of Colorado.

3.2 The structural basis of H3 recognition by p300 ZZ domain

Through collaboration with Dr. Tatiana Kutateladze's lab at University of Colorado School of Medicine, we determined the crystal structure of the p300 ZZ-H3 complex at 2.0 Å resolution. The complex structure was obtained using a chimeric construct containing residues 1-6 of H3 linked to residues 1663-1713 of p300. The structure showed that two H3-ZZ fusion proteins form complexes in which the H3 region of one molecule is bound to the ZZ domain of another molecule (Figure 11A). The p300 ZZ domain adopts a cross-brace topology stabilized by two zinc-binding clusters, a couple of twisted two- and three-stranded anti-parallel β -sheets, and a short α -helix (Figure 11B). The histone residues pair with the first β -strand (residues 1665-1669 of ZZ), creating the third anti-parallel β -strand and make extensive intermolecular contacts with the domain (Figure 11B). Characteristic β -sheet interactions are observed between the backbone amides of Ala1, Thr3 and Gln5 of H3 and T1669, V1667 and R1665 of the ZZ domain. Ala1 occupies a highly negatively charged binding site where the NH_3^+ group of Ala1 is anchored through the hydrogen bonds with T1669 and N1671 and a salt bridge with D1690 (Figure 11C, D). The guanidinium moiety of Arg2 is restrained via a salt bridge with the carboxyl group of D1688 and hydrogen bonds with the backbone carbonyl oxygen of E1687, whereas the backbone amide of Arg2 is involved in direct and water-mediated hydrogen bonding contacts with D1688. The side chain of Lys4 lays in a groove formed by the aromatic ring of F1666 and the side chain of D1664, the negatively charged carboxylic group of which forms a salt bridge with the ϵ -amino group of Lys4

(Figure 11B, E). The formation of the salt bridge most likely accounts for the indifference of p300 ZZ domain towards PTMs on H3K4, which would augment cation- π and hydrophobic interactions with F1666 but diminish the electrostatic contact with D1664. The side chain of Gln5 is hydrogen bonded to the guanidinium group of R1665 (Figure 11E).

This structural mechanism for the recognition of H3 distinguishes p300 ZZ domain from all currently known histone H3 readers. For example, BHC80 PHD finger, a H3 reader domain specifically recognizing K4-unmodified H3 tail (164), also forms a negatively charged cavity to bind the Ala1 of H3 (Figure 11F). However, this binding cavity is located on the opposite side of this domain as compared with p300 ZZ (Figure 11C). In addition, unlike ZZ, BHC80 PHD contains another site with negative charge to accommodate unmodified Lys4 (Figure 11F). Methylation on Lys4 disrupts its binding to this negatively charged site of BHC80 PHD (164), but does not affect its interaction with p300 ZZ domain because ZZ does not have this Lys4-accomadating site (Figure 11C). Therefore, the molecular basis of ZZ-H3 interaction indicates that the ZZ domain represents a novel family of histone readers.

Substitution of N1671, D1688 or D1690, the ZZ domain residues that are responsible for binding Ala1 and Arg2 of H3, with an alanine or lysine, abolished the ZZ-H3 interaction in peptide pull-down or calf thymus histone pull-down assays (Figure 12A, B). Further, mutation of D1664, F1666 or Y1668 also substantially reduced the binding, pointing to the essential role of the Lys4 coordination (Figure 12A, B).

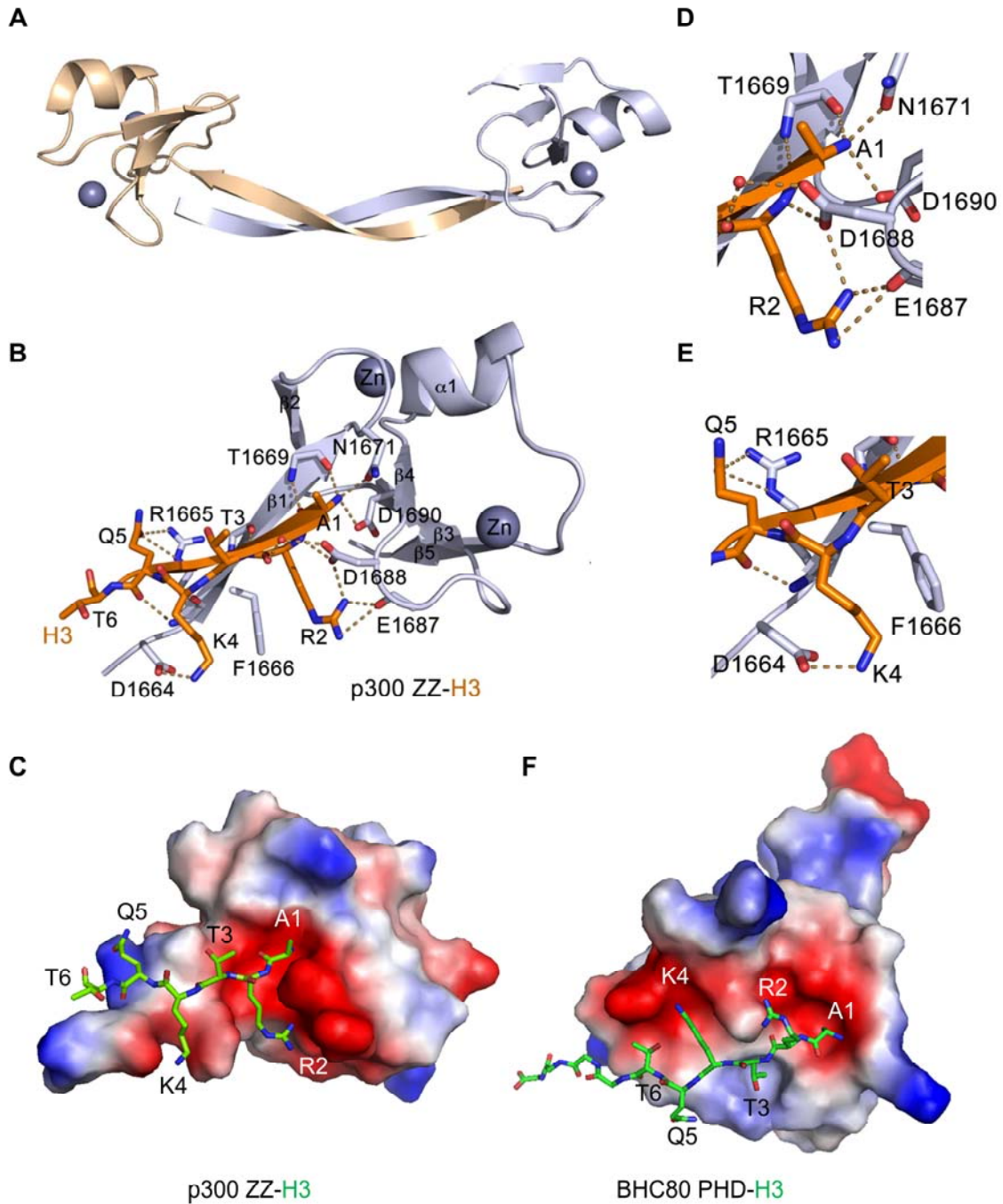


Figure 11. Structure of the p300 ZZ-H3 complex.

(A) The crystal structure of the linked H3-ZZ construct. (B) A ribbon diagram of the p300 ZZ domain (light blue) in complex with histone H3 tail (residues 1-6) (orange). (C) Electrostatic surface potential of p300 ZZ domain is colored blue

(positive charge) and red (negative charge) with the bound histone H3 tail shown in stick (green). (D) Zoom-in view of the histone H3 Ala1 binding site. (E) Zoom-in view of the histone H3 Lys4 binding site. (F) The electrostatic surface potential plot of the PHD finger of BHC80 recognizing the N-terminal sequence of histone H3 (PDB: 2PUY) (164).

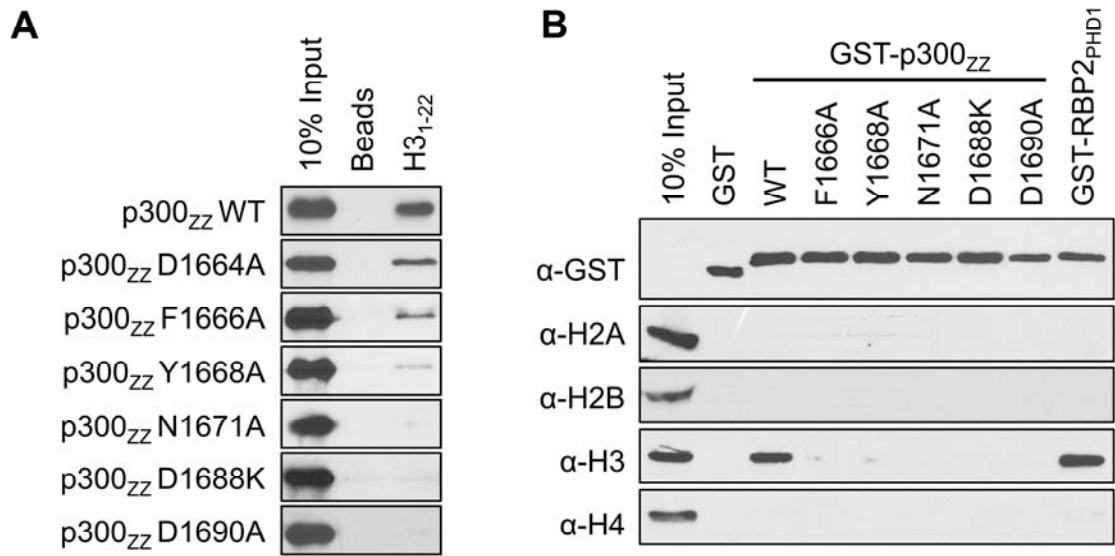


Figure 12. Key residues required for ZZ-H3 binding.

(A) Peptide pull-down assays using wild type and mutated p300 ZZ domain. (B) Calf thymus histone pull-down assays of the wild type p300 ZZ domain and the indicated mutants.

3.3 Recognition of H3 by the ZZ domain is required for p300-chromatin association

Our *in vitro* data reveal that p300 ZZ domain specifically recognizes the histone H3 tail. However, whether the ZZ-H3 interaction is important to the functions of p300 in cells is unknown.

First, we asked the question whether the H3 recognition by ZZ is required for p300-chromatin association. To address this question, we attempted to determine the chromatin occupancy of the full-length wild-type (WT) p300 or ZZ-mutants in cultured cells. We cloned the full-length coding DNA sequences (CDS) of *EP300* gene into either lentiviral vector (pCDH) or retroviral vector (pBABE), and delivered the expressing vectors into H1299 cell line through viral infection. Unfortunately, the stable cells thus established failed to express full-length p300, likely due to the failure of the viruses in packaging the extra-large CDS (7.2 kb) of p300.

To overcome this difficulty, we decided to use the p300 core fragment (p300_{BRPHZT}) that contains the BRD, RING, PHD, HAT, ZZ and TAZ2 domains (Figure 13A) in our experimental system. The p300_{BRPHZT} fragment cloned in the pCDH-3XFLAG vector can be successfully introduced and stably expressed in H1299 cells at a reasonable expression level. Therefore, using this p300_{BRPHZT} core fragment, we deleted the individual BRD, ZZ, AIL or BRD+ZZ to evaluate the importance of these domains to chromatin binding of the p300 core fragment in cells (Figure 13A).

We performed salt fractionation assay in the cells stably expressing WT p300_{BRPHZT} fragment or its counterparts with individual domain deleted (Figure 13B). The more tightly a protein binds to chromatin, the higher salt concentration is needed to wash it off from chromatin. WT p300_{BRPHZT} bound strongly to chromatin in cells, as wash buffer containing 0.6 M salt was needed to completely wash it off from chromatin. In contrast, ZZ- or BRD-deleted fragments bound more weakly to chromatin, as 0.3 M salt can wash them off from chromatin. The BRD of p300 is known to bind acetylated histones, preferentially acetylated H4 (27). It has been reported that BRD is required for p300 to form stable interaction with chromatin (165). The reduced chromatin binding as a result of BRD deletion in our salt fractionation assays is consistent with the published data. Importantly, simultaneous deletion of both BRD and ZZ domain caused a more profound decrease in chromatin binding than single deletions, implying an additive effect. As expected, deletion of AIL did not affect chromatin binding (Figure 13B).

Next, we performed chromatin immunoprecipitation (ChIP) using FLAG M2 antibody followed by western blotting (ChIP-WB) of histone H3 to evaluate chromatin association of the p300_{BRPHZT} core fragment and the domain-deletion mutants (Figure 13C). All FLAG-tagged p300 fragments were expressed at a similar level, while the amount of histone H3 pulled down by the ZZ- or BRD-deletion mutants was much less than that of the WT p300_{BRPHZT}, indicating that loss of either domain reduces chromatin binding. Deletion of both domains led to a further reduction whereas AIL deletion had little effect. All together, these

results suggest that both ZZ and BRD are required for p300-chromatin association.

To further determine the importance of the H3-binding activity of the ZZ domain in p300-chromatin association, we introduced histone-binding deficient point mutations (N1671A and D1690A, named as ZZmu1 and ZZmu2) into the p300_{BRPHZT} fragment (Figure 14A). A BRD point mutant, N1132A (named as BRDmu), that fails to bind histone acetylation (27) was also tested. In addition, we also constructed p300 fragment carrying D1690A and N1132A double mutations (named as ZZmu+BRDmu).

Both salt fractionation and ChIP-Western assays revealed that mutation of either domain reduced p300_{BRPHZT} binding to chromatin and mutations of both showed a more severe defect (Figure 14B, C), suggesting that the H3-binding activity of the ZZ domain and the histone acetylation binding activity of BRD are both required for chromatin association of p300 in cells.

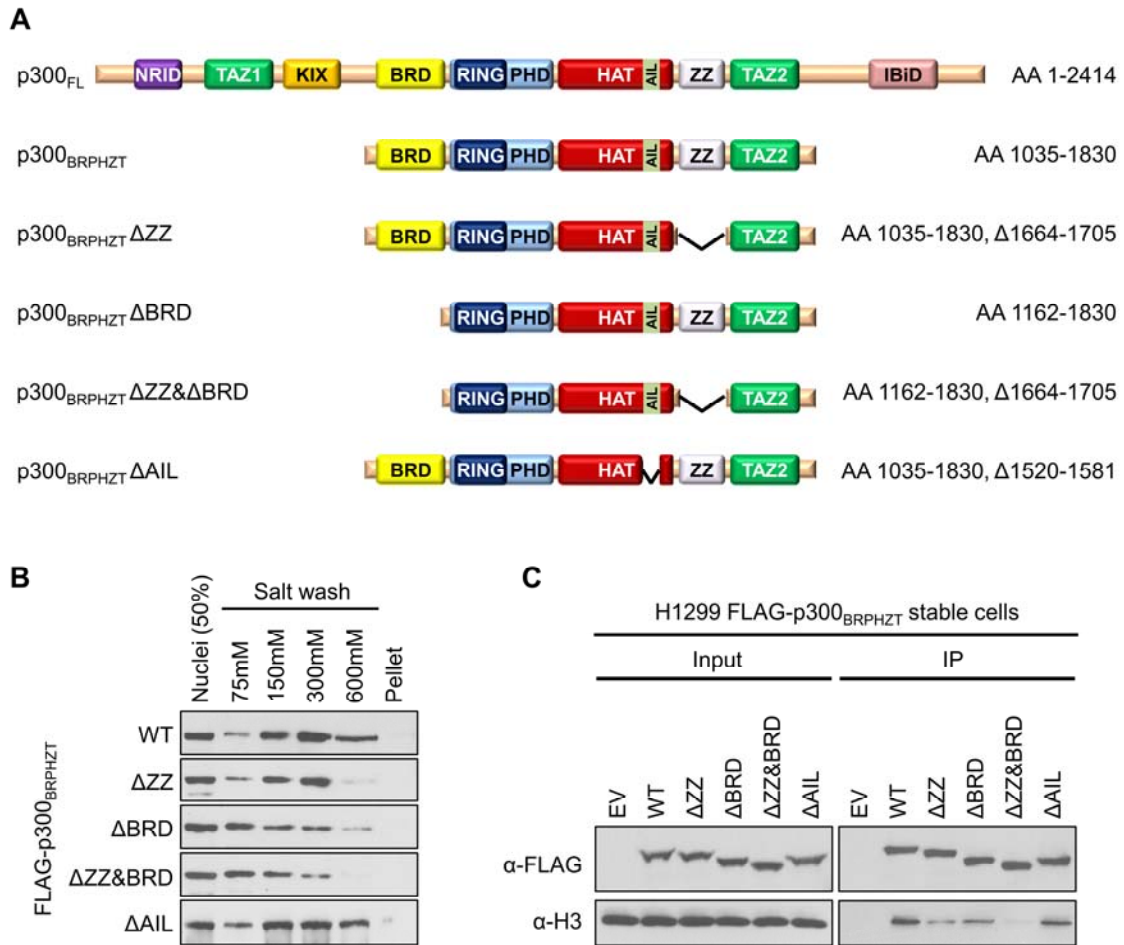


Figure 13. Both ZZ domain and BRD are required by p300 for chromatin association.

(A) Schematic representation of full-length p300 protein and the p300 fragments stably expressed in H1299 cells. (B) Salt fractionation of H1299 cells stably expressing wild type or deletion-mutated FLAG-p300_{BRPHZT}. The workflow for salt fractionation assay is shown in Figure 7. (C) ChIP-WB analysis of wild type or deletion-mutated FLAG-p300_{BRPHZT} in H1299 stable cells.

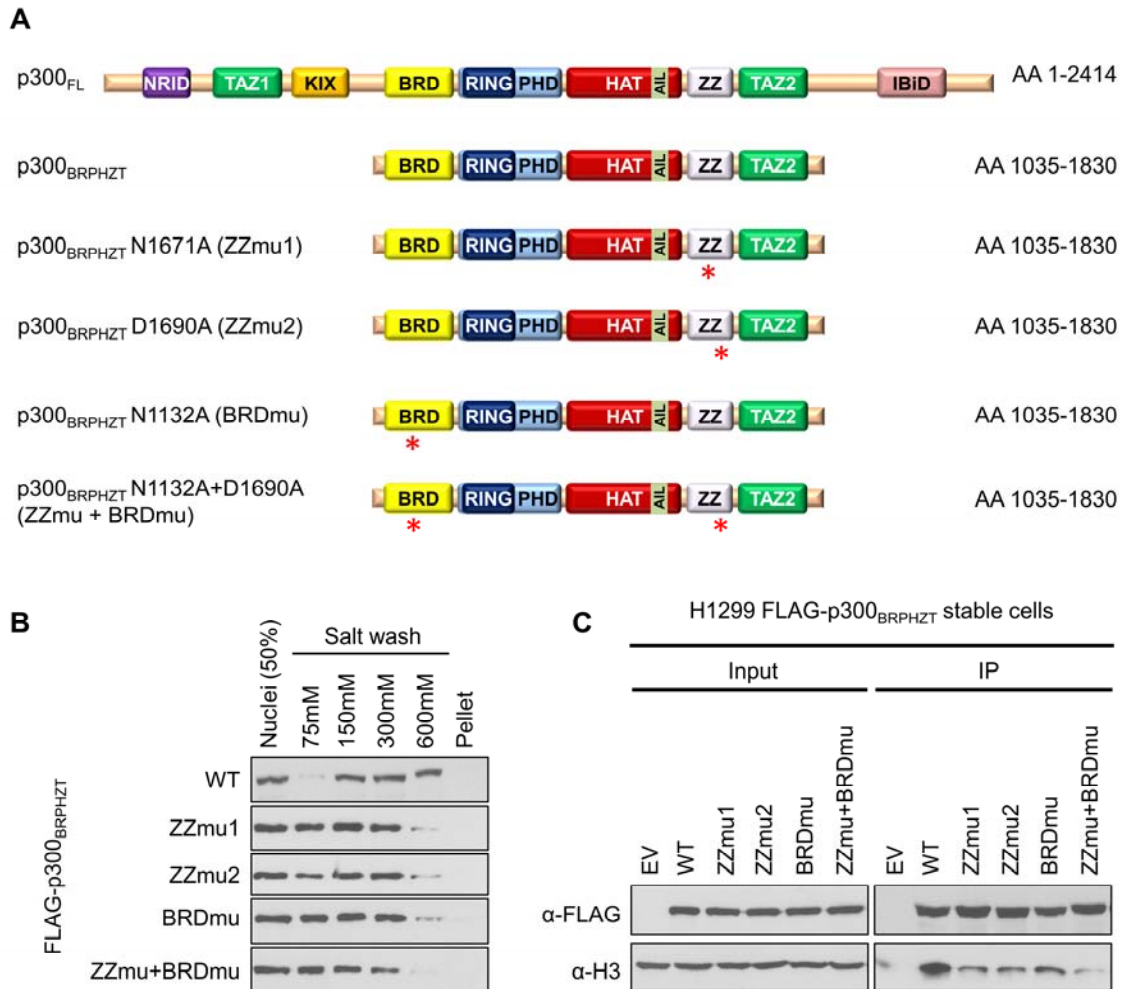


Figure 14. Both the H3-recognition ability of ZZ domain and the acetylysine binding activity of BRD are required by p300 for chromatin association.

(A) Schematic representation of full-length p300 protein and the p300 fragments stably expressed in H1299 cells. (B) Salt fractionation of H1299 cells stably expressing wild type or mutated FLAG-p300_{BRPHZT}. The workflow for salt fractionation assay is shown in Figure 7. (C) ChIP-WB analysis of wild type or mutated FLAG-p300_{BRPHZT} in H1299 stable cells.

3.4 Recognition of H3 by the ZZ domain facilitates the acetylation of H3K18 and H3K27 by the HAT domain

Both BRD and the ZZ domain of p300 are adjacent to the catalytic HAT domain. As we discussed in Chapter 1.2, recognition of acetylated histone H4 by BRD increases the accessibility of nucleosome substrates to CBP/p300 HAT domain, thus contributing to histone acetylation (39). So we speculated that ZZ may regulate the enzymatic activity of HAT through a similar mechanism.

To test this hypothesis, we purified recombinant GST-tagged p300_{BRPHZ} fragment (encompassing BRD, RING, PHD, HAT and ZZ domains) and the same fragment bearing various deletions/mutations (Figure 15A) and compared their enzymatic activity on nucleosomes by *in vitro* HAT assays. These deletions/mutations include ZZ domain deletion, AIL deletion, HAT catalytic dead mutation D1399A (HATmu) (166), ZZ domain mutations N1671A or D1690A (named as ZZmu1 or ZZmu2, respectively), BRD mutation N1132A (BRDmu), D1690A and N1132A double mutations (ZZmu+BRDmu). All the mutations or deletions did not affect the protein stability during purification.

Next we used these fragments as enzymes and recombinant mononucleosomes (without pre-existing modifications) as substrate for *in vitro* HAT assays. Equal molar amount of each fragment was used in the assays for easy comparison (Figure 15B). Samples were collected at different time points: 0, 10, 20, 40, 60 and 80 min after reaction, and immunoblotted using specific antibodies against H3K4ac, H3K9ac, H3K18ac, and H3K27ac. Total H3 was also blotted as a loading control. The fluorescence intensity of each band was

measured using Odyssey system. To compare signals from different gels, we used pre-modified nucleosomes as a standard to run on each SDS-PAGE gel. All values of fluorescence intensity across different gels were compared to the common standard sample. All quantifications were based on three biological replicates.

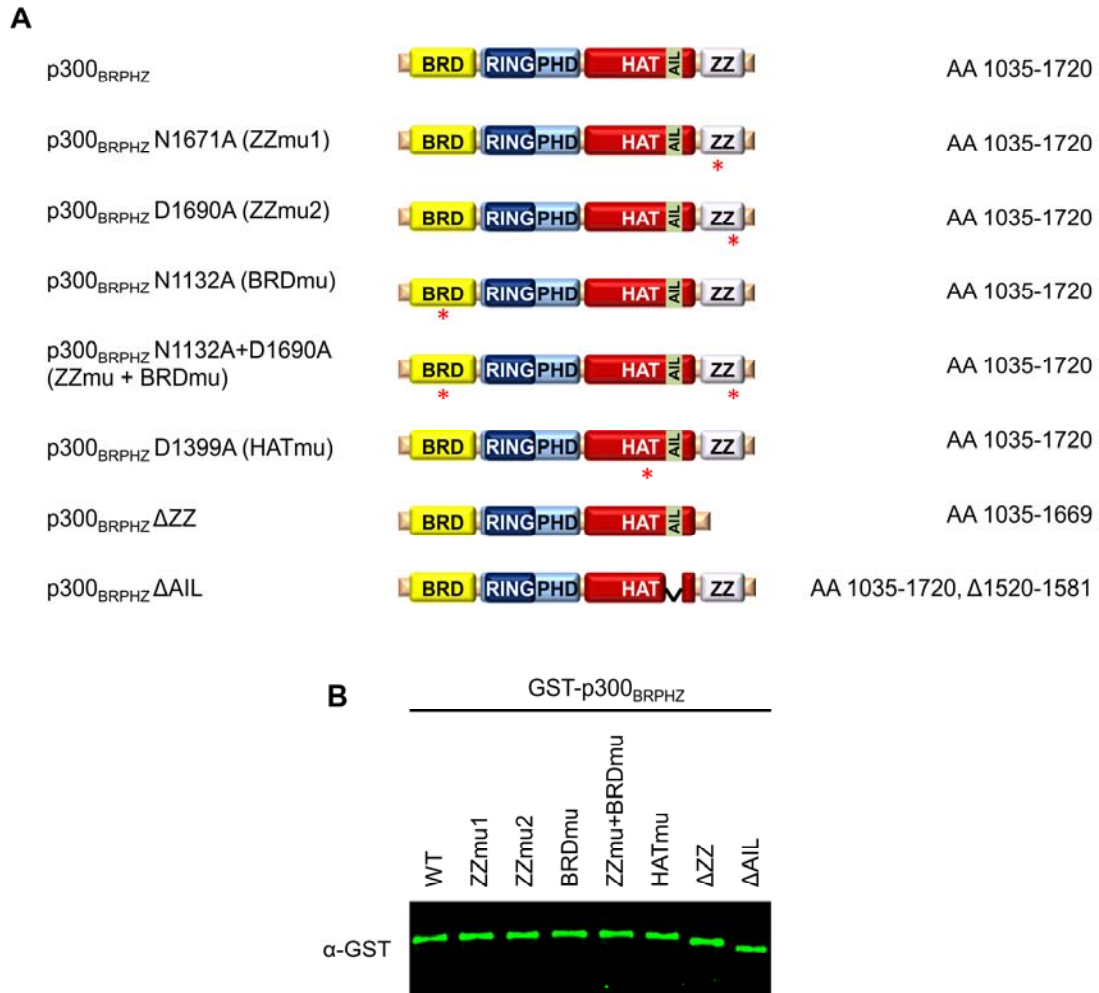


Figure 15. The p300 fragments used in *in vitro* HAT assays.

(A) Schematic representation of p300 fragments used in *in vitro* HAT assays. (B) Western blot analysis showing equal amount of p300 fragments used in the HAT assays.

As shown in Figure 16, histone acetylation signals gradually increased during the time course, indicating the accumulation of products of the HAT reaction. All four lysine residues tested, H3K27, H3K18, H3K9 and H3K4, can be acetylated by the WT p300_{BRPHZ} enzyme *in vitro*. Interestingly, deletion of ZZ domain greatly reduced acetylation on H3K27 and H3K18 (Figure 16A, B) but not on H3K9 and H3K4 (Figure 16C, D), suggesting that the ZZ domain is required for efficient acetylation specifically on H3K27 and K18.

It has been previously reported that deletion of AIL can release the active site creating a constitutively active HAT (28). Consistent with this, we found deletion of AIL dramatically accelerated the acetylation at all lysine residues at early time points such as 10, 20 and 40 min (Figure 16A-D). At 80 min, the histone acetylation levels were comparable between reactions with WT and AIL-deleted enzymes, implying that all substrates were fully acetylated at the last time point. This is in agreement with a previously proposed model that the hypoacetylated AIL contacts a negatively charged patch on the HAT domain surface blocking the active site, whereas acetylation of AIL by HAT releases the inhibitory loop, thus freeing the active site (28, 31). As a negative control, HAT domain mutation D1399A abolished the acetylation of all sites tested.

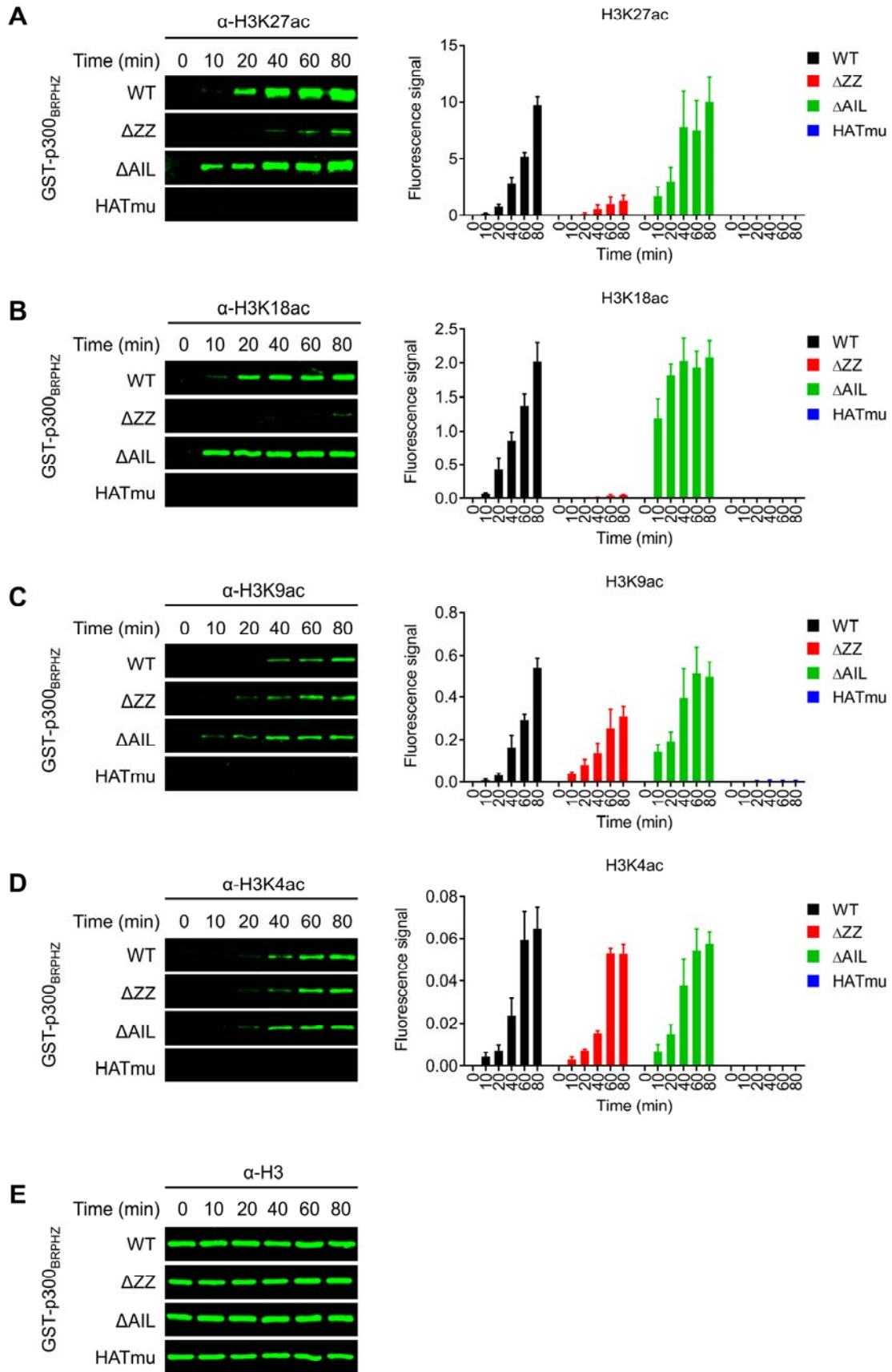


Figure 16. Deletion of ZZ domain specifically attenuated the acetylation of H3K27 and H3K18.

H3K27ac (A), H3K18ac (B), H3K9ac (C), H3K4ac (D) and H3 (E) western blot analysis of *in vitro* HAT assays using WT p300_{BRPHZ} or its counterpart harboring either ZZ deletion, AIL deletion or loss-of-catalytic activity HAT mutation (D1399A), and the reconstituted mononucleosome. Quantification of the HAT activity on each lysine was based on the fluorescence signal from three biological replicates. A common standard sample is used for normalization in each replicate.

To further determine whether the regulatory role of ZZ on the HAT activity of p300 is dependent on its H3-binding capability, we carried out the same *in vitro* HAT assays to compare WT and ZZ-mutated p300_{BRPHZ} fragment (ZZmu1 or ZZmu2) (Figure 17). BRDmu and ZZmu+BRDmu were also included as controls. Similar to deletion of ZZ, ZZ point mutations exhibited a much lower HAT activity on H3K27 and H3K18 (Figure 17A, B), whereas acetylation of H3K9 and H3K4 were not reduced compared to the WT p300 fragment (Figure 17C, D). Different from ZZ mutations that specific attenuated H3K18 and H3K27 acetylation, BRD mutation led to a substantial decrease in acetylation of all lysine residues tested (Figure 17A-D). Furthermore, double mutations of both ZZ and BRD totally abolished the acetylation of all tested residues (Figure 17A-D). Together, these results suggest that the acetyllysine binding function of BRD is necessary for the overall catalytic activity of p300_{BRPHZ} on histones, whereas recognition of H3 by ZZ domain is specifically required for p300_{BRPHZ} to acetylate H3K18 and H3K27. Mutations simultaneously disrupting the functions of both domains may completely disable p300's access to nucleosomes, abolishing acetylation of all histone substrates.

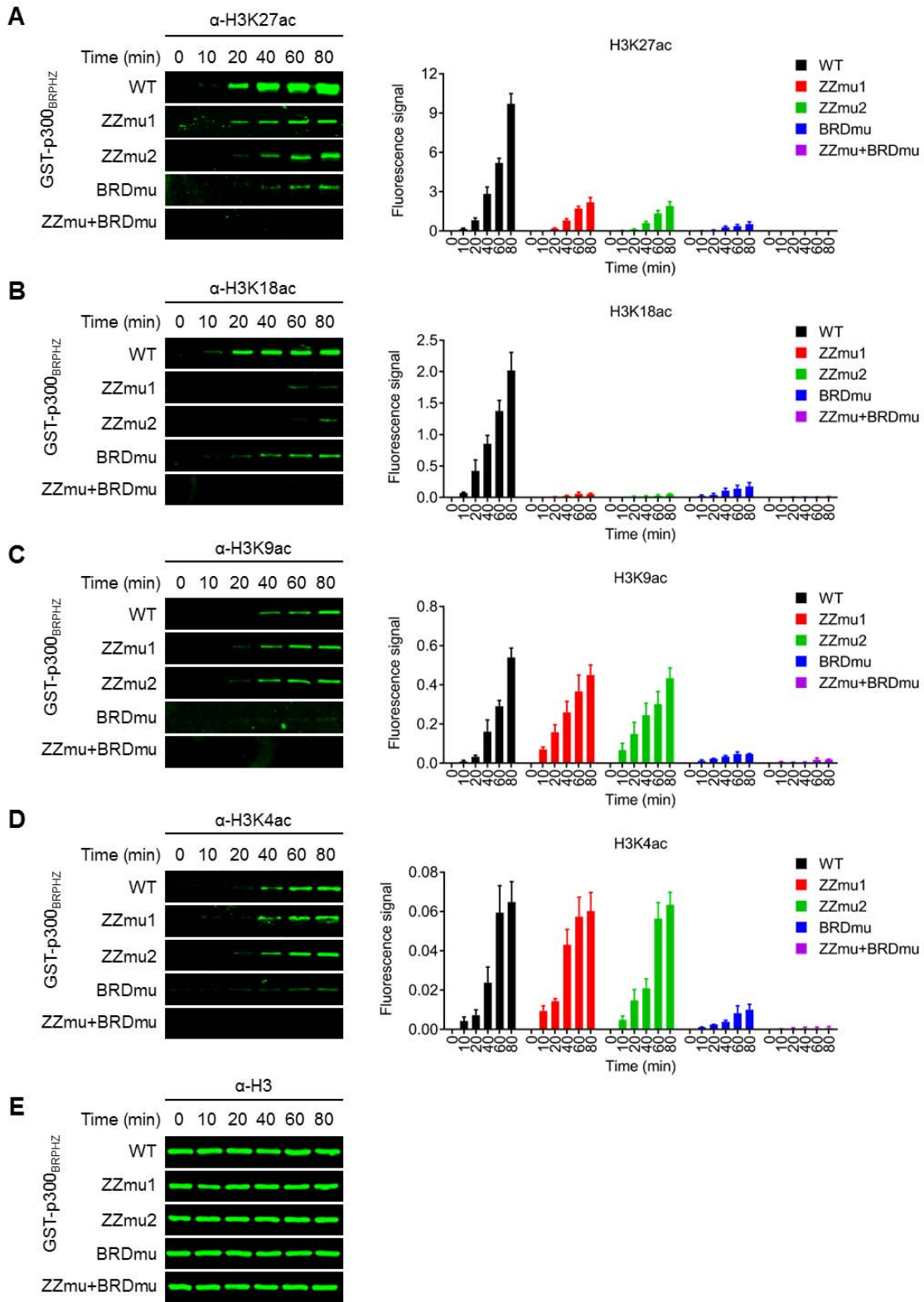


Figure 17. H3 binding by ZZ domain facilitates p300 HAT activity on H3K18 and H3K27.

H3K27ac (A), H3K18ac (B), H3K9ac (C), H3K4ac (D) and H3 (E) western blot analysis of *in vitro* HAT assays using WT or mutated p300_{BRPHZ} and the reconstituted mononucleosome. Quantification of the HAT activity on each lysine was based on the fluorescence signal from three biological replicates. A common standard sample is used for normalization in each replicate.

Because the first two residues of H3 (Ala1-Arg2) are critical to the ZZ-H3 interaction, we speculated that the very N-terminal residues of H3 are also required for the acetylation of H3K18 and H3K27 by p300 HAT. To test this hypothesis, we carried out *in vitro* HAT assays of the WT p300_{BRPHZ} fragment using recombinant mononucleosomes containing full-length H3 (rNUC_H3_FL) or H3 with the first two amino acid residues deleted (rNUC_H3_ΔN). We found that the removal of Ala1-Arg2 of histone H3 dramatically decreased acetylation of H3K27 and H3K18 by p300 HAT (Figure 18A-B), likely due to the reduced ZZ-H3 interaction. However, since each nucleosome contains two H3 subunits, this experiment cannot distinguish whether the recognition of H3 by p300 ZZ facilitates the acetylation of K27 and K18 on the same H3 subunit (*in cis*) or on the other H3 subunit in the same or adjacent nucleosomes (*in trans*). To clarify this mechanism, we performed *in vitro* HAT assays using histone peptides as substrates. We incubated the WT p300_{BRPHZ} with the H3₁₋₃₃ peptide or the same H3 peptide with the first two amino acids deleted (H3₃₋₃₃). Similar to the results of the HAT assays on mononucleosomes, p300_{BRPHZ} catalyzed H3K18ac and H3K27ac more efficiently on H3₁₋₃₃ than on H3₃₋₃₃ (Figure 18C), supporting the *in cis* model (but not excluding the *in trans* model).

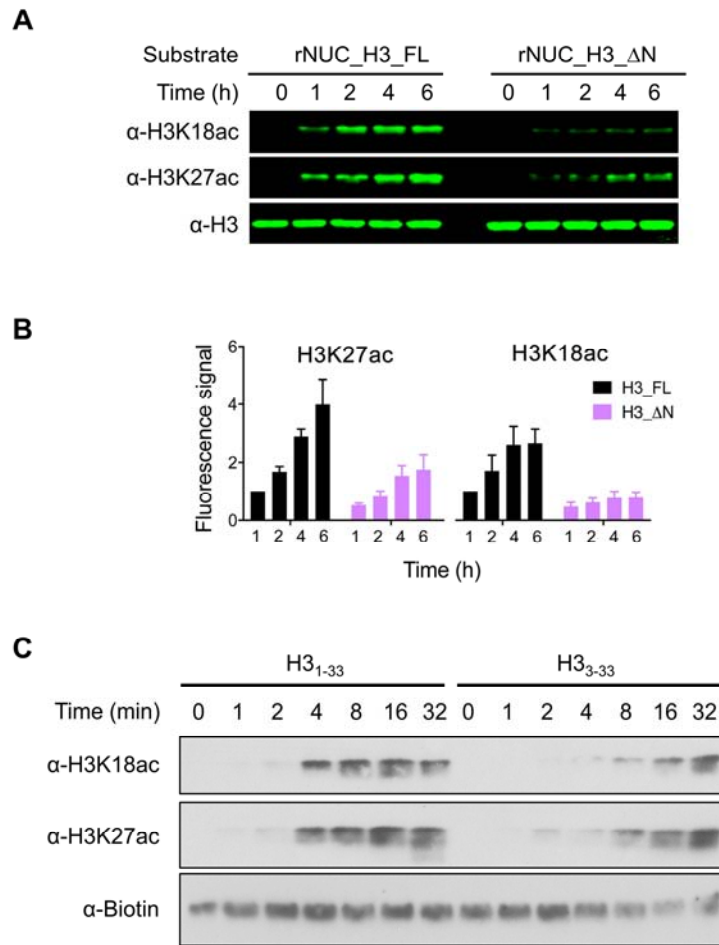


Figure 18. The first two residues of H3 are required for the acetylation of H3K18 and H3K27.

(A) *In vitro* HAT assays using WT p300_{BRPHZ} and the reconstituted mononucleosome carrying either intact H3.1 (rNUC_H3_FL) or N-terminally truncated H3.1 (rNUC_H3_ΔN, Ala1 and Arg2 of both H3.1 are deleted). (B) Quantification of the HAT activity on H3K18 and H3K27 based on the fluorescence signal in (A) from three biological replicates. The 1 hr sample of rNUC_H3_FL is used for normalization. (C) *In vitro* HAT assays using WT p300_{BRPHZ} and biotinylated H3 peptides.

The *in vitro* HAT assays demonstrate that recognition of H3 by the ZZ domain is required for the HAT domain of p300 to acetylate histone on H3K18 and H3K27. Next we asked whether this recognition has the same regulatory role in cells. To address this question, we utilized the H1299 stable cells systems established in Chapter 3.3 and evaluated global histone acetylation levels of these H1299 cells by Western blot analysis. First, we compared various H3 and H4 acetylation levels in the cells stably expressing WT FLAG-p300_{BRPHZT}, ZZ, BRD, or AIL deletion mutants as well as ZZ and BRD double deletion mutants (Figure 19A). The Western blotting band intensities were quantified using Odyssey and normalized by total H3 or H4 values. Heatmaps were generated using the mean values of fold changes relative to the vector controls from three biological replicates (Figure 19B). Compared with the control cells infected with an empty vector, WT p300_{BRPHZT}-expressing cells showed higher levels of global H3K4ac, H3K18ac, H3K27ac and H4 tetra-acetylation (5~8-fold) and a moderately higher H3K9ac level (~2-fold) (Figure 19A, B). Compared with the WT p300_{BRPHZT}-expressing cells, BRD deletion markedly reduced the acetylation levels on all sites tested. In contrast, deletion of the ZZ domain specifically decreased H3K18ac and H3K27ac levels, whereas the levels of H3K4ac, H3K9ac or H4ac remained largely unchanged. Deletion of both ZZ and BRD further reduced acetylation on H3K18 and H3K27 to an undetectable level (Figure 19A, B). These results suggest that both BRD and the ZZ domain are required for maintaining H3K18 and H3K27 acetylation in cells. Unlike the *in vitro* HAT assays results, deletion of AIL did not dramatically change the acetylation

levels of any site in cells (Figure 19A, B). One possible explanation is that the ALL region of the ectopic p300_{BRPHZT} fragment is hyperacetylated and stretching out from the HAT active site, thus having a minimal inhibitory effect.

The results above demonstrate that while BRD is required for acetylating all lysine residues, the ZZ domain is specifically required by p300 in acetylating H3K18 and H3K27 in cells. Next, we sought to determine whether the importance of ZZ and BRD in histone acetylation is dependent on their histone-binding capabilities. In this regard, we compared the global histone acetylation levels of H1299 cells stably expressing WT FLAG-p300_{BRPHZT} and those expressing FLAG-p300_{BRPHZT} bearing point mutations in ZZ, BRD or both domains. Similar to their respective deletion mutants, the BRD mutant failed to acetylate almost all histone H3 and H4 lysine residues tested, and the two ZZ point mutations were specifically defective in acetylating H3K18 and H3K27 (Figure 19C, D). Mutations in both domains led to a more severe drop in H3K18ac and H3K27ac levels compared to the ZZ or BRD single domain mutations (Figure 19C, D).

Furthermore, in a transient expression system expressing full-length p300 in 293T cells, introducing the loss-of-function mutations into the ZZ domain also attenuated the full-length p300 in acetylating H3K18 and H3K27 (Figure 20A, B). Together, these findings reveal that recognition of H3 by the ZZ domain plays a critical role in facilitating p300-mediated H3K18 and H3K27 acetylation in cells whereas the binding of acetylated histone by BRD is required for the acetylation of all lysine residues on H3 and H4.

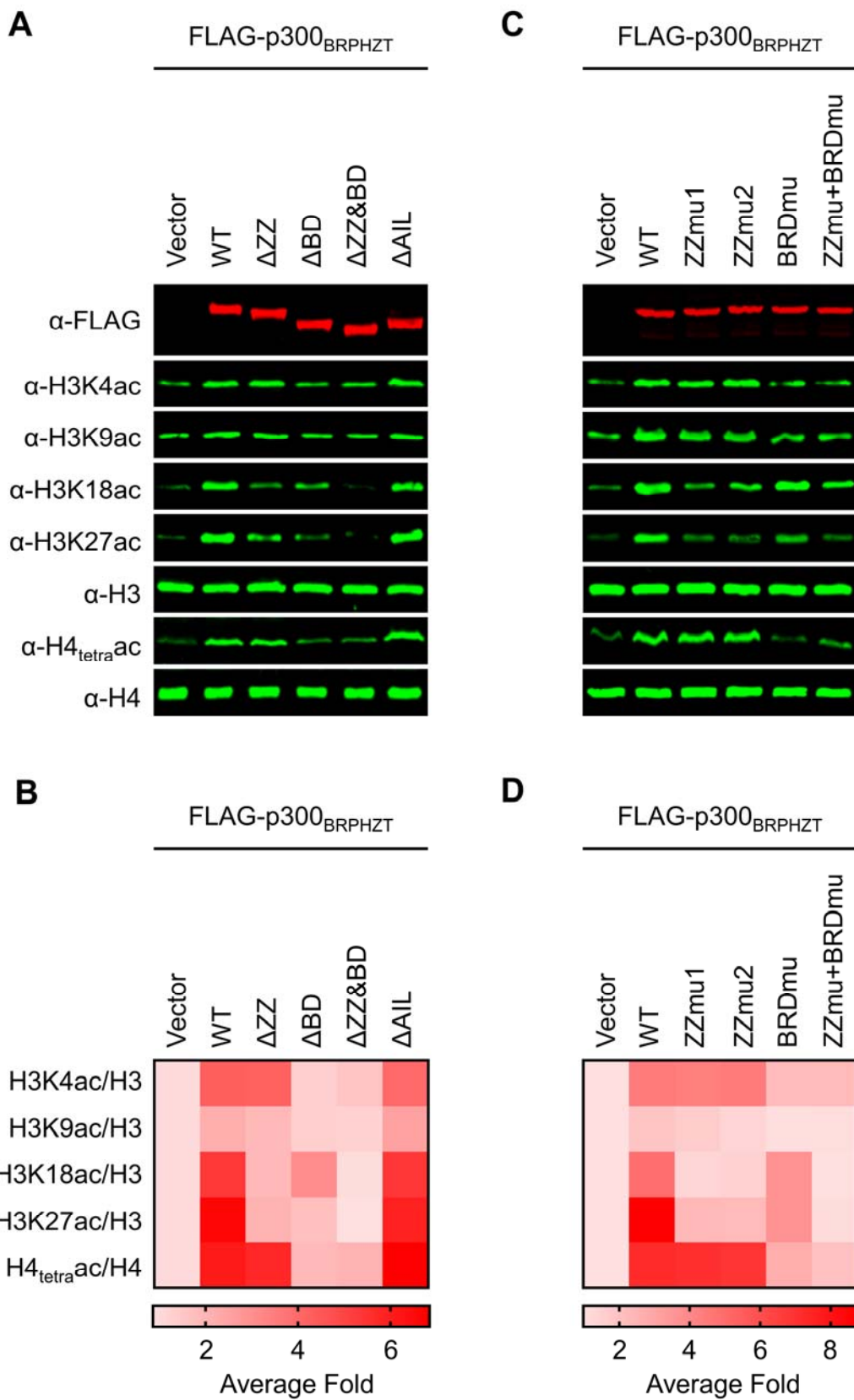


Figure 19. H3 recognition by ZZ domain is critical to p300-mediated H3K18 and H3K27 acetylation in cells.

(A) Western blot analysis of histone acetylation levels in whole cell extract of H1299 cells stably expressing wild type or deletion-mutated FLAG-p300_{BRPHZT}.

(B) Heatmap of quantification of the indicated histone acetylation levels from three biological replicates as in (A). Total H3 or H4 was used for normalization.

(C) Western blot analysis of histone acetylation levels in whole cell extract of H1299 cells stably expressing wild type FLAG-p300_{BRPHZT} or the indicated mutants.

(D) Heatmap of quantification of the indicated histone acetylation levels from three biological replicates as in (C). Total H3 or H4 was used for normalization.

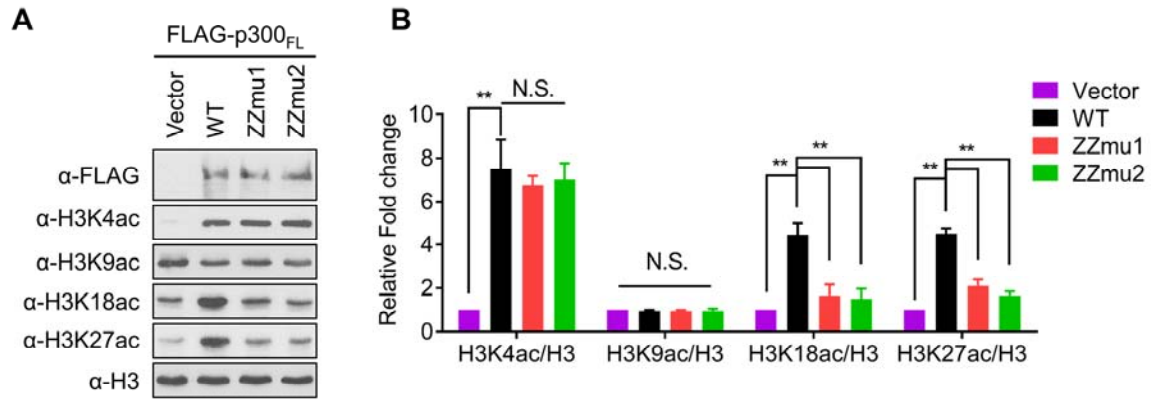


Figure 20. H3 recognition by ZZ domain is required by full-length p300 to acetylate H3K18 and H3K27 in cells.

(A) Western blot analysis of histone acetylation levels in whole cell extract of 293T cells transiently expressing full-length p300 or the ZZ mutants. (B) Quantification of the indicated histone acetylation levels from three biological replicates as in (A). Total H3 was used for normalization.

3.5 Recognition of H3 by the ZZ domain is required for genome-wide p300 occupancy and p300-dependent deposition of H3K18ac and H3K27ac

To gain a deeper insight into the role of p300 ZZ domain in regulating p300 occupancy and p300-dependent deposition of H3K18ac and H3K27ac genome-wide, we performed ChIP-seq analysis in H1299 cells stably expressing FLAG-p300_{BRPHZT} or its counterpart harboring ZZ loss-of-function mutations, N1671A or D1690A (Figure 21A-C). Western blotting analysis showed that the WT and mutant FLAG-p300_{BRPHZT} fragments are expressed at similar levels (Figure 21B). We used the anti-Flag M2 antibody to ChIP for FLAG-p300_{BRPHZT} fragments and anti-H3K18ac and anti-H3K27ac antibodies to ChIP for respective histone acetylation. The ChIPed DNA was sequenced using the Illumina Solexa HiSeq 3000 at MD Anderson Cancer Center Science Park Next-Generation Sequencing (NGS) Facility. We collaborated with Jiejun Shi from Dr. Wei Li's lab in Baylor College of Medicine (BCM) to analyze the ChIP-seq data. Our lab's previous data of anti-H3K4me1, anti-H3K27me3 and anti-H3K27ac ChIP-seq in parental H1299 cells were also used in our analysis.

Anti-FLAG ChIP in the cells expressing WT FLAG-p300_{BRPHZT} identified 679 p300_{BRPHZT} binding sites. Compared with the previously published full-length p300 binding sites (25, 167), p300_{BRPHZT} binding sites are much broader and the peaks are less sharp. To ensure to include the majority of p300_{BRPHZT} binding sites, we analyzed ChIP-seq signals spanning a \pm 20 kb window centered on binding peaks (Figure 21D). Based on pre-existing PTMs on H3K27 in H1299 cells, we divided the p300_{BRPHZT} binding sites into two groups: H3K27 pre-

acetylated regions (Group 1) and H3K27 pre-methylated regions (Group 2) (Figure 21D). Group 1 sites are enriched with H3K27ac and H3K4me1, indicating they are probably active enhancers and are likely targets of endogenous p300/CBP. Because the peaks are already hyperacetylated, ectopic expression of the p300_{BRPHZT} fragment is not able to further increase acetylation levels at the peaks. In contrast, a significant increase in H3K18ac and H3K27ac levels at the hypoacetylated peak flanking regions was observed when ectopically expressing WT p300_{BRPHZT} (compared with the control cells expressing an empty vector) (Figure 21D, Figure 22). Group 2 binding sites are preoccupied by H3K27me3 but not by H3K27ac or H3K18ac. This is not surprising as it has been shown previously that p300/CBP also bind to a large number of poised regulatory regions that are low in H3K27ac and high in H3K27me3 (167-169). Because H3K27 at these regions is largely methylated across the entire +/- 20 kb windows thus less accessible to p300 HAT, no significant increase in H3K18ac or H3K27ac level was observed, despite the strong binding of p300_{BRPHZT} in these regions (Figure 21D).

In contrast to the WT p300_{BRPHZT} protein, the two ZZ domain mutants, N1671A and D1690A, were much less capable of gaining the chromatin binding at both groups of sites, and consequently, the increase in H3K18ac and H3K27ac occupancies at those sites was attenuated in the cells expressing these mutants (Figure 21D, Figure 22).

We show in Figure 23 genome-browser views of four representative p300-bound genes: *NBPF1*, *NOTCH2NL*, *PDE4DIP* and *DMPK*. While endogenous

histone acetylation is strongly enriched at gene promoters, FLAG-p300_{BRPHZT} binds to much broader regions not only at promoters, but also in gene bodies and intergenic regions. Binding of p300_{BRPHZT} enhanced local histone acetylation levels on both H3K18 and H3K27. However, loss-of-function mutations in ZZ domain abolished p300_{BRPHZT} bindings at those regions and consequently, impaired acetylation on H3K18 and H3K27. These ChIP-seq results were validated by ChIP-qPCR (Figure 24). Notably, the mutations of the ZZ domain that abolish its H3-binding ability considerably decreased binding of p300_{BRPHZT} to individual genes (Figure 24A) and led to a notable reduction in the H3K18 (Figure 24B) and H3K27 (Figure 24C) acetylation levels on these genes. In contrast, the H3K18 and H3K27 acetylation levels on *ASCL1* and *INSM1*, the negative control sites without p300_{BRPHZT} binding, were not significantly changed by ZZ mutations.

Similarly, the N1132A mutation that abrogates acetyllysine binding activity of BRD resulted in a drastic decrease in p300_{BRPHZT} occupancy and H3K18ac and H3K27ac deposition at *NBPF1*, *NOTCH2NL* and *DMPK* target regions but not the negative control regions (Figure 25). However, the p300_{BRPHZT} occupancy and H3K18ac and H3K27ac levels of *PDE4DIP* upstream regions were not significantly affected by BRD mutation, indicating the chromatin association and histone acetylation of p300_{BRPHZT} are specifically dependent on ZZ-H3 recognition but not on BRD's function at this site.

Together, these data suggest that both ZZ-H3 and BRD-acetyllysine interactions are required for binding of p300 to chromatin and efficient histone

H3K18/K27 acetylation in cells, corroborating the findings in salt fractionation (Figure 14B), ChIP-WB (Figure 14C), *in vitro* HAT assay (Figure 17) and *in vivo* histone acetylation analysis (Figures 19-20) described above.

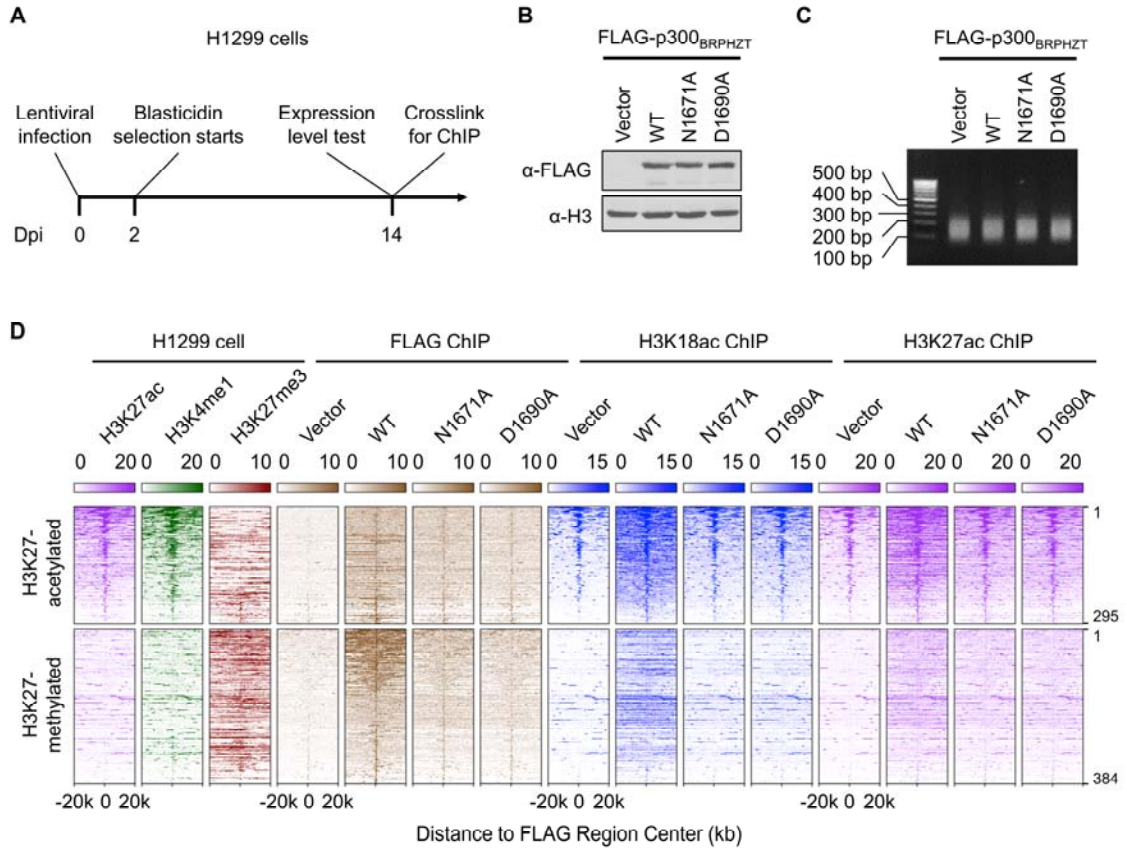


Figure 21. The ZZ domain is necessary to p300's chromatin binding and acetylation activity on H3K18 and H3K27 in cells.

(A) The workflow of samples preparation for ChIP-seq assay. (B) Western blot analysis of the expression levels of wild type or mutated FLAG-p300_{BRPHZT} level. (C) Electrophoresis of sonicated DNAs for ChIP-seq. (D) Heatmap of normalized H3K27ac (purple), H3K4me1 (green), H3K27me3 (scarlet), FLAG (brown) and H3K18ac (blue) ChIP-seq signals centered on FLAG binding sites in a ± 20 kb window in H1299 control cells and H1299 cells stably expressing wild type FLAG-p300_{BRPHZT} or the indicated ZZ mutants. The color keys represent signal density.

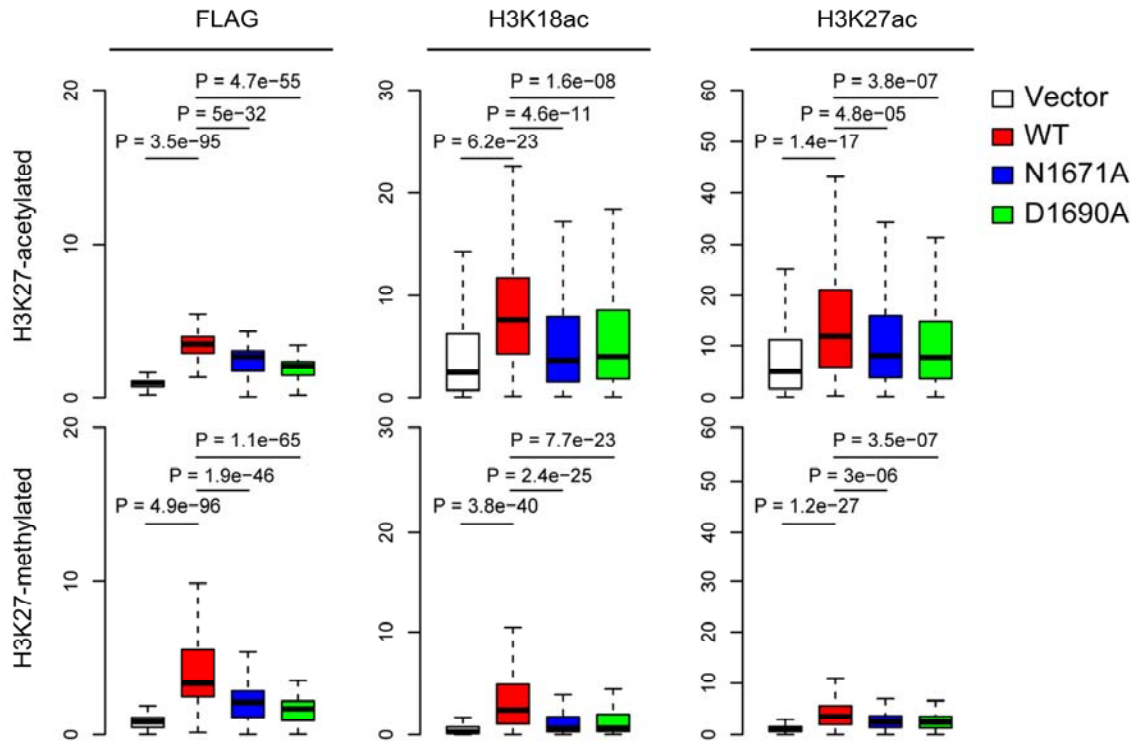


Figure 22. Box plots comparing FLAG, H3K18ac and H3K27ac occupancies in different samples at FLAG-p300_{BRPHZT} binding peaks.

All FLAG-p300_{BRPHZT} peaks are divided into two groups as in Figure 21D. The centerline of box represents the median and box limits indicate the 25th and 75th percentiles. Two-tailed paired Student's t-test was used for statistical analyses.

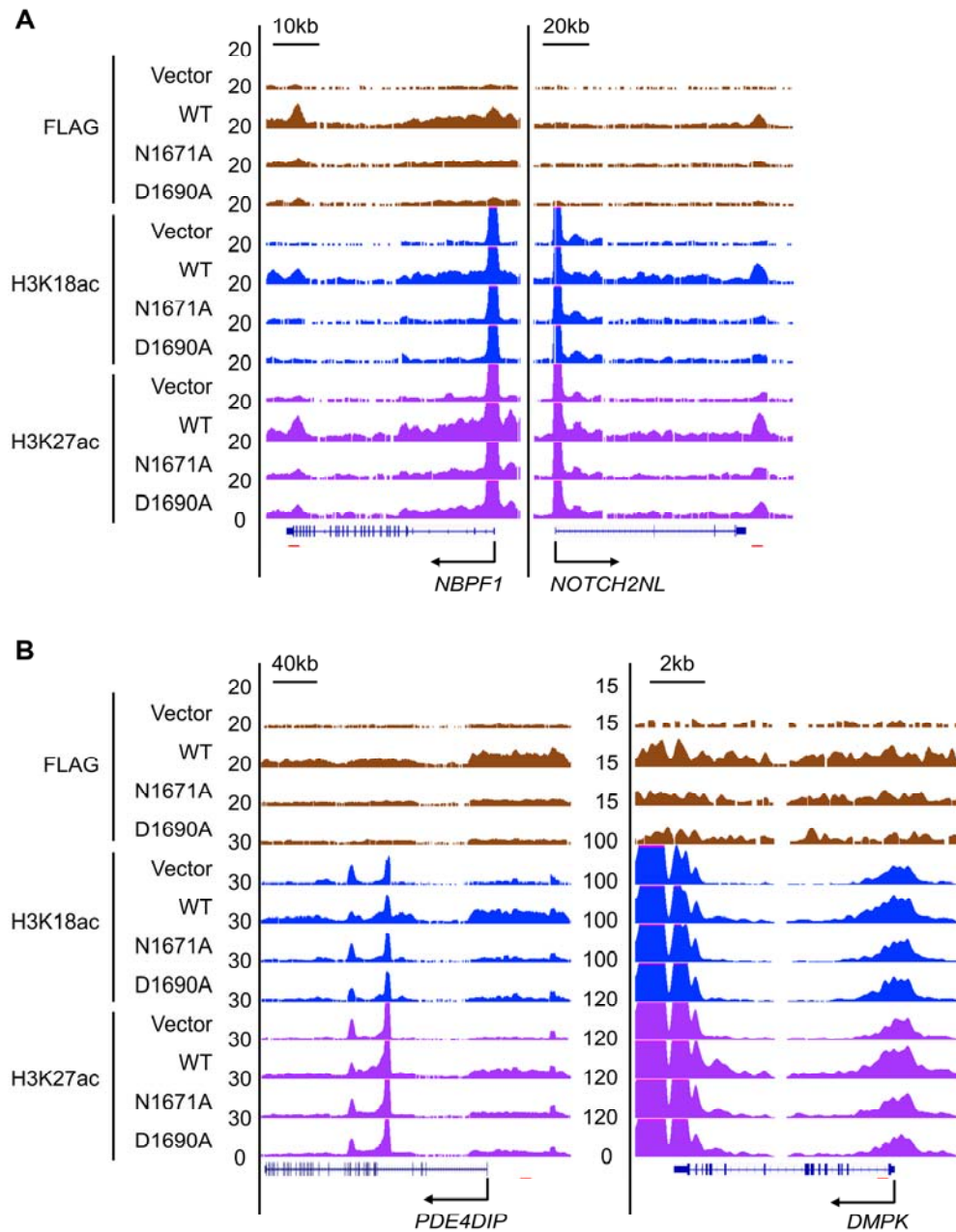


Figure 23. Representative genome-browser views of ChIP-seq data.

Representative genome-browser views of the FLAG (brown), H3K18ac (blue) and H3K27ac (purple) ChIP-seq signals on the indicated genes. The red lines indicate the sites for ChIP-qPCR validation.

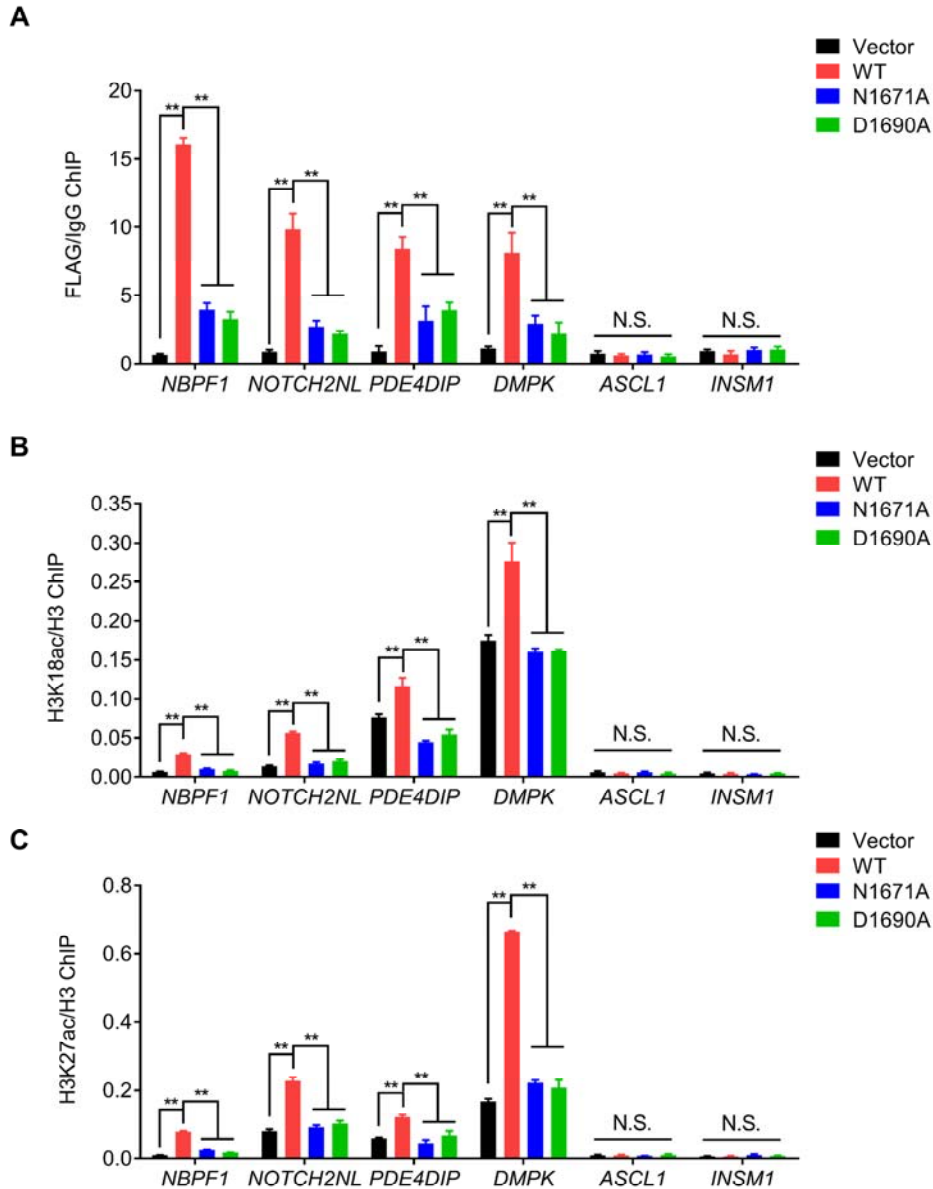


Figure 24. ChIP-qPCR in H1299 cells stably expressing wild type FLAG-p300_{BRPHZT} or the ZZ mutants.

qPCR analysis of the FLAG-p300_{BRPHZT}, H3K18ac and H3K27ac ChIP at target loci (locations indicated by red line in Figure 23) and two negative control loci in H1299 cells stably expressing wild type FLAG-p300_{BRPHZT} or the ZZ mutants. IgG or H3 ChIP was used for normalization.

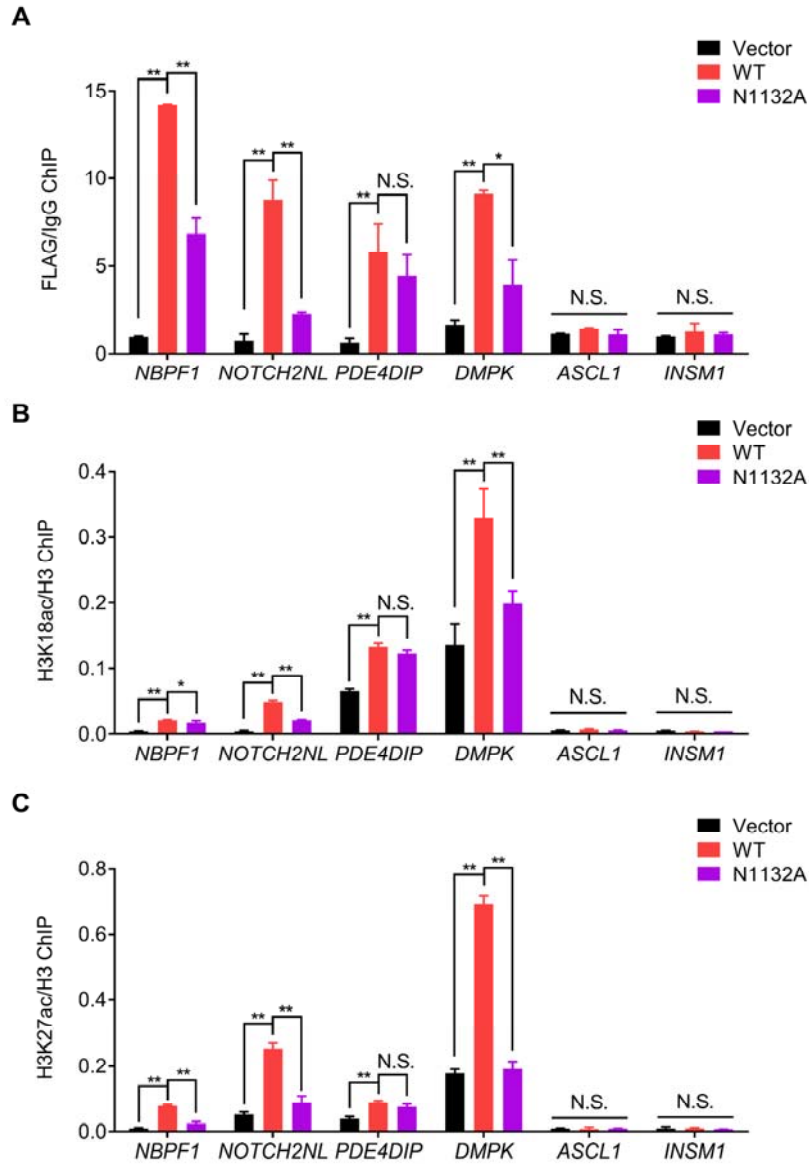


Figure 25. ChIP-qPCR in H1299 cells stably expressing wild type FLAG-p300_{BRPHZT} or the BRD mutant.

qPCR analysis of the FLAG-p300_{BRPHZT}, H3K18ac and H3K27ac ChIP at target loci and two negative control loci in H1299 cells stably expressing wild type FLAG-p300_{BRPHZT} or the N1132A mutant. IgG or H3 ChIP was used for normalization.

3.6 Conclusions

Our studies identify the ZZ domain of p300 as a reader specifically recognizing the N-terminus of histone H3. This recognition is insensitive to methylation or acetylation on H3 tail, a binding pattern distinct from all known H3 readers, suggesting the ZZ domain may constitute a novel group of histone readers. Crystal structure of the ZZ-H3 complex reveals a negatively charged cavity of ZZ that coordinates Ala1 and Arg2 of H3, suggesting a novel recognition mode.

The H3-binding capability of ZZ and the acetyllysine binding ability of BRD are both essential for chromatin association of p300 and acetylation of histones. Specifically, the BRD-acetyllysine binding is necessary for p300 to catalyze acetylation of virtually all lysine residues in H3 and H4, whereas the ZZ domain is specifically required for p300 to acetylate primarily H3K27 and H3K18. Collectively, the binding of p300 ZZ domain to H3 N-terminus provides a novel intramolecular mechanism in regulating both chromatin recruitment and substrate selectivity of p300.

3.7 Discussion

Transcriptional coactivators p300 and CBP play critical roles in multiple fundamental cellular processes such as cell proliferation, differentiation and apoptosis. They contain multiple domains and most of these domains have been well studied. However, the function of their ZZ domain is still elusive. In this study, we discover that p300 ZZ domain is a reader for histone H3. It specifically recognizes the first a few residues of H3 N-terminus, regardless of methylation or acetylation status on H3. This unique feature distinguishes ZZ from all known readers, as other readers are all sensitive to histone PTMs. The K_d value for the p300 ZZ-H3 interaction is 8.8 μM (Figure 10B), which is in the range of binding affinities exhibited by the majority of histone-binding modules (170-172), corroborating the notion that the ZZ domain of p300 is a new member of epigenetic readers that select for histone H3.

The ZZ domain of p300 possesses a novel structural mechanism for histone H3 recognition. Importantly, key residues forming the negatively charged binding site to contact with the Ala1 and Arg2 of H3, such as N1671, D1688 and D1690, are highly conserved in multiple members of ZZ domain family (Figure 4B). It will be interesting to test whether other ZZ domains containing these conserved residues also have H3-binding ability.

Although coactivator functions of p300/CBP are largely dependent on their chromatin-binding capability (165, 173), the mechanism underlying p300/CBP-chromatin association is not well studied. Transcription factors that bind specific DNA sequences and other chromatin-binding factors can recruit p300/CBP to

chromatin through protein-protein interaction (46). Independent of the recruitment by other proteins, p300 itself can directly bind to chromatin (165), which requires the acetyllysine-binding ability of p300 BRD. We found that recognition of H3 by p300 ZZ domain is also required for p300-chromatin association, which provides another mechanism for recruiting p300 to chromatin. By ChIP and salt fractionation assays, we revealed the importance of ZZ and BRD for p300's binding to chromatin, as deletion or loss-of-function mutations of either domain dramatically reduced p300-chromatin association globally and at specific target regions (Figures 13, 14, 24 and 25). Furthermore, simultaneous mutations of both domains further reduced chromatin binding compared with single domain deficiencies, indicating that ZZ and BRD may collaborate in promoting p300's chromatin recruitment. Interestingly, double mutations did not completely abolish p300's chromatin binding (Figures 13 and 14), suggesting that mechanisms other than ZZ and BRD may exist. For instance, the TAZ2 domain can recruit p300 to chromatin through interacting with transcription factors (46).

Genome-wide analysis of p300_{BRPHZT} occupancy by ChIP-seq analysis identified 679 peaks, which are much fewer than that of full-length p300 (25, 167). This is likely because the p300_{BRPHZT} fragment lacks a number of protein-interacting domains in the full-length protein that also contribute to p300-chromatin binding. Nevertheless, the p300_{BRPHZT} binding sites can be classified into two groups based on the pre-existing modifications on H3K27: H3K27 pre-acetylated regions (Group 1) and H3K27 pre-methylated regions (Group 2) (Figure 21D). Group 1 sites are likely active enhancers containing high level of

H3K4me1 and H3K27ac while Group 2 binding sites are probably silenced or poised enhancers. Both BRD and ZZ domains are required for p300 binding at both groups of sites, however, certain level of specificity still remains. For example, the p300_{BRPHZT} occupies the *PDE4DIP* upstream region; mutations of the ZZ mutation, but not BRD, affect the binding. As H4 acetylation levels may be low in this region, it is likely that the ZZ-H3 interaction plays a dominant role in p300 chromatin binding.

Most known histone readers recognize specific histone modifications, thus promoting recruitment of the protein or protein complex to specific chromatin loci. However, the ZZ-H3 binding is independent of any H3 modifications, suggesting that ZZ domain alone is not be able to recruit p300 to specific chromatin regions. So, what is the significance of the “non-specific” ZZ-H3 interaction in p300’s chromatin recruitment? Inspired by the ideas of Manning et al. (165), we proposed the following model (Figure 26). Prior to p300 being recruited to specific target regions by interacting with transcription factors, the recognition of H3 by ZZ domain may account for the initial step of p300 to associate with chromatin (Figure 26A). This close chromatin proximity would allow DNA-bound transcription factors to quickly find p300 and then to recruit it to specific target regions (Figure 26B). Alternatively, after p300 is recruited to specific regions by transcription factors, the ZZ-H3 binding stabilizes p300’s association with chromatin to ensure transcription is successfully activated (Figure 26C). More biochemical and cell-based experiments need to be done to test this model.

Both p300 and CBP are promiscuous acetyltransferases with hundreds of substrates, including multiple sites of all core histones (19). However, depletion of both p300 and CBP specifically reduces global levels of H3K18ac and H3K27ac in mammalian cells (12, 13). The reason why acetylation on H3K18 and H3K27 is dominantly dependent on p300/CBP is currently unknown. We show that the ability of p300 to acetylate primarily H3K18 and H3K27 largely relies on the binding of the ZZ domain to the N-terminus of H3. A model of the p300_{HAT+ZZ}-H3 complex (generated by Yi Zhang from Kutateladze lab) using the simulated annealing method and the crystal structures of p300_{BRPH} and p300 ZZ-H3 reveals a ~38 Å distance between the H3A1-binding site of ZZ and the catalytic site in the HAT domain (Figure 27). This distance is too long for Lys4 or Lys9 of H3 to occupy the active site of the HAT domain and thus be acetylated *in cis* when the N-terminus of H3 is locked through the interaction with ZZ. However, the distal lysine residues (K18 and K27) in the H3 tail can reach the active site. Furthermore, the substrate-binding groove of the HAT domain is highly negatively charged and would favor the binding of positively-charged H3 tail. Our *in vitro* and *in vivo* data and the structure model collectively suggest that binding of p300 ZZ domain to the N-terminus of H3 provides selectivity of the adjacent HAT domain toward the distal lysine sites in H3, such as H3K18 and H3K27.

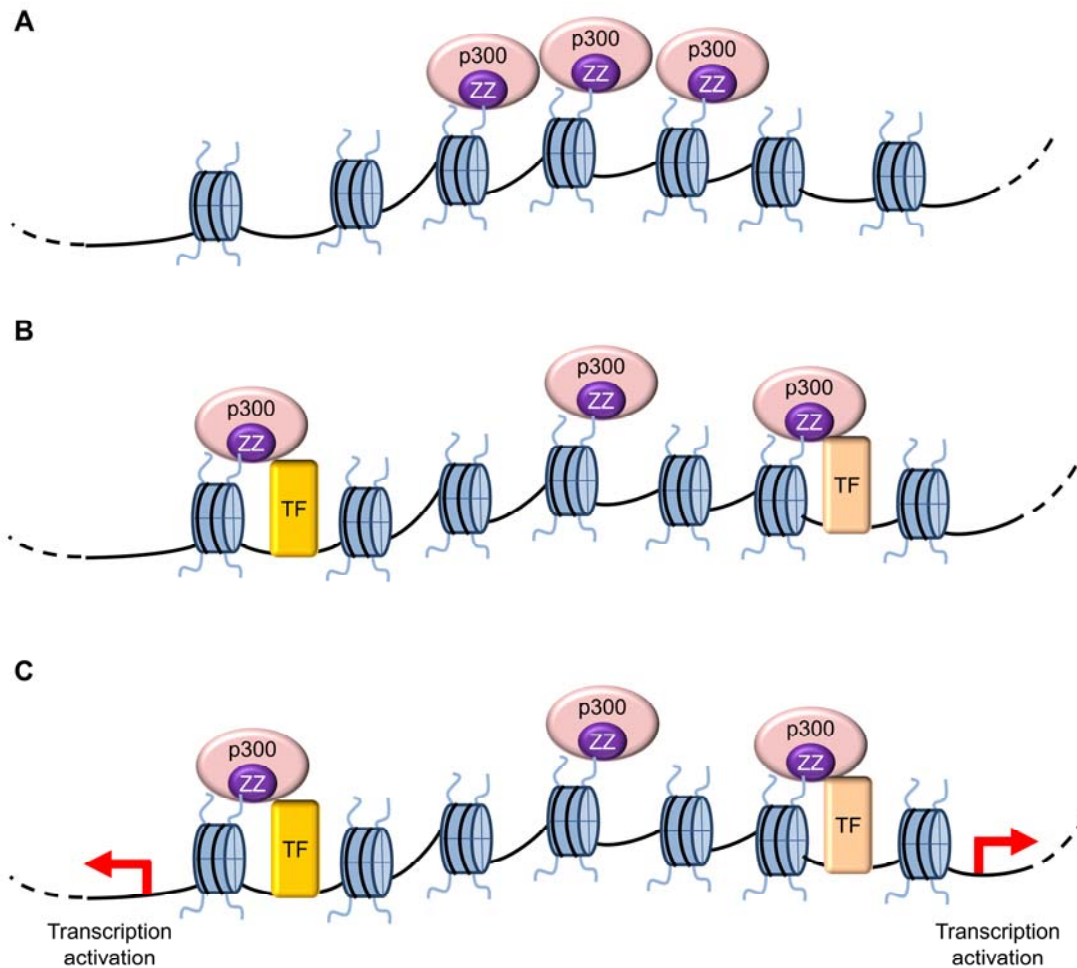


Figure 26. The proposed functions of ZZ domain-mediated p300 chromatin recruitment.

(A) Before p300 is recruited to specific target regions by transcription factors, the recognition of H3 by ZZ domain may represent the initial step to associate p300 with chromatin. (B) This association would then allow DNA-bound transcription factors to recruit p300 from chromatin, rather than from solution, to specific target regions more efficiently. (C) After p300 is recruited to specific regions by transcription factors, its interaction with chromatin is stabilized by the ZZ-H3 binding to ensure transcription is successfully activated.

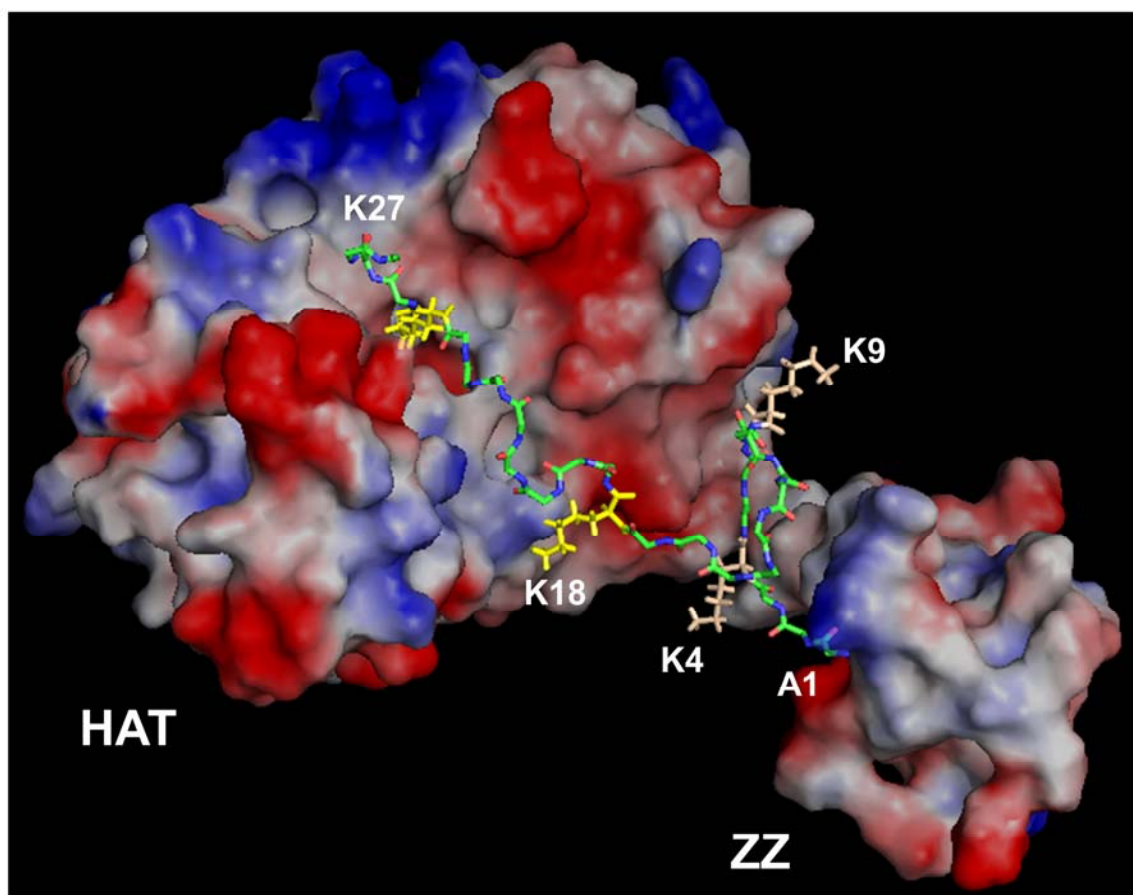


Figure 27. The structural basis of ZZ-mediated HAT specificity toward the distal lysine sites in H3.

A model of the p300_{HAT+ZZ} region in complex with H3₁₋₃₁ peptide generated by Yi Zhang from Kutateladze lab. Electrostatic surface potential of p300 HAT is colored blue (positive charge) and red (negative charge) with the histone H3 peptide shown in green. The side chains of H3K4, K9, K18 and K27 are colored yellow.

Chapter 4. p300 Is Required for Maintenance of SCLC Cell Growth

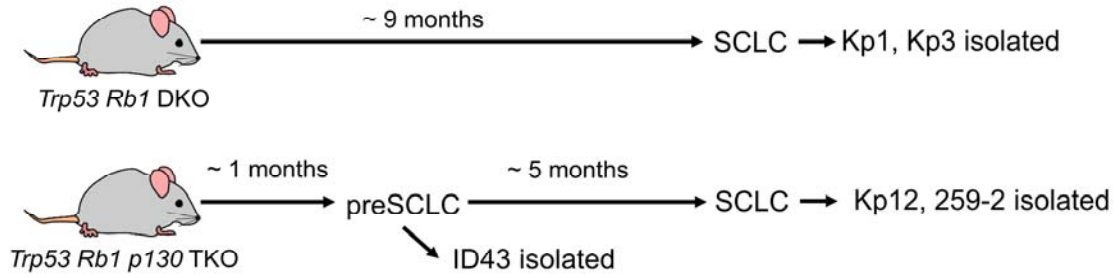
4.1 Depletion of p300 impedes SCLC cell proliferation

Cancer cells are highly dependent on dysregulated transcriptional programs gained during tumorigenesis to maintain their continued growth, a phenomenon called “transcriptional addiction” (174). As transcriptional coactivators, p300/CBP have been extensively studied in many types of cancers, however, their roles in SCLC are elusive. High p300/CBP expression was reported to be associated with poor overall survival for resected SCLC patients (111). In SCLC, disease maintenance is addicted to overexpression of oncogenes such as *MYC*, *MYCL*, *MYCN*, *NFIB* and *SOX2*, which is driven by super-enhancers containing extraordinarily high level of H3K27 acetylation (153). Considering p300 and CBP are the dominant HATs catalyzing H3K27 acetylation, they likely play important roles in maintaining active super-enhancers in SCLC. Based on these known facts, we hypothesized that p300/CBP are required for SCLC disease maintenance by activating oncogenes.

First, we examined the expression levels of p300/CBP in a number of mouse and human SCLC cells. SCLC cells isolated from primary tumors of genetically engineered mouse models (GEMM) constitute a good model because of their simple genetic background. Kp1 and Kp3 are two primary SCLC tumor cell lines isolated from the GEMM with conditional *Trp53 Rb1* double knockout in lung (175); Kp12 and 259-2 cells are isolated from conditional *Trp53 Rb1 p130* triple knockout GEMM that have accelerated SCLC tumorigenesis compared with

Trp53 Rb1 double knockout GEMM (176) (Figure 28A). ID43 cells are lung epithelial neuroendocrine cells isolated from conditional *Trp53 Rb1 p130* triple knockout GEMM before they become malignant (preSC), thus serving as a non-tumorigenic control for SCLC cells (177) (Figure 28A). By analyzing the whole cell lysate of these cells, we found that most GEMM SCLC cells have higher p300 levels than the ID43 preSC cells (Figure 28B). The expression levels of CBP are also slightly higher in the GEMM SCLC cells. However, despite of the increased p300/CBP levels, we did not observe a dramatic elevation of global H3K27ac level in GEMM SCLC cells compared with ID43 cell (Figure 28B).

A



B

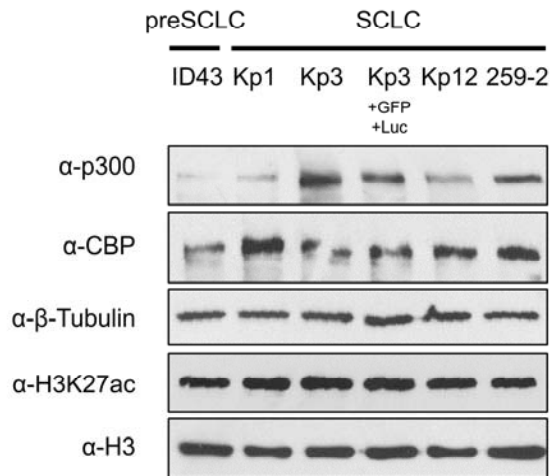


Figure 28. p300 is overexpressed in murine SCLC cell lines.

(A) The sources of GEMM SCLC cell lines. (B) Western blot analysis of p300, CBP and H3K27ac levels in the indicated SCLC cell lines.

To determine the role of p300/CBP in maintenance of SCLC cell growth, we depleted *Ep300* or *Crebbp* gene using a lentiviral CRISPR-Cas9 system. Two distinct gRNAs targeting the 5' end of the CDS were used for each gene and non-targeting (NT) gRNA served as control. Western blotting confirmed that each target gene was successfully depleted at protein level in all cell lines without significantly affecting the level of its close paralog (Figure 29A). Proliferation assays showed that p300-depleted Kp1, Kp3, Kp12 and 259-2 cells grow much more slowly than their NT control cells (Fig 29B). Compared to p300 depletion, CBP depletion had little (Kp1 and 259-2) or no (Kp3 and Kp12) proliferation defect (Fig 29B). Together, these results demonstrate that p300, but not CBP, is essential to murine SCLC cell proliferation.

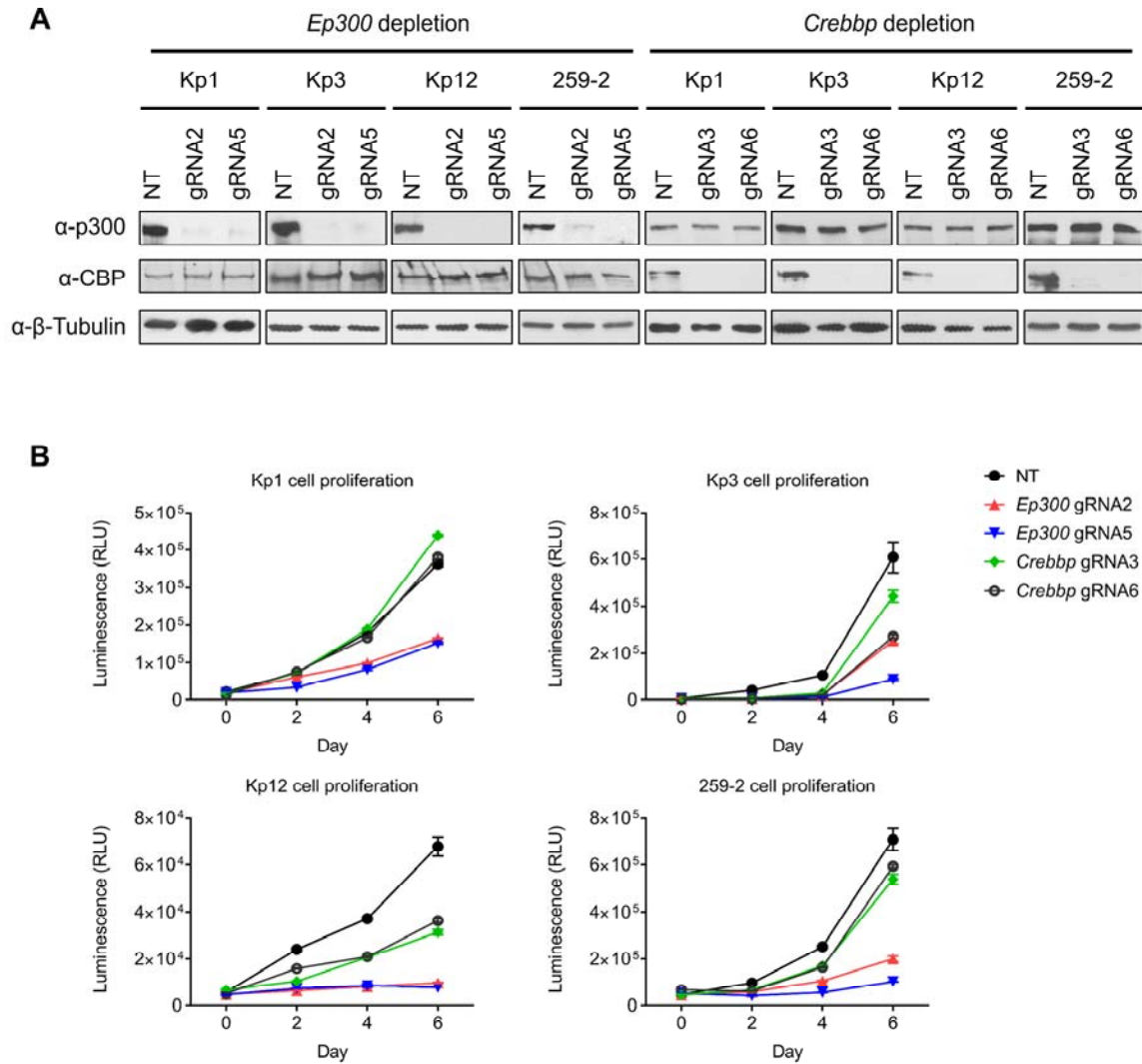


Figure 29. The depletion of p300 impedes murine SCLC cells proliferation.

(A) Western blot analysis of p300 and CBP levels in the control and p300/CBP-depleted murine SCLC cells. (B) The proliferation of control and p300/CBP-depleted murine SCLC cells.

Compared with GEMM SCLC cells, human SCLC cells are much more heterogeneous both genetically and epigenetically. For example, they have distinct mutation status of *CREBBP/EP300* genes, amplification of different *MYC* family genes, and various expression levels of neuroendocrine transcription factors. To study the role of CBP/p300 in human SCLC cells with different backgrounds, we chose SCLC cells with (1) WT CBP and WT p300 (H69, H82 and H2171); (2) WT p300 and mutated CBP (H1048 and H209); and (3) WT CBP and mutated p300 (H524 and H1836). The detailed mutation information of those cells is listed in Table 5. Immortalized human bronchial epithelial cell (HBEC) was used as a non-cancer control. Western blot analysis showed that all SCLC cell lines except H1836 have much higher levels of p300 than HBEC and all cell lines except H209 have greatly increased CBP level compared with HBEC cells (Figure 30). Loss of CBP in H209 cell is due to translocation and loss-of-heterozygosity (LOH) (90, 158). It is interesting that cell lines carrying mutated p300 (H524) or CBP (H1048) still had higher levels of p300 and CBP, respectively, than control cells. There are two possibilities: (1) the mutations are heterozygous and the remaining WT allele is still functional; or (2) the mutations do not completely abolish the proteins' functions. For example, the CBP mutation, S1680del, in H1048 cells is not located within any known domain (Table 5), therefore its functional consequence is hard to predict. In H524 cells, although the mutation in the HAT domain abrogates the HAT activity (95), the mutant p300 may still interacts with other proteins to help to assemble an

activating complex. Nevertheless, our results suggest that p300 and CBP are overexpressed in human SCLC cells regardless of their genetic mutation status.

We next examined global H3K18ac and H3K27ac levels in these cells (Figure 30). Although the levels of H3K27ac in SCLC cells are not significantly higher than the non-tumorigenic HBEC cells, H3K18ac levels are much higher in the SCLC cells compared with HBEC. The global H3K18ac and H3K27ac levels correlate with the total levels of p300 and CBP proteins in most human SCLC cells except for the H69 cells.

Cell line	Cell type	<i>EP300</i> status	<i>CREBBP</i> status
HBEC	Human control cell	WT	WT
A549	Human NSCLC	WT	WT
H1299	Human NSCLC	WT	WT
H1048	Human SCLC	WT	p.S1680del
H1836	Human SCLC	p.S1396P	WT
H209	Human SCLC	WT	Homozygous Deletions
H2171	Human SCLC	WT	WT
H524	Human SCLC	p.F1090L, Y1503S	WT
H69	Human SCLC	WT	WT
H82	Human SCLC	WT	WT
ID43	Mouse pre-SCLC	WT	WT
Kp1	Mouse SCLC	WT	WT
Kp3	Mouse SCLC	WT	WT
Kp3 ^{+GFP+Luc}	Mouse SCLC	WT	WT
Kp12	Mouse SCLC	WT	WT
259-2	Mouse SCLC	WT	WT

Table 5. The mutation status of *EP300* and *CREBBP* genes in lung cancer cell lines used in this study.

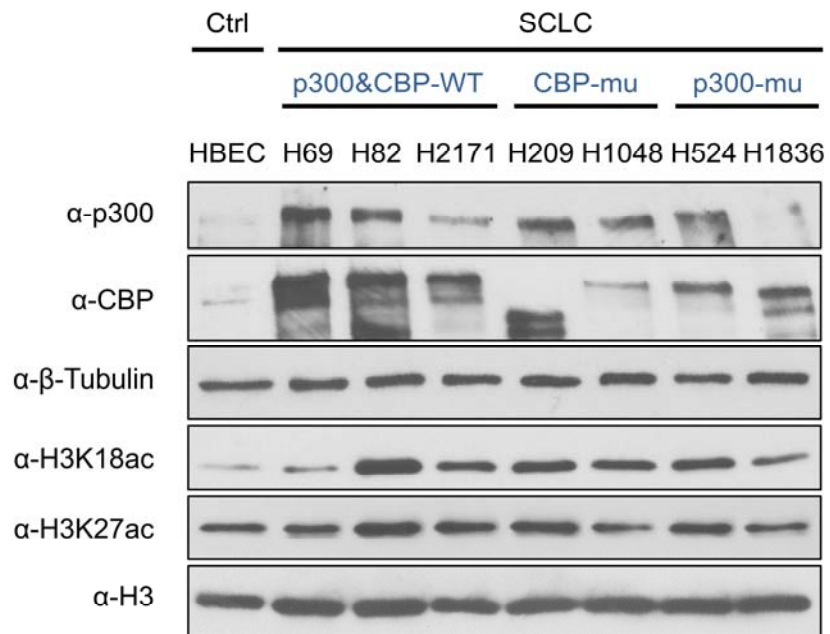


Figure 30. p300 and CBP are overexpressed in human SCLC cell lines.

Western blot analysis of p300, CBP, H3K18ac and H3K27ac levels in the indicated SCLC cell lines.

Human SCLC cells can be classified by the expression levels of NE lineage transcription factors, *ASCL1* or *NEUROD1*. *ASCL1*-high (cells expressing high level of *ASCL1* but low level of *NEUROD1*) and *NEUROD1*-high (cells expressing high level of *NEUROD1* but low level of *ASCL1*) are two dominant groups (178) that have different epigenetic landscapes (179). To examine the role of p300/CBP in both groups of human SCLC cells, we depleted *CREBBP/EP300* in both *ASCL1*-high (H69 cells) and *NEUROD1*-high (H82 cells) cells and determined cell proliferation. Two distinct gRNAs targeting the 5' end of the CDS were used for each gene and non-targeting (NT) gRNA served as control. Western blotting confirmed that each target gene was successfully depleted at protein level in both cell lines without significantly affecting the level of its close paralog (Figure 31A). Depleting p300 or CBP did not significantly affect the global H3K27ac level in these two cell lines (Figure 31A), suggesting the potential redundancy between p300 and CBP in maintaining the global H3K27ac level.

Proliferation assays showed that p300 depletion led to a severe proliferation defect in both H69 and H82 cells, whereas CBP depletion only slightly impeded cell proliferation (Figure 31B), suggesting that p300, but not CBP, is crucial to human SCLC cell proliferation. Those results are in agreement with our observations in murine SCLC cells.

NSCLC is another subtype of lung cancer accounting for ~85% of lung cancer cases. To examine whether p300 and CBP are required by NSCLC, we depleted *EP300* or *CREBBP* gene in two representative NSCLC cell lines, A549

and H1299, and HBEC cell, and measured cell proliferation. Surprisingly, cell proliferation was not affected by p300 or CBP depletion in these cell lines (Figure 32), indicating that the dependency on p300 is specific to SCLC but not to NSCLC or normal lung cells.

In summary, we found that p300 is overexpressed in both murine and human SCLC cells. It is required for the maintenance of cell growth in both murine and human SCLC cells. Although CBP is also overexpressed in human SCLC, but in most SCLC cells, CBP is not absolutely required for cell growth maintenance.

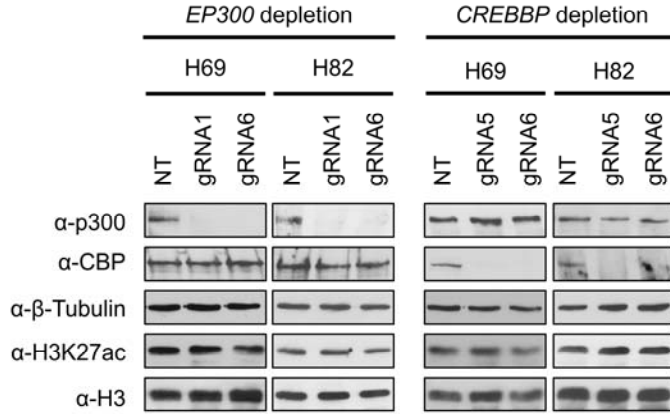
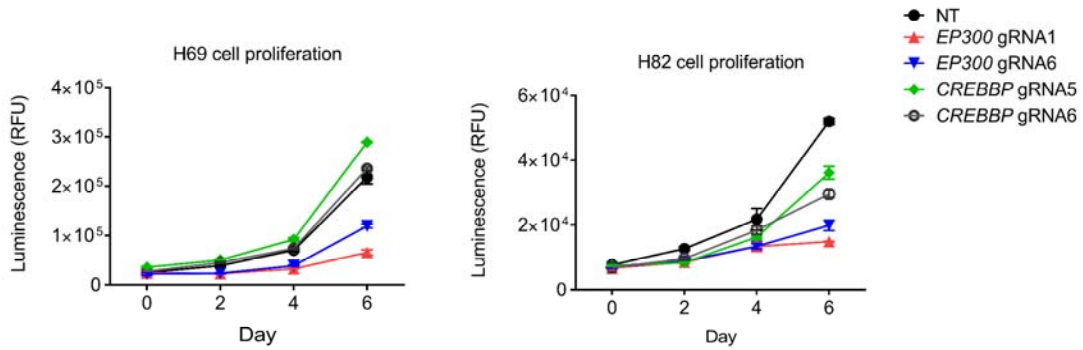
A**B**

Figure 31. The depletion of p300 impedes human SCLC cells proliferation.

(A) Western blot analysis of p300 and CBP levels in the control and p300/CBP-depleted human SCLC cells. (B) The proliferation of control and p300/CBP-depleted H69 and H82 cells.

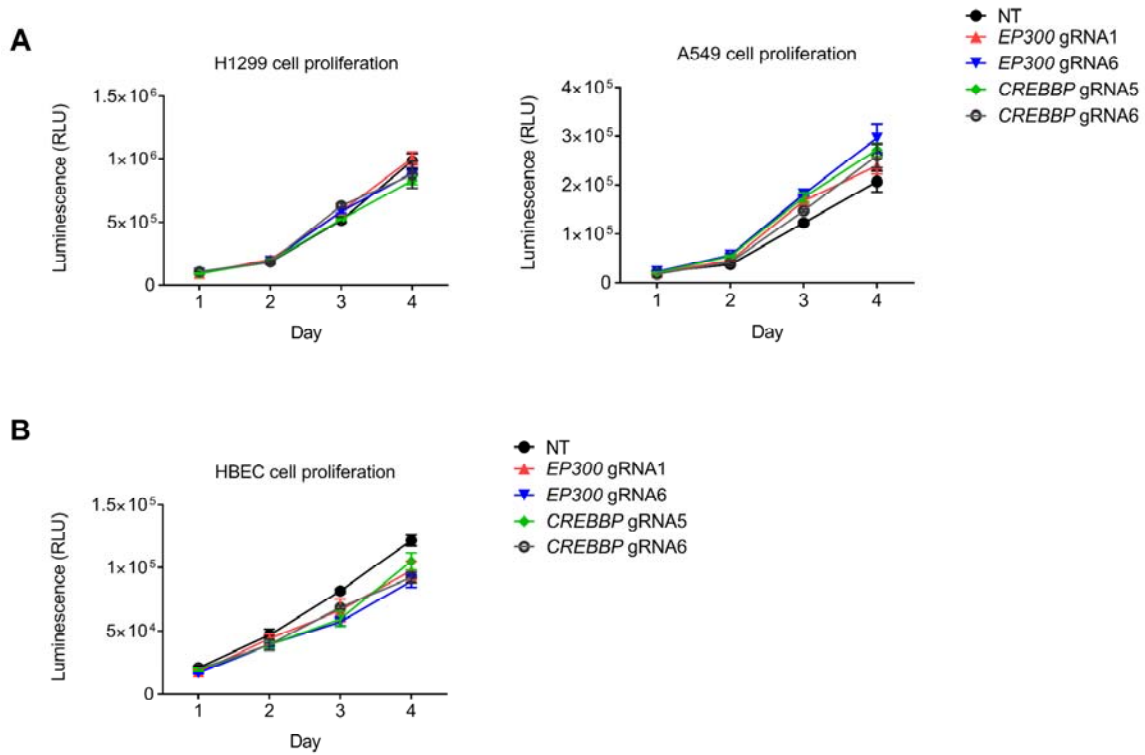


Figure 32. The depletion of p300 does not affect the proliferation of human NSCLC cells and normal lung epithelial cell.

(A) The proliferation of control and p300/CBP-depleted H1299 and A549 cells.

(B) The proliferation of control and p300/CBP-depleted HBEC cells.

4.2 Depletion of p300 attenuates oncogene activation in SCLC cells

CBP/p300 are critical transcriptional coactivators that control the expression of key cancer-related genes, especially those associated with super-enhancers (103). To determine the functional differences between p300 and CBP in SCLC cell proliferation, we assessed the expression of a few key oncogenes in p300 or CBP depleted cells. We chose to study the expression changes of *MYC* family genes because: (1) *MYC* family genes are known to play critical roles in the tumorigenesis/maintenance of both murine (177, 180) and human (151, 156) SCLCs; (2) *MYC* family genes are associated with super-enhancers in human SCLCs and are thus likely direct targets of p300/CBP (153). *MYC* family genes include 3 members: *MYC*, *MYCL1* and *MYCN*. A large number of human SCLCs have the amplification of one *MYC* family gene. For example, H69 cell is *MYCN*-amplified whereas H82 has *MYC* amplification. The amplified *MYC* member usually has much higher expression level than the other 2 members and becomes the dominant one in that cell (156, 181). We performed RT-qPCR assays to compare the expression levels of *MYC*, *MYCL* and *MYCN* in these two cell lines (Figure 33A). Consistent with the amplification status, *MYC* levels in H82 are ~1,000-fold higher than that in H69 while its *MYCN* level was ~1,000-fold lower than that of H69. We also observed that H82 has higher *MYCL1* expression level than H69. It is possible that among the *MYC* family members, *MYCN* or *MYC* plays the most dominant oncogenic role in H69 or H82, respectively.

Interestingly, in H69, depletion of p300 or CBP reduced the expression of *MYCN* and *MYC* but not *MYCL1*. The decrease in *MYCN* level was much more significant in p300-depleted cells than in CBP-depleted cells (Figure 33B). The decreased expression of *MYCN* was also observed in p300- or CBP-depleted H82 cells. But the reduction of *MYC* level was only found in p300-depleted H82 cells but not in CBP-depleted ones (Figure 33B). These results suggest that expression of the dominant *MYC* family member shows more dependency on p300 than CBP in both cell lines. This may partially explain why p300 depletion caused much more severe proliferation defect than CBP depletion (Figure 31B).

According to the work of Drs. Kwok-kin Wong and Richard Young (153), *MYCN* is driven by super-enhancers in H69 but not in H82 while *MYC* is driven by super-enhancers in H82 but not in H69 (Figure 34A), which is consistent with their relative expression levels (Figure 33A) and amplification status in these 2 cell lines. Considering p300 is one of the main acetyltransferases of H3K18ac and H3K27ac, we proposed that p300 is required for the acetylation of H3K18 and H3K27 at super-enhancers associated with the dominant *MYC* family gene in SCLC cell. We chose two regions of the published *MYC* super-enhancer in H82 cell as examples and performed H3K18ac and H3K27ac ChIP-qPCR in p300-depleted and NT control H82 cells. Significant decrease of H3K27ac level at both regions was observed in p300-depleted cells (Figure 34B). The depletion of p300 also led to a severe drop of H3K18ac level at SE1 region. The decrease of both histone markers at *MYC* super-enhancers resulted from p300 depletion is consistent with the reduced *MYC* expression. Taken together, we found p300 is

required for sustaining the histone acetylation and expression of super-enhancers-associated oncogenes in SCLC cells.

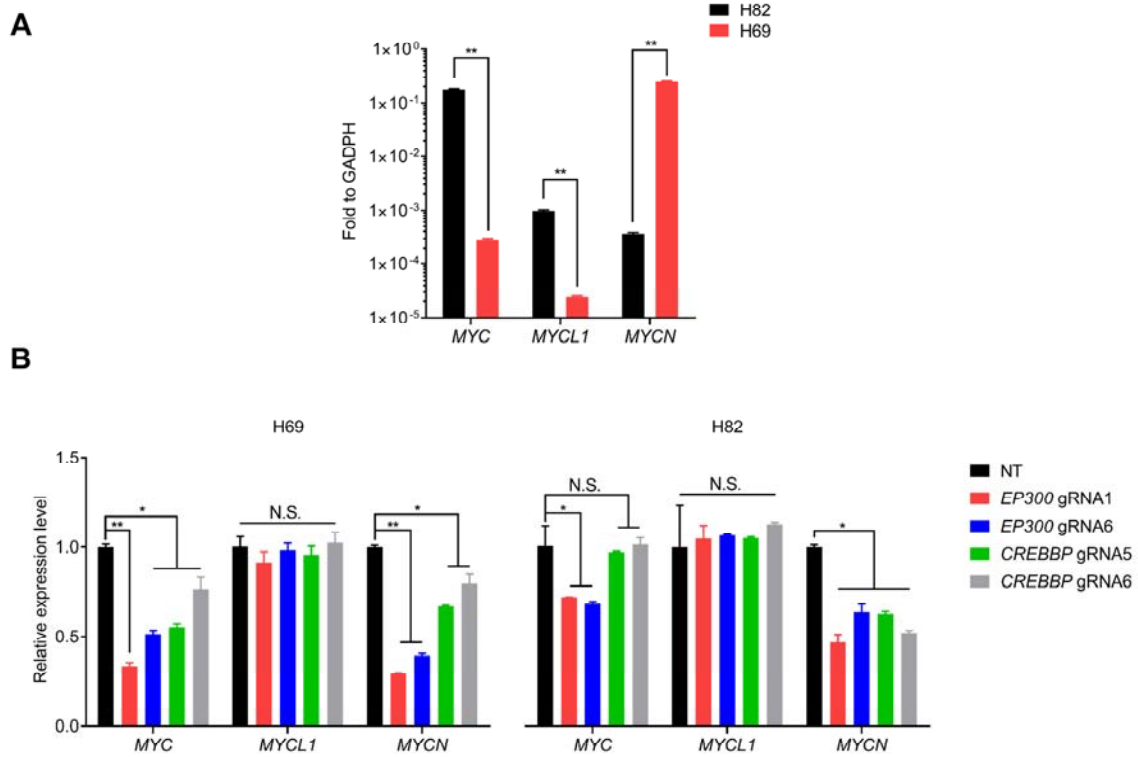


Figure 33. Expression activation of the dominant *MYC* family gene is dependent on p300.

(A) RT-qPCR analysis of 3 *MYC* family genes in H69 and H82 cells. (B) RT-qPCR analysis of 3 *MYC* family genes in control and p300/CBP-depleted H69 and H82 cells.

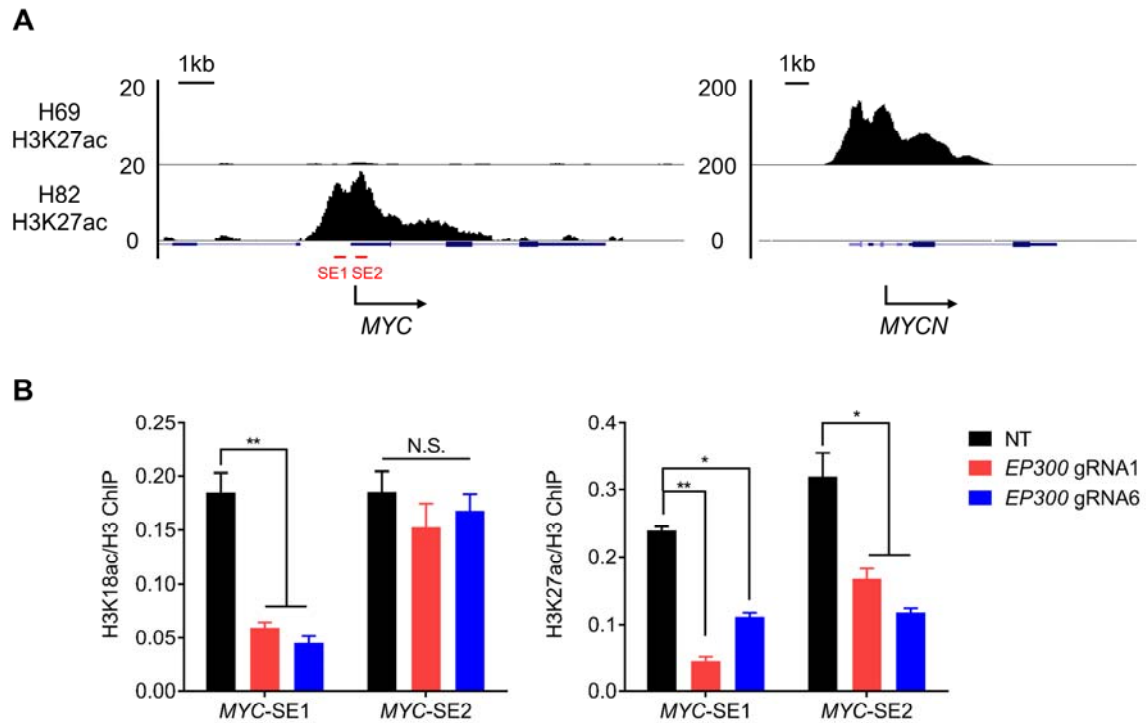


Figure 34. Histone acetylation at *MYC* super-enhancer regions requires p300.

(A) The genome-browser views of H3K27ac at *MYC* and *MYCN* super-enhancer regions. The raw data tracks are from Gene Expression Omnibus with the accession number GSE62614 (153). The red lines indicate the sites for ChIP-qPCR in (B). SE: super-enhancer. (B) qPCR analysis of the H3K27ac level at two *MYC* super-enhancer regions.

4.3 Conclusions

In this study, we show that p300 and CBP are overexpressed in both murine and human SCLC cells. Depletion of p300, but not CBP, impedes SCLC cell proliferation. Both p300 and CBP are required for sustaining the expression of oncogenes, for example, the *MYC* family genes, in SCLC cells. However, the expression of the dominant *MYC* family gene that is associated with super-enhancers shows more dependency on p300 than CBP. Consistently, p300, but not CBP, is essential for maintenance of SCLC cell growth.

4.4 Discussion

SCLC is the most aggressive subtype of lung cancer with an unmet need for effective treatment (182). The molecular basis of this disease is poorly understood. Here we found that p300 is required for the proliferation of both murine and human SCLC cells. The proliferation defect caused by p300 depletion was observed in all SCLC cell lines tested. However, more cell lines need to be tested before we can conclude that p300 dependency is a ubiquitous mechanism in SCLC, a highly heterogeneous disease. It will also be important to test in the future whether p300 depletion also attenuates SCLC tumor growth in a xenograft or allograft model. Importantly, p300 depletion does not dramatically affect the proliferation of NSCLC cells or normal lung epithelial cell, implying that inhibiting p300 may be a potential SCLC treatment method with low toxicity to normal lung cell.

Despite of the high sequence similarity between p300 and CBP, CBP is not required for cell proliferation in the SCLC cell lines tested. Because of the relatively high mutation rate (13~15%) of *CREBBP/EP300* in SCLC (95, 136), it has been previously predicted that both *CREBBP* and *EP300* are tumor suppressor genes (183). Most *CREBBP* alterations are nonsense mutations, deletions, frameshifts and translocations (Figure 5B), which are likely loss-of-function. Consistent with the mutation status of *CREBBP*, the laboratory of Dr. David MacPherson recently reported that lung neuroendocrine-specific triple knockout of *Trp53*, *Rb1* and *Crebbp* in mice accelerates SCLC tumorigenesis compared with *Trp53 Rb1* double knockout mice, indicating *Crebbp* is a tumor

suppressor gene in murine SCLC (184). However, this paper did not mention the role of p300 in SCLC. In fact, the mutation pattern of *EP300* in SCLC is distinct from that of *CREBBP*. The majority of *EP300* alterations are missense mutations with unknown consequences, though only a few of mutations within p300 HAT domain have been confirmed to reduce HAT activity (95). Therefore, the mutation status of *EP300* in SCLC does not conflict with our results that p300 is required in maintaining the continuous growth of SCLC cells.

An explanation for the functional differences between p300 and CBP in SCLC may be that they target different genes (185). In H69 and H82 cells, activation of the dominant *MYC* family gene that is associated with super-enhancers relies more on p300 than on CBP, which may reflect the differences in their target genes. Unfortunately, we only have a small amount of preliminary data on how p300 and CBP regulate oncogenes in SCLC cells. RNA-seq and H3K27ac ChIP-seq analysis using control cell, p300- or CBP-depleted cells will provide more comprehensive information to help us understand the molecular basis of the p300-dependency in SCLC cell proliferation in the future.

Overall, although still preliminary, our data start to shed light on the critical functions of p300 in SCLC. Future studies will bring further insights into the molecular mechanisms of SCLC maintenance and evaluate p300 inhibition as a new therapeutic strategy for SCLC patients.

Chapter 5. Future Directions

5.1 Determining the physiological importance of p300 ZZ domain

p300 is a key transcription coactivator important to both development and diseases. Our findings that the ZZ domain is required for both chromatin binding and histone acetylation, the basic molecular functions of p300, suggesting that the ZZ domain is likely critical for p300 to exert its functions in both physiological and pathological settings. It is particularly interesting to me to determine the functional importance of the ZZ domain in human cancers.

Although there is no cancer-related mutation hotspot in p300 ZZ domain reported in TCGA, we did find dozens of genetic mutations occurring in the ZZ domain coding regions, albeit with low frequency, from cBioPortal (<https://www.cbioportal.org>) (119, 120) and Catalogue of Somatic Mutations in Cancer (COSMIC, <https://cancer.sanger.ac.uk/cosmic>) (186). All up-to-date mutations located in p300 ZZ domain are listed in Table 6 and Figure 35A. The effect of those mutations on p300 ZZ's function is currently unknown.

In our preliminary studies, we expressed and purified recombinant ZZ domain mutants mimicking a few TCGA mutations, including R1680C/H, W1681* and D1688H (Figure 35B) and tested their histone-binding activity. Histone peptide pull-down assays showed that the H3-binding activity is reduced in R1680C and W1681A and abolished in the D1688K mutant (Figure 35C). These preliminary data suggest that cancer-related mutations can abrogate the function of ZZ, implying the histone-binding activity of p300 ZZ domain is indeed

important to tumorigenesis. In the future, it will be interesting to study the function of p300 ZZ domain in tumorigenesis using a proper cancer model. For instance, the colon cancer mutation of ZZ domain, R1680C, can be introduced into endogenous *EP300* gene by CRISPR/Cas9-mediated DNA cutting followed by homology-directed repair using single-stranded oligodeoxynucleotides in colon epithelial cells. Single clones containing a R1680C point mutation will be selected and examined for their cell growth and survival in culture. We'll also establish xenograft models using those cells for measuring tumor growth *in vivo*. Mechanistically, the epigenome and transcriptome of parental and ZZ-mutated cells will be assessed by p300 and histone ChIP-seq and RNA-seq, respectively.

The ZZ domain is required for p300-dependent H3K18 and H3K27 acetylation and the BRD is required for the acetylation of all lysine residues on H3 and H4 by p300. Importantly, these two domains seem to cooperate in regulating the HAT activity of p300. The inhibitors of p300 BRD showed good anti-cancer effect in hematopoietic malignancies (43, 118). In the future, we also plan to determine whether ZZ mutations can sensitize cells to those BRD inhibitor, which will be beneficial to the development of targeted therapies.

Sample ID	Cancer Study	Gene	AA change	Type
MFE296 cell line	CCLC (Novartis/Broad 2012)	<i>EP300</i>	R1665H	Missense
ATLL_A-01	Lymphoma/leukemia (COSMIC)	<i>EP300</i>	T1669I	Missense
ATL014	Lymphoma/leukemia (COSMIC)	<i>EP300</i>	T1669I	Missense
TCGA-BG-A0MG-01	Uterine (TCGA)	<i>EP300</i>	E1672*	Nonsense
OSCC-GB_01670111	Oral (COSMIC)	<i>EP300</i>	E1672*	Nonsense
ESCC_E11	Esophagus (COSMIC)	<i>EP300</i>	C1673Y	Missense
MBC_71	MBL (Sickkids 2016)	<i>EP300</i>	E1678Q	Missense
Pat_59_B	Melanoma (COSMIC)	<i>EP300</i>	T1679I	Missense
TCGA-DM-A1D0-01	Colon (TCGA)	<i>EP300</i>	R1680H	Missense
TCGA-F5-6813-01	Colon (TCGA)	<i>EP300</i>	R1680H	Missense
PLK106Ca	Colon (COSMIC)	<i>EP300</i>	R1680C	Missense
TCGA-ZR-A9CJ-01	Esophagus (TCGA)	<i>EP300</i>	R1680C	Missense
PD8141a	AML (COSMIC)	<i>EP300</i>	W1681*	Nonsense
ATL359	Lymphoma/leukemia (COSMIC)	<i>EP300</i>	C1683Y	Missense
coadread_dfci_2016_2768	Colorectal (DFCI 2016)	<i>EP300</i>	V1685I	Missense
T2768	Colon (COSMIC)	<i>EP300</i>	V1685I	Missense
Pat_24_Pre	Melanoma (Broad 2012)	<i>EP300</i>	C1686Y	Missense
PAJ MVC	Kidney (COSMIC)	<i>EP300</i>	C1686*	Nonsense
ID32	AML (COSMIC)	<i>EP300</i>	C1686fs	FS del
SW948 cell line	CCLC (Novartis/Broad 2012)	<i>EP300</i>	X1687_splice	Splice
MTS-T0713	Breast (METABRIC)	<i>EP300</i>	D1688H	Missense
TCGA-P3-A5Q5-01	Head & neck (TCGA)	<i>EP300</i>	D1688H	Missense
TCGA-GR-A4D6-01	DLBC (TCGA)	<i>EP300</i>	T1694A	Missense
HCT-116 cell line	NCI-60	<i>EP300</i>	N1700fs	FS del
P-0003104-T01-IM5	MSK-IMPACT	<i>EP300</i>	H1703Y	Missense
P-0010591-T01-IM5	MSK-IMPACT	<i>EP300</i>	E1706*	Nonsense

Table 6. Mutations in p300 ZZ domain occurring in cancers.

Data are collected from cBioPortal (www.cbioportal.org) (119, 120) and COSMIC (<https://cancer.sanger.ac.uk/cosmic>) (186). The diagram view of these listed mutations is in Figure 35A.

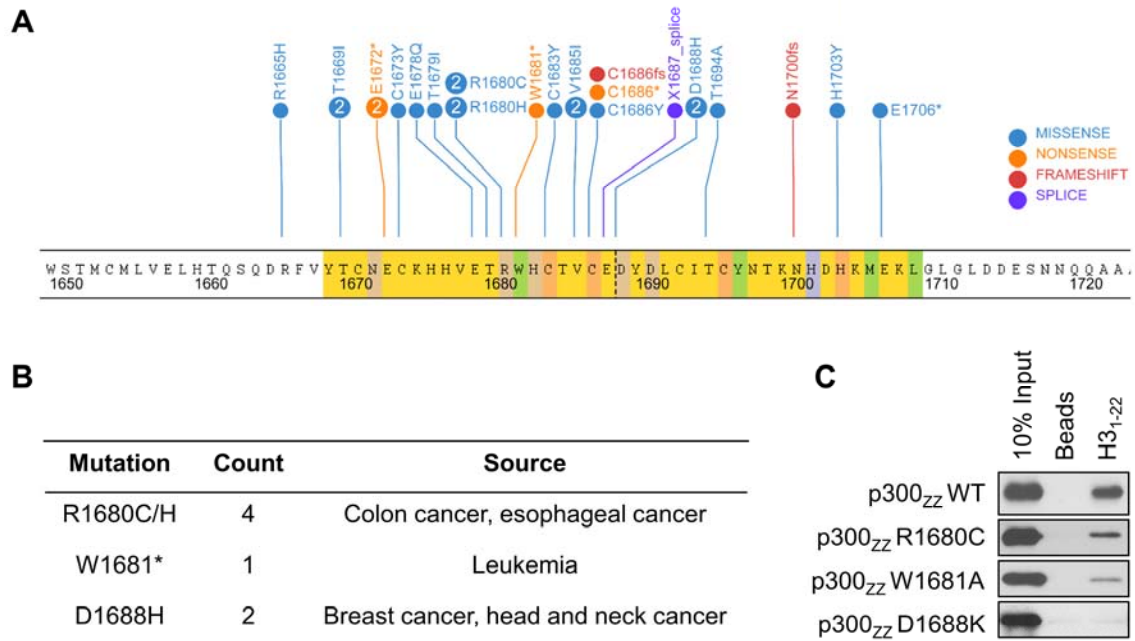


Figure 35. Mutations of p300 ZZ domain occurring in cancers.

(A) The diagram view of all the mutations of p300 ZZ domain occurring in cancers (also listed in Table 6). Diagram is generated using the online tool ProteinPaint (<https://pecan.stjude.cloud/proteinpaint>) (187). (B) Examples of p300 ZZ domain mutations that occur in cancers. (C) Peptide pull-down assays using wild type and mutated p300 ZZ domain.

5.2 Determining the role of p300 in SCLC maintenance

Our preliminary data has shown that p300 is necessary to SCLC cell proliferation in cell culture. This is an interesting observation, however, much more need to be done to reveal the role of p300 in SCLC maintenance. It would be of great interest to determine in the future whether p300 depletion impedes SCLC tumor growth in xenograft or allograft models. We can perform RNA-seq and ChIP-seq to further examine the transcriptomic and epigenomic changes resulted from p300, CBP, or double depletions. It is anticipated that depletion of p300, CBP or both will lead to a drastic decrease in the expression of oncogenes associated with super-enhancers in SCLC tumors.

Interestingly, a recent report shows that SCLC cells are not sensitive to A-485, a potent small molecule inhibitor targeting p300/CBP HAT domain (15), indicating that the function of p300 in SCLC cell proliferation may not require the HAT activity. Indeed, p300 is essential for the assembly of a transcription activation complex using protein-interaction domains, which may contribute to disease maintenance independent of its HAT activity. This makes it urgent to identify the protein domains or minimal regions of p300 that are critical for its biological functions in SCLC. To identify such essential domains, we will perform a CRISPR/Cas9-based dropout screening in SCLC cells using a tiling gRNA library targeting the *EP300* gene exons encoding the full-length p300 protein. The gRNAs targeting critical domains or regions are expected to have significantly lower enrichment. After the critical domains/regions are identified, rescue assays will be performed using constructs containing the deletion of each

critical domain or region in p300-depleted SCLC cells. If specific inhibitors for the critical domains are available, we will also test whether SCLC cells are sensitive to those compounds.

Collectively, these studies will depict a detailed picture of the molecular mechanisms of p300 and extend our understanding of critical roles of p300 in important biological processes. Furthermore, elucidating the role of p300 in SCLC will help to bring insights into the molecular basis of SCLC maintenance and may provide p300 as a new therapeutic target for treatment of SCLC.

Chapter 6. References

1. Arany, Z., W. R. Sellers, D. M. Livingston, and R. Eckner. 1994. E1A-associated p300 and CREB-associated CBP belong to a conserved family of coactivators. *Cell* 77: 799-800.
2. Vo, N., and R. H. Goodman. 2001. CREB-binding protein and p300 in transcriptional regulation. *The Journal of biological chemistry* 276: 13505-13508.
3. Yee, S. P., and P. E. Branton. 1985. Detection of cellular proteins associated with human adenovirus type 5 early region 1A polypeptides. *Virology* 147: 142-153.
4. Whyte, P., N. M. Williamson, and E. Harlow. 1989. Cellular targets for transformation by the adenovirus E1A proteins. *Cell* 56: 67-75.
5. Stein, R. W., M. Corrigan, P. Yaciuk, J. Whelan, and E. Moran. 1990. Analysis of E1A-mediated growth regulation functions: binding of the 300-kilodalton cellular product correlates with E1A enhancer repression function and DNA synthesis-inducing activity. *Journal of virology* 64: 4421-4427.
6. Eckner, R., M. E. Ewen, D. Newsome, M. Gerdes, J. A. DeCaprio, J. B. Lawrence, and D. M. Livingston. 1994. Molecular cloning and functional analysis of the adenovirus E1A-associated 300-kD protein (p300) reveals a protein with properties of a transcriptional adaptor. *Genes & development* 8: 869-884.

7. Chrivia, J. C., R. P. Kwok, N. Lamb, M. Hagiwara, M. R. Montminy, and R. H. Goodman. 1993. Phosphorylated CREB binds specifically to the nuclear protein CBP. *Nature* 365: 855-859.
8. Ogryzko, V. V., R. L. Schiltz, V. Russanova, B. H. Howard, and Y. Nakatani. 1996. The transcriptional coactivators p300 and CBP are histone acetyltransferases. *Cell* 87: 953-959.
9. Bannister, A. J., and T. Kouzarides. 1996. The CBP co-activator is a histone acetyltransferase. *Nature* 384: 641-643.
10. Farria, A., W. Li, and S. Y. Dent. 2015. KATs in cancer: functions and therapies. *Oncogene* 34: 4901-4913.
11. Schiltz, R. L., C. A. Mizzen, A. Vassilev, R. G. Cook, C. D. Allis, and Y. Nakatani. 1999. Overlapping but distinct patterns of histone acetylation by the human coactivators p300 and PCAF within nucleosomal substrates. *The Journal of biological chemistry* 274: 1189-1192.
12. Jin, Q., L. R. Yu, L. Wang, Z. Zhang, L. H. Kasper, J. E. Lee, C. Wang, P. K. Brindle, S. Y. Dent, and K. Ge. 2011. Distinct roles of GCN5/PCAF-mediated H3K9ac and CBP/p300-mediated H3K18/27ac in nuclear receptor transactivation. *The EMBO journal* 30: 249-262.
13. Horwitz, G. A., K. Zhang, M. A. McBrian, M. Grunstein, S. K. Kurdistani, and A. J. Berk. 2008. Adenovirus small e1a alters global patterns of histone modification. *Science* 321: 1084-1085.
14. Weinert, B. T., T. Narita, S. Satpathy, B. Srinivasan, B. K. Hansen, C. Scholz, W. B. Hamilton, B. E. Zucconi, W. W. Wang, W. R. Liu, J. M.

- Brickman, E. A. Kesicki, A. Lai, K. D. Bromberg, P. A. Cole, and C. Choudhary. 2018. Time-Resolved Analysis Reveals Rapid Dynamics and Broad Scope of the CBP/p300 Acetylome. *Cell* 174: 231-244 e212.
15. Lasko, L. M., C. G. Jakob, R. P. Edalji, W. Qiu, D. Montgomery, E. L. Digiammarino, T. M. Hansen, R. M. Risi, R. Frey, V. Manaves, B. Shaw, M. Algire, P. Hessler, L. T. Lam, T. Uziel, E. Faivre, D. Ferguson, F. G. Buchanan, R. L. Martin, M. Torrent, G. G. Chiang, K. Karukurichi, J. W. Langston, B. T. Weinert, C. Choudhary, P. de Vries, J. H. Van Drie, D. McElligott, E. Kesicki, R. Marmorstein, C. Sun, P. A. Cole, S. H. Rosenberg, M. R. Michaelides, A. Lai, and K. D. Bromberg. 2017. Discovery of a selective catalytic p300/CBP inhibitor that targets lineage-specific tumours. *Nature* 550: 128-132.
16. Das, C., M. S. Lucia, K. C. Hansen, and J. K. Tyler. 2009. CBP/p300-mediated acetylation of histone H3 on lysine 56. *Nature* 459: 113-117.
17. Vempati, R. K., R. S. Jayani, D. Notani, A. Sengupta, S. Galande, and D. Haldar. 2010. p300-mediated acetylation of histone H3 lysine 56 functions in DNA damage response in mammals. *The Journal of biological chemistry* 285: 28553-28564.
18. Chen, C. C., J. J. Carson, J. Feser, B. Tamburini, S. Zabaronick, J. Linger, and J. K. Tyler. 2008. Acetylated lysine 56 on histone H3 drives chromatin assembly after repair and signals for the completion of repair. *Cell* 134: 231-243.

19. Dancy, B. M., and P. A. Cole. 2015. Protein lysine acetylation by p300/CBP. *Chemical reviews* 115: 2419-2452.
20. Chan, H. M., and N. B. La Thangue. 2001. p300/CBP proteins: HATs for transcriptional bridges and scaffolds. *Journal of cell science* 114: 2363-2373.
21. Kalkhoven, E. 2004. CBP and p300: HATs for different occasions. *Biochemical pharmacology* 68: 1145-1155.
22. Chen, J., and Q. Li. 2011. Life and death of transcriptional co-activator p300. *Epigenetics : official journal of the DNA Methylation Society* 6: 957-961.
23. Wang, Z., C. Zang, K. Cui, D. E. Schones, A. Barski, W. Peng, and K. Zhao. 2009. Genome-wide mapping of HATs and HDACs reveals distinct functions in active and inactive genes. *Cell* 138: 1019-1031.
24. Heintzman, N. D., R. K. Stuart, G. Hon, Y. Fu, C. W. Ching, R. D. Hawkins, L. O. Barrera, S. Van Calcar, C. Qu, K. A. Ching, W. Wang, Z. Weng, R. D. Green, G. E. Crawford, and B. Ren. 2007. Distinct and predictive chromatin signatures of transcriptional promoters and enhancers in the human genome. *Nature genetics* 39: 311-318.
25. Visel, A., M. J. Blow, Z. Li, T. Zhang, J. A. Akiyama, A. Holt, I. Plajzer-Frick, M. Shoukry, C. Wright, F. Chen, V. Afzal, B. Ren, E. M. Rubin, and L. A. Pennacchio. 2009. ChIP-seq accurately predicts tissue-specific activity of enhancers. *Nature* 457: 854-858.

26. Park, S., R. L. Stanfield, M. A. Martinez-Yamout, H. J. Dyson, I. A. Wilson, and P. E. Wright. 2017. Role of the CBP catalytic core in intramolecular SUMOylation and control of histone H3 acetylation. *Proceedings of the National Academy of Sciences of the United States of America* 114: E5335-E5342.
27. Delvecchio, M., J. Gaucher, C. Aguilar-Gurrieri, E. Ortega, and D. Panne. 2013. Structure of the p300 catalytic core and implications for chromatin targeting and HAT regulation. *Nature structural & molecular biology* 20: 1040-1046.
28. Thompson, P. R., D. Wang, L. Wang, M. Fulco, N. Pediconi, D. Zhang, W. An, Q. Ge, R. G. Roeder, J. Wong, M. Levrero, V. Sartorelli, R. J. Cotter, and P. A. Cole. 2004. Regulation of the p300 HAT domain via a novel activation loop. *Nature structural & molecular biology* 11: 308-315.
29. Karanam, B., L. Jiang, L. Wang, N. L. Kelleher, and P. A. Cole. 2006. Kinetic and mass spectrometric analysis of p300 histone acetyltransferase domain autoacetylation. *The Journal of biological chemistry* 281: 40292-40301.
30. Ortega, E., S. Rengachari, Z. Ibrahim, N. Hoghoughi, J. Gaucher, A. S. Holehouse, S. Khochbin, and D. Panne. 2018. Transcription factor dimerization activates the p300 acetyltransferase. *Nature*.
31. Liu, X., L. Wang, K. Zhao, P. R. Thompson, Y. Hwang, R. Marmorstein, and P. A. Cole. 2008. The structural basis of protein acetylation by the p300/CBP transcriptional coactivator. *Nature* 451: 846-850.

32. Black, J. C., J. E. Choi, S. R. Lombardo, and M. Carey. 2006. A mechanism for coordinating chromatin modification and preinitiation complex assembly. *Molecular cell* 23: 809-818.
33. Rack, J. G., T. Lutter, G. E. Kjaereng Bjerga, C. Guder, C. Ehrhardt, S. Varv, M. Ziegler, and R. Aasland. 2014. The PHD finger of p300 influences its ability to acetylate histone and non-histone targets. *Journal of molecular biology* 426: 3960-3972.
34. Shi, X., T. Hong, K. L. Walter, M. Ewalt, E. Michishita, T. Hung, D. Carney, P. Pena, F. Lan, M. R. Kaadige, N. Lacoste, C. Cayrou, F. Davrazou, A. Saha, B. R. Cairns, D. E. Ayer, T. G. Kutateladze, Y. Shi, J. Cote, K. F. Chua, and O. Gozani. 2006. ING2 PHD domain links histone H3 lysine 4 methylation to active gene repression. *Nature* 442: 96-99.
35. Sanchez, R., and M. M. Zhou. 2011. The PHD finger: a versatile epigenome reader. *Trends in biochemical sciences* 36: 364-372.
36. Park, S., M. A. Martinez-Yamout, H. J. Dyson, and P. E. Wright. 2013. The CH2 domain of CBP/p300 is a novel zinc finger. *FEBS letters* 587: 2506-2511.
37. Hammitzsch, A., C. Tallant, O. Fedorov, A. O'Mahony, P. E. Brennan, D. A. Hay, F. O. Martinez, M. H. Al-Mossawi, J. de Wit, M. Vecellio, C. Wells, P. Wordsworth, S. Muller, S. Knapp, and P. Bowness. 2015. CBP30, a selective CBP/p300 bromodomain inhibitor, suppresses human Th17 responses. *Proceedings of the National Academy of Sciences of the United States of America* 112: 10768-10773.

38. Ghosh, S., A. Taylor, M. Chin, H. R. Huang, A. R. Conery, J. A. Mertz, A. Salmeron, P. J. Dakle, D. Mele, A. Cote, H. Jayaram, J. W. Setser, F. Poy, G. Hatzivassiliou, D. DeAlmeida-Nagata, P. Sandy, C. Hatton, F. A. Romero, E. Chiang, T. Reimer, T. Crawford, E. Pardo, V. G. Watson, V. Tsui, A. G. Cochran, L. Zawadzke, J. C. Harmange, J. E. Audia, B. M. Bryant, R. T. Cummings, S. R. Magnuson, J. L. Grogan, S. F. Bellon, B. K. Albrecht, R. J. Sims, 3rd, and J. M. Lora. 2016. Regulatory T Cell Modulation by CBP/EP300 Bromodomain Inhibition. *The Journal of biological chemistry* 291: 13014-13027.
39. Nguyen, U. T., L. Bittova, M. M. Muller, B. Fierz, Y. David, B. Houck-Loomis, V. Feng, G. P. Dann, and T. W. Muir. 2014. Accelerated chromatin biochemistry using DNA-barcoded nucleosome libraries. *Nature methods* 11: 834-840.
40. Kraus, W. L., E. T. Manning, and J. T. Kadonaga. 1999. Biochemical analysis of distinct activation functions in p300 that enhance transcription initiation with chromatin templates. *Molecular and cellular biology* 19: 8123-8135.
41. Tang, Z., W. Y. Chen, M. Shimada, U. T. Nguyen, J. Kim, X. J. Sun, T. Sengoku, R. K. McGinty, J. P. Fernandez, T. W. Muir, and R. G. Roeder. 2013. SET1 and p300 act synergistically, through coupled histone modifications, in transcriptional activation by p53. *Cell* 154: 297-310.
42. Fonte, C., J. Grenier, A. Trousson, A. Chauchereau, O. Lahuna, E. E. Baulieu, M. Schumacher, and C. Massaad. 2005. Involvement of {beta}-

- catenin and unusual behavior of CBP and p300 in glucocorticosteroid signaling in Schwann cells. *Proceedings of the National Academy of Sciences of the United States of America* 102: 14260-14265.
43. Conery, A. R., R. C. Centore, A. Neiss, P. J. Keller, S. Joshi, K. L. Spillane, P. Sandy, C. Hatton, E. Pardo, L. Zawadzke, A. Bommi-Reddy, K. E. Gascoigne, B. M. Bryant, J. A. Mertz, and R. J. Sims. 2016. Bromodomain inhibition of the transcriptional coactivators CBP/EP300 as a therapeutic strategy to target the IRF4 network in multiple myeloma. *eLife* 5.
44. Chakravarti, D., V. J. LaMorte, M. C. Nelson, T. Nakajima, I. G. Schulman, H. Juguilon, M. Montminy, and R. M. Evans. 1996. Role of CBP/P300 in nuclear receptor signalling. *Nature* 383: 99-103.
45. Goodman, R. H., and S. Smolik. 2000. CBP/p300 in cell growth, transformation, and development. *Genes & development* 14: 1553-1577.
46. Wang, F., C. B. Marshall, and M. Ikura. 2013. Transcriptional/epigenetic regulator CBP/p300 in tumorigenesis: structural and functional versatility in target recognition. *Cellular and molecular life sciences : CMLS* 70: 3989-4008.
47. Mayr, B., and M. Montminy. 2001. Transcriptional regulation by the phosphorylation-dependent factor CREB. *Nature reviews. Molecular cell biology* 2: 599-609.
48. Kwok, R. P., J. R. Lundblad, J. C. Chrivia, J. P. Richards, H. P. Bachinger, R. G. Brennan, S. G. Roberts, M. R. Green, and R. H. Goodman. 1994.

- Nuclear protein CBP is a coactivator for the transcription factor CREB.
Nature 370: 223-226.
49. Radhakrishnan, I., G. C. Perez-Alvarado, D. Parker, H. J. Dyson, M. R. Montminy, and P. E. Wright. 1997. Solution structure of the KIX domain of CBP bound to the transactivation domain of CREB: a model for activator:coactivator interactions. *Cell* 91: 741-752.
 50. Berk, A. J. 2005. Recent lessons in gene expression, cell cycle control, and cell biology from adenovirus. *Oncogene* 24: 7673-7685.
 51. Hamamori, Y., V. Sartorelli, V. Ogryzko, P. L. Puri, H. Y. Wu, J. Y. Wang, Y. Nakatani, and L. Kedes. 1999. Regulation of histone acetyltransferases p300 and PCAF by the bHLH protein twist and adenoviral oncoprotein E1A. *Cell* 96: 405-413.
 52. Chakravarti, D., V. Ogryzko, H. Y. Kao, A. Nash, H. Chen, Y. Nakatani, and R. M. Evans. 1999. A viral mechanism for inhibition of p300 and PCAF acetyltransferase activity. *Cell* 96: 393-403.
 53. Perissi, V., J. S. Dasen, R. Kurokawa, Z. Wang, E. Korkus, D. W. Rose, C. K. Glass, and M. G. Rosenfeld. 1999. Factor-specific modulation of CREB-binding protein acetyltransferase activity. *Proceedings of the National Academy of Sciences of the United States of America* 96: 3652-3657.
 54. Madison, D. L., P. Yaciuk, R. P. Kwok, and J. R. Lundblad. 2002. Acetylation of the adenovirus-transforming protein E1A determines

- nuclear localization by disrupting association with importin-alpha. *The Journal of biological chemistry* 277: 38755-38763.
55. Saint Just Ribeiro, M., M. L. Hansson, and A. E. Wallberg. 2007. A proline repeat domain in the Notch co-activator MAML1 is important for the p300-mediated acetylation of MAML1. *The Biochemical journal* 404: 289-298.
 56. Hansson, M. L., A. E. Popko-Scibor, M. Saint Just Ribeiro, B. M. Dancy, M. J. Lindberg, P. A. Cole, and A. E. Wallberg. 2009. The transcriptional coactivator MAML1 regulates p300 autoacetylation and HAT activity. *Nucleic acids research* 37: 2996-3006.
 57. Fryer, C. J., E. Lamar, I. Turbachova, C. Kintner, and K. A. Jones. 2002. Mastermind mediates chromatin-specific transcription and turnover of the Notch enhancer complex. *Genes & development* 16: 1397-1411.
 58. Bose, D. A., G. Donahue, D. Reinberg, R. Shiekhattar, R. Bonasio, and S. L. Berger. 2017. RNA Binding to CBP Stimulates Histone Acetylation and Transcription. *Cell* 168: 135-149 e122.
 59. Kim, T. K., M. Hemberg, J. M. Gray, A. M. Costa, D. M. Bear, J. Wu, D. A. Harmin, M. Laptewicz, K. Barbara-Haley, S. Kuersten, E. Markenscoff-Papadimitriou, D. Kuhl, H. Bito, P. F. Worley, G. Kreiman, and M. E. Greenberg. 2010. Widespread transcription at neuronal activity-regulated enhancers. *Nature* 465: 182-187.
 60. Huang, W. C., and C. C. Chen. 2005. Akt phosphorylation of p300 at Ser-1834 is essential for its histone acetyltransferase and transcriptional activity. *Molecular and cellular biology* 25: 6592-6602.

61. Chen, Y. J., Y. N. Wang, and W. C. Chang. 2007. ERK2-mediated C-terminal serine phosphorylation of p300 is vital to the regulation of epidermal growth factor-induced keratin 16 gene expression. *The Journal of biological chemistry* 282: 27215-27228.
62. Wan, W., Z. You, Y. Xu, L. Zhou, Z. Guan, C. Peng, C. C. L. Wong, H. Su, T. Zhou, H. Xia, and W. Liu. 2017. mTORC1 Phosphorylates Acetyltransferase p300 to Regulate Autophagy and Lipogenesis. *Molecular cell* 68: 323-335 e326.
63. Yuan, L. W., J. W. Soh, and I. B. Weinstein. 2002. Inhibition of histone acetyltransferase function of p300 by PKCdelta. *Biochimica et biophysica acta* 1592: 205-211.
64. Jang, E. R., J. D. Choi, G. Jeong, and J. S. Lee. 2010. Phosphorylation of p300 by ATM controls the stability of NBS1. *Biochemical and biophysical research communications* 397: 637-643.
65. Wang, Q. E., C. Han, R. Zhao, G. Wani, Q. Zhu, L. Gong, A. Battu, I. Racoma, N. Sharma, and A. A. Wani. 2013. p38 MAPK- and Akt-mediated p300 phosphorylation regulates its degradation to facilitate nucleotide excision repair. *Nucleic acids research* 41: 1722-1733.
66. Lee, Y. H., S. A. Coonrod, W. L. Kraus, M. A. Jelinek, and M. R. Stallcup. 2005. Regulation of coactivator complex assembly and function by protein arginine methylation and demethylation. *Proceedings of the National Academy of Sciences of the United States of America* 102: 3611-3616.

67. Xu, W., H. Chen, K. Du, H. Asahara, M. Tini, B. M. Emerson, M. Montminy, and R. M. Evans. 2001. A transcriptional switch mediated by cofactor methylation. *Science* 294: 2507-2511.
68. Chevillard-Briet, M., D. Trouche, and L. Vandel. 2002. Control of CBP co-activating activity by arginine methylation. *The EMBO journal* 21: 5457-5466.
69. Ceschin, D. G., M. Walia, S. S. Wenk, C. Duboe, C. Gaudon, Y. Xiao, L. Fauquier, M. Sankar, L. Vandel, and H. Gronemeyer. 2011. Methylation specifies distinct estrogen-induced binding site repertoires of CBP to chromatin. *Genes & development* 25: 1132-1146.
70. Girdwood, D., D. Bumpass, O. A. Vaughan, A. Thain, L. A. Anderson, A. W. Snowden, E. Garcia-Wilson, N. D. Perkins, and R. T. Hay. 2003. P300 transcriptional repression is mediated by SUMO modification. *Molecular cell* 11: 1043-1054.
71. Kuo, H. Y., C. C. Chang, J. C. Jeng, H. M. Hu, D. Y. Lin, G. G. Maul, R. P. Kwok, and H. M. Shih. 2005. SUMO modification negatively modulates the transcriptional activity of CREB-binding protein via the recruitment of Daxx. *Proceedings of the National Academy of Sciences of the United States of America* 102: 16973-16978.
72. Tanaka, Y., I. Naruse, T. Hongo, M. Xu, T. Nakahata, T. Maekawa, and S. Ishii. 2000. Extensive brain hemorrhage and embryonic lethality in a mouse null mutant of CREB-binding protein. *Mech Dev* 95: 133-145.

73. Yao, T. P., S. P. Oh, M. Fuchs, N. D. Zhou, L. E. Ch'ng, D. Newsome, R. T. Bronson, E. Li, D. M. Livingston, and R. Eckner. 1998. Gene dosage-dependent embryonic development and proliferation defects in mice lacking the transcriptional integrator p300. *Cell* 93: 361-372.
74. Oike, Y., N. Takakura, A. Hata, T. Kaname, M. Akizuki, Y. Yamaguchi, H. Yasue, K. Araki, K. Yamamura, and T. Suda. 1999. Mice homozygous for a truncated form of CREB-binding protein exhibit defects in hematopoiesis and vasculo-angiogenesis. *Blood* 93: 2771-2779.
75. Kung, A. L., V. I. Rebel, R. T. Bronson, L. E. Ch'ng, C. A. Sieff, D. M. Livingston, and T. P. Yao. 2000. Gene dose-dependent control of hematopoiesis and hematologic tumor suppression by CBP. *Genes & development* 14: 272-277.
76. Tanaka, Y., I. Naruse, T. Maekawa, H. Masuya, T. Shiroishi, and S. Ishii. 1997. Abnormal skeletal patterning in embryos lacking a single Cbp allele: a partial similarity with Rubinstein-Taybi syndrome. *Proceedings of the National Academy of Sciences of the United States of America* 94: 10215-10220.
77. Petrij, F., R. H. Giles, H. G. Dauwerse, J. J. Saris, R. C. Hennekam, M. Masuno, N. Tommerup, G. J. van Ommen, R. H. Goodman, D. J. Peters, and et al. 1995. Rubinstein-Taybi syndrome caused by mutations in the transcriptional co-activator CBP. *Nature* 376: 348-351.
78. Solomon, B. D., D. L. Bodian, A. Khromykh, G. G. Mora, B. C. Lanpher, R. K. Iyer, R. Baveja, J. G. Vockley, and J. E. Niederhuber. 2015. Expanding

- the phenotypic spectrum in EP300-related Rubinstein-Taybi syndrome. *American journal of medical genetics. Part A* 167: 1111-1116.
79. Rubinstein, J. H., and H. Taybi. 1963. Broad thumbs and toes and facial abnormalities. A possible mental retardation syndrome. *Am J Dis Child* 105: 588-608.
80. Oike, Y., A. Hata, T. Mamiya, T. Kaname, Y. Noda, M. Suzuki, H. Yasue, T. Nabeshima, K. Araki, and K. Yamamura. 1999. Truncated CBP protein leads to classical Rubinstein-Taybi syndrome phenotypes in mice: implications for a dominant-negative mechanism. *Human molecular genetics* 8: 387-396.
81. Kasper, L. H., F. Boussouar, P. A. Ney, C. W. Jackson, J. Rehg, J. M. van Deursen, and P. K. Brindle. 2002. A transcription-factor-binding surface of coactivator p300 is required for haematopoiesis. *Nature* 419: 738-743.
82. Rebel, V. I., A. L. Kung, E. A. Tanner, H. Yang, R. T. Bronson, and D. M. Livingston. 2002. Distinct roles for CREB-binding protein and p300 in hematopoietic stem cell self-renewal. *Proceedings of the National Academy of Sciences of the United States of America* 99: 14789-14794.
83. Korzus, E., M. G. Rosenfeld, and M. Mayford. 2004. CBP histone acetyltransferase activity is a critical component of memory consolidation. *Neuron* 42: 961-972.
84. Alarcon, J. M., G. Malleret, K. Touzani, S. Vronskaya, S. Ishii, E. R. Kandel, and A. Barco. 2004. Chromatin acetylation, memory, and LTP are

- impaired in CBP+/- mice: a model for the cognitive deficit in Rubinstein-Taybi syndrome and its amelioration. *Neuron* 42: 947-959.
85. Barrett, R. M., M. Malvaez, E. Kramar, D. P. Matheos, A. Arrizon, S. M. Cabrera, G. Lynch, R. W. Greene, and M. A. Wood. 2011. Hippocampal focal knockout of CBP affects specific histone modifications, long-term potentiation, and long-term memory. *Neuropsychopharmacology : official publication of the American College of Neuropsychopharmacology* 36: 1545-1556.
86. Korzus, E. 2017. Rubinstein-Taybi Syndrome and Epigenetic Alterations. *Advances in experimental medicine and biology* 978: 39-62.
87. Martincorena, I., and P. J. Campbell. 2015. Somatic mutation in cancer and normal cells. *Science* 349: 1483-1489.
88. Gayther, S. A., S. J. Batley, L. Linger, A. Bannister, K. Thorpe, S. F. Chin, Y. Daigo, P. Russell, A. Wilson, H. M. Sowter, J. D. Delhanty, B. A. Ponder, T. Kouzarides, and C. Caldas. 2000. Mutations truncating the EP300 acetylase in human cancers. *Nature genetics* 24: 300-303.
89. Bryan, E. J., V. J. Jokubaitis, N. L. Chamberlain, S. W. Baxter, E. Dawson, D. Y. Choong, and I. G. Campbell. 2002. Mutation analysis of EP300 in colon, breast and ovarian carcinomas. *International journal of cancer. Journal international du cancer* 102: 137-141.
90. Kishimoto, M., T. Kohno, K. Okudela, A. Otsuka, H. Sasaki, C. Tanabe, T. Sakiyama, C. Hirama, I. Kitabayashi, J. D. Minna, S. Takenoshita, and J. Yokota. 2005. Mutations and deletions of the CBP gene in human lung

- cancer. *Clinical cancer research : an official journal of the American Association for Cancer Research* 11: 512-519.
91. Li, Y. Y., G. J. Hanna, A. C. Laga, R. I. Haddad, J. H. Lorch, and P. S. Hammerman. 2015. Genomic analysis of metastatic cutaneous squamous cell carcinoma. *Clinical cancer research : an official journal of the American Association for Cancer Research* 21: 1447-1456.
92. Pasqualucci, L., D. Dominguez-Sola, A. Chiarenza, G. Fabbri, A. Grunn, V. Trifonov, L. H. Kasper, S. Lerach, H. Tang, J. Ma, D. Rossi, A. Chadburn, V. V. Murty, C. G. Mullighan, G. Gaidano, R. Rabadan, P. K. Brindle, and R. Dalla-Favera. 2011. Inactivating mutations of acetyltransferase genes in B-cell lymphoma. *Nature* 471: 189-195.
93. Morin, R. D., M. Mendez-Lago, A. J. Mungall, R. Goya, K. L. Mungall, R. D. Corbett, N. A. Johnson, T. M. Severson, R. Chiu, M. Field, S. Jackman, M. Krzywinski, D. W. Scott, D. L. Trinh, J. Tamura-Wells, S. Li, M. R. Firme, S. Rogic, M. Griffith, S. Chan, O. Yakovenko, I. M. Meyer, E. Y. Zhao, D. Smailus, M. Moksa, S. Chittaranjan, L. Rimsza, A. Brooks-Wilson, J. J. Spinelli, S. Ben-Neriah, B. Meissner, B. Woolcock, M. Boyle, H. McDonald, A. Tam, Y. Zhao, A. Delaney, T. Zeng, K. Tse, Y. Butterfield, I. Birol, R. Holt, J. Schein, D. E. Horsman, R. Moore, S. J. Jones, J. M. Connors, M. Hirst, R. D. Gascoyne, and M. A. Marra. 2011. Frequent mutation of histone-modifying genes in non-Hodgkin lymphoma. *Nature* 476: 298-303.

94. Haery, L., J. G. Lugo-Pico, R. A. Henry, A. J. Andrews, and T. D. Gilmore. 2014. Histone acetyltransferase-deficient p300 mutants in diffuse large B cell lymphoma have altered transcriptional regulatory activities and are required for optimal cell growth. *Molecular cancer* 13: 29.
95. Peifer, M., L. Fernandez-Cuesta, M. L. Sos, J. George, D. Seidel, L. H. Kasper, D. Plenker, F. Leenders, R. Sun, T. Zander, R. Menon, M. Koker, I. Dahmen, C. Muller, V. Di Cerbo, H. U. Schildhaus, J. Altmuller, I. Baessmann, C. Becker, B. de Wilde, J. Vandesompele, D. Bohm, S. Ansen, F. Gabler, I. Wilkening, S. Heynck, J. M. Heuckmann, X. Lu, S. L. Carter, K. Cibulskis, S. Banerji, G. Getz, K. S. Park, D. Rauh, C. Grutter, M. Fischer, L. Pasqualucci, G. Wright, Z. Wainer, P. Russell, I. Petersen, Y. Chen, E. Stoelben, C. Ludwig, P. Schnabel, H. Hoffmann, T. Muley, M. Brockmann, W. Engel-Riedel, L. A. Muscarella, V. M. Fazio, H. Groen, W. Timens, H. Sietsma, E. Thunnissen, E. Smit, D. A. Heideman, P. J. Snijders, F. Cappuzzo, C. Ligorio, S. Damiani, J. Field, S. Solberg, O. T. Brustugun, M. Lund-Iversen, J. Sanger, J. H. Clement, A. Soltermann, H. Moch, W. Weder, B. Solomon, J. C. Soria, P. Validire, B. Besse, E. Brambilla, C. Brambilla, S. Lantuejoul, P. Lorimier, P. M. Schneider, M. Hallek, W. Pao, M. Meyerson, J. Sage, J. Shendure, R. Schneider, R. Buttner, J. Wolf, P. Nurnberg, S. Perner, L. C. Heukamp, P. K. Brindle, S. Haas, and R. K. Thomas. 2012. Integrative genome analyses identify key somatic driver mutations of small-cell lung cancer. *Nature genetics* 44: 1104-1110.

96. Sobulo, O. M., J. Borrow, R. Tomek, S. Reshmi, A. Harden, B. Schlegelberger, D. Housman, N. A. Doggett, J. D. Rowley, and N. J. ZeleznikLe. 1997. MLL is fused to CBP, a histone acetyltransferase, in therapy-related acute myeloid leukemia with a t(11;16)(q23;p13.3). *Proceedings of the National Academy of Sciences of the United States of America* 94: 8732-8737.
97. Rowley, J. D., S. Reshmi, O. Sobulo, T. Musvee, J. Anastasi, S. Raimondi, N. R. Schneider, J. C. Barredo, E. S. Cantu, B. Schlegelberger, F. Behm, N. A. Doggett, J. Borrow, and N. ZeleznikLe. 1997. All patients with the T(11;16)(q23;p13.3) that involves MLL and CBP have treatment-related hematologic disorders. *Blood* 90: 535-541.
98. Ida, K., I. Kitabayashi, T. Taki, M. Taniwaki, K. Noro, M. Yamamoto, M. Ohki, and Y. Hayashi. 1997. Adenoviral E1A-associated protein p300 is involved in acute myeloid leukemia with t(11;22)(q23;q13). *Blood* 90: 4699-4704.
99. Giles, R. H., J. G. Dauwerse, C. Higgins, F. Petrij, J. W. Wessels, G. C. Beverstock, H. Dohner, M. Jotterand-Bellomo, J. H. F. Falkenburg, R. M. Slater, G. J. B. van Ommen, A. Hagemeijer, B. A. van der Reijden, and M. H. Breuning. 1997. Detection of CBP rearrangements in acute myelogenous leukemia with t(8;16). *Leukemia* 11: 2087-2096.
100. Kitabayashi, I., Y. Aikawa, A. Yokoyama, F. Hosoda, M. Nagai, N. Kakazu, T. Abe, and M. Ohki. 2001. Fusion of MOZ and p300 histone

- acetyltransferases in acute monocytic leukemia with a t(8;22)(p11;q13) chromosome translocation. *Leukemia* 15: 89-94.
101. Ionov, Y., S. Matsui, and J. K. Cowell. 2004. A role for p300/CREB binding protein genes in promoting cancer progression in colon cancer cell lines with microsatellite instability. *Proceedings of the National Academy of Sciences of the United States of America* 101: 1273-1278.
102. Iyer, N. G., S. F. Chin, H. Ozdag, Y. Daigo, D. E. Hu, M. Cariati, K. Brindle, S. Aparicio, and C. Caldas. 2004. p300 regulates p53-dependent apoptosis after DNA damage in colorectal cancer cells by modulation of PUMA/p21 levels. *Proceedings of the National Academy of Sciences of the United States of America* 101: 7386-7391.
103. Jiang, Y., A. Ortega-Molina, H. Geng, H. Y. Ying, K. Hatzi, S. Parsa, D. McNally, L. Wang, A. S. Doane, X. Agirre, M. Teater, C. Meydan, Z. Li, D. Poloway, S. Wang, D. Ennishi, D. W. Scott, K. R. Stengel, J. E. Kranz, E. Holson, S. Sharma, J. W. Young, C. S. Chu, R. G. Roeder, R. Shaknovich, S. W. Hiebert, R. D. Gascoyne, W. Tam, O. Elemento, H. G. Wendel, and A. M. Melnick. 2017. CREBBP Inactivation Promotes the Development of HDAC3-Dependent Lymphomas. *Cancer discovery* 7: 38-53.
104. Zhang, J., S. Vlasevska, V. A. Wells, S. Nataraj, A. B. Holmes, R. Duval, S. N. Meyer, T. Mo, K. Basso, P. K. Brindle, S. Hussein, R. Dalla-Favera, and L. Pasqualucci. 2017. The CREBBP Acetyltransferase Is a

- Haploinsufficient Tumor Suppressor in B-cell Lymphoma. *Cancer discovery*.
105. Horton, S. J., G. Giotopoulos, H. Yun, S. Vohra, O. Sheppard, R. Bashford-Rogers, M. Rashid, A. Clipson, W. I. Chan, D. Sasca, L. Yiangou, H. Osaki, F. Basheer, P. Gallipoli, N. Burrows, A. Erdem, A. Sybirna, S. Foerster, W. Zhao, T. Sustic, A. Petrunkina Harrison, E. Laurenti, J. Okosun, D. Hodson, P. Wright, K. G. Smith, P. Maxwell, J. Fitzgibbon, M. Q. Du, D. J. Adams, and B. J. P. Huntly. 2017. Early loss of Crebbp confers malignant stem cell properties on lymphoid progenitors. *Nature cell biology* 19: 1093-1104.
 106. Garcia-Ramirez, I., S. Tadros, I. Gonzalez-Herrero, A. Martin-Lorenzo, G. Rodriguez-Hernandez, D. Moore, L. Ruiz-Roca, O. Blanco, D. Alonso-Lopez, J. L. Rivas, K. Hartert, R. Duval, D. Klinkebiel, M. Bast, J. Vose, M. Lunning, K. Fu, T. Greiner, F. Rodrigues-Lima, R. Jimenez, F. J. G. Criado, M. B. G. Cenador, P. Brindle, C. Vicente-Duenas, A. Alizadeh, I. Sanchez-Garcia, and M. R. Green. 2017. Crebbp loss cooperates with Bcl2 overexpression to promote lymphoma in mice. *Blood* 129: 2645-2656.
 107. Okosun, J., C. Bodor, J. Wang, S. Araf, C. Y. Yang, C. Pan, S. Boller, D. Cittaro, M. Bozek, S. Iqbal, J. Matthews, D. Wrench, J. Marzec, K. Tawana, N. Popov, C. O'Riain, D. O'Shea, E. Carlotti, A. Davies, C. H. Lawrie, A. Matolcsy, M. Calaminici, A. Norton, R. J. Byers, C. Mein, E. Stupka, T. A. Lister, G. Lenz, S. Montoto, J. G. Gribben, Y. Fan, R.

- Grosschedl, C. Chelala, and J. Fitzgibbon. 2014. Integrated genomic analysis identifies recurrent mutations and evolution patterns driving the initiation and progression of follicular lymphoma. *Nature genetics* 46: 176-181.
108. Debes, J. D., T. J. Sebo, C. M. Lohse, L. M. Murphy, D. A. Haugen, and D. J. Tindall. 2003. p300 in prostate cancer proliferation and progression. *Cancer research* 63: 7638-7640.
109. Yokomizo, C., K. Yamaguchi, Y. Itoh, T. Nishimura, A. Umemura, M. Minami, K. Yasui, H. Mitsuyoshi, H. Fujii, N. Tochiki, T. Nakajima, T. Okanoue, and T. Yoshikawa. 2011. High expression of p300 in HCC predicts shortened overall survival in association with enhanced epithelial mesenchymal transition of HCC cells. *Cancer Lett* 310: 140-147.
110. Hou, X., Y. Li, R. Z. Luo, J. H. Fu, J. H. He, L. J. Zhang, and H. X. Yang. 2012. High expression of the transcriptional co-activator p300 predicts poor survival in resectable non-small cell lung cancers. *European journal of surgical oncology : the journal of the European Society of Surgical Oncology and the British Association of Surgical Oncology* 38: 523-530.
111. Gao, Y., J. Geng, X. Hong, J. Qi, Y. Teng, Y. Yang, D. Qu, and G. Chen. 2014. Expression of p300 and CBP is associated with poor prognosis in small cell lung cancer. *International journal of clinical and experimental pathology* 7: 760-767.
112. Zhong, J., L. Ding, L. R. Bohrer, Y. Pan, P. Liu, J. Zhang, T. J. Sebo, R. J. Karnes, D. J. Tindall, J. van Deursen, and H. Huang. 2014. p300

- acetyltransferase regulates androgen receptor degradation and PTEN-deficient prostate tumorigenesis. *Cancer research* 74: 1870-1880.
113. Ianculescu, I., D. Y. Wu, K. D. Siegmund, and M. R. Stallcup. 2012. Selective roles for cAMP response element-binding protein binding protein and p300 protein as coregulators for androgen-regulated gene expression in advanced prostate cancer cells. *The Journal of biological chemistry* 287: 4000-4013.
114. Lee, J. H., B. Yang, A. J. Lindahl, N. Damaschke, M. D. Boersma, W. Huang, E. Corey, D. F. Jarrard, and J. M. Denu. 2017. Identifying Dysregulated Epigenetic Enzyme Activity in Castrate-Resistant Prostate Cancer Development. *ACS chemical biology* 12: 2804-2814.
115. Giotopoulos, G., W. I. Chan, S. J. Horton, D. Ruau, P. Gallipoli, A. Fowler, C. Crawley, E. Papaemmanuil, P. J. Campbell, B. Gottgens, J. M. Van Deursen, P. A. Cole, and B. J. Huntly. 2016. The epigenetic regulators CBP and p300 facilitate leukemogenesis and represent therapeutic targets in acute myeloid leukemia. *Oncogene* 35: 279-289.
116. Pattabiraman, D. R., J. Sun, D. H. Dowhan, S. Ishii, and T. J. Gonda. 2009. Mutations in multiple domains of c-Myb disrupt interaction with CBP/p300 and abrogate myeloid transforming ability. *Mol Cancer Res* 7: 1477-1486.
117. Pattabiraman, D. R., C. McGirr, K. Shakhbazov, V. Barbier, K. Krishnan, P. Mukhopadhyay, P. Hawthorne, A. Trezise, J. Ding, S. M. Grimmond, P. Papathanasiou, W. S. Alexander, A. C. Perkins, J. P. Levesque, I. G.

- Winkler, and T. J. Gonda. 2014. Interaction of c-Myb with p300 is required for the induction of acute myeloid leukemia (AML) by human AML oncogenes. *Blood* 123: 2682-2690.
118. Picaud, S., O. Fedorov, A. Thanasopoulou, K. Leonards, K. Jones, J. Meier, H. Olzscha, O. Monteiro, S. Martin, M. Philpott, A. Tumber, P. Filippakopoulos, C. Yapp, C. Wells, K. H. Che, A. Bannister, S. Robson, U. Kumar, N. Parr, K. Lee, D. Lugo, P. Jeffrey, S. Taylor, M. L. Vecellio, C. Bountra, P. E. Brennan, A. O'Mahony, S. Velichko, S. Muller, D. Hay, D. L. Daniels, M. Urh, N. B. La Thangue, T. Kouzarides, R. Prinjha, J. Schwaller, and S. Knapp. 2015. Generation of a Selective Small Molecule Inhibitor of the CBP/p300 Bromodomain for Leukemia Therapy. *Cancer research* 75: 5106-5119.
119. Cerami, E., J. Gao, U. Dogrusoz, B. E. Gross, S. O. Sumer, B. A. Aksoy, A. Jacobsen, C. J. Byrne, M. L. Heuer, E. Larsson, Y. Antipin, B. Reva, A. P. Goldberg, C. Sander, and N. Schultz. 2012. The cBio cancer genomics portal: an open platform for exploring multidimensional cancer genomics data. *Cancer discovery* 2: 401-404.
120. Gao, J., B. A. Aksoy, U. Dogrusoz, G. Dresdner, B. Gross, S. O. Sumer, Y. Sun, A. Jacobsen, R. Sinha, E. Larsson, E. Cerami, C. Sander, and N. Schultz. 2013. Integrative analysis of complex cancer genomics and clinical profiles using the cBioPortal. *Sci Signal* 6: pl1.
121. Legge, G. B., M. A. Martinez-Yamout, D. M. Hambly, T. Trinh, B. M. Lee, H. J. Dyson, and P. E. Wright. 2004. ZZ domain of CBP: an unusual zinc

- finger fold in a protein interaction module. *Journal of molecular biology* 343: 1081-1093.
122. Ponting, C. P., D. J. Blake, K. E. Davies, J. Kendrick-Jones, and S. J. Winder. 1996. ZZ and TAZ: new putative zinc fingers in dystrophin and other proteins. *Trends in biochemical sciences* 21: 11-13.
123. Barresi, R., and K. P. Campbell. 2006. Dystroglycan: from biosynthesis to pathogenesis of human disease. *Journal of cell science* 119: 199-207.
124. Ishikawa-Sakurai, M., M. Yoshida, M. Imamura, K. E. Davies, and E. Ozawa. 2004. ZZ domain is essentially required for the physiological binding of dystrophin and utrophin to beta-dystroglycan. *Human molecular genetics* 13: 693-702.
125. Sanz, L., M. T. Diaz-Meco, H. Nakano, and J. Moscat. 2000. The atypical PKC-interacting protein p62 channels NF-kappaB activation by the IL-1-TRAF6 pathway. *The EMBO journal* 19: 1576-1586.
126. Danielsen, J. R., L. K. Povlsen, B. H. Villumsen, W. Streicher, J. Nilsson, M. Wikstrom, S. Bekker-Jensen, and N. Mailand. 2012. DNA damage-inducible SUMOylation of HERC2 promotes RNF8 binding via a novel SUMO-binding Zinc finger. *J Cell Biol* 197: 179-187.
127. Diehl, C., M. Akke, S. Bekker-Jensen, N. Mailand, W. Streicher, and M. Wikstrom. 2016. Structural analysis of a complex between small ubiquitin-like modifier 1 (SUMO1) and the ZZ domain of CREB-binding Protein (CBP/p300) reveals a new interaction surface on SUMO. *The Journal of biological chemistry*.

128. Semenova, E. A., R. Nagel, and A. Berns. 2015. Origins, genetic landscape, and emerging therapies of small cell lung cancer. *Genes & development* 29: 1447-1462.
129. Kato, Y., T. B. Ferguson, D. E. Bennett, and T. H. Burford. 1969. Oat cell carcinoma of the lung. A review of 138 cases. *Cancer* 23: 517-524.
130. Sutherland, K. D., N. Proost, I. Brouns, D. Adriaensen, J. Y. Song, and A. Berns. 2011. Cell of origin of small cell lung cancer: inactivation of Trp53 and Rb1 in distinct cell types of adult mouse lung. *Cancer cell* 19: 754-764.
131. Park, K. S., M. C. Liang, D. M. Raiser, R. Zamponi, R. R. Roach, S. J. Curtis, Z. Walton, B. E. Schaffer, C. M. Roake, A. F. Zmoos, C. Kriegel, K. K. Wong, J. Sage, and C. F. Kim. 2011. Characterization of the cell of origin for small cell lung cancer. *Cell cycle* 10: 2806-2815.
132. Micke, P., A. Faldum, T. Metz, K. M. Beeh, F. Bittinger, J. G. Hengstler, and R. Buhl. 2002. Staging small cell lung cancer: Veterans Administration Lung Study Group versus International Association for the Study of Lung Cancer--what limits limited disease? *Lung Cancer* 37: 271-276.
133. Kalemkerian, G. P., W. Akerley, P. Bogner, H. Borghaei, L. Q. Chow, R. J. Downey, L. Gandhi, A. K. Ganti, R. Govindan, J. C. Greco, J. Hayman, R. S. Heist, L. Horn, T. Jahan, M. Koczywas, B. W. Loo, Jr., R. E. Merritt, C. A. Moran, H. B. Niell, J. O'Malley, J. D. Patel, N. Ready, C. M. Rudin, C. C. Williams, Jr., K. Gregory, M. Hughes, and N. National

- Comprehensive Cancer. 2013. Small cell lung cancer. *Journal of the National Comprehensive Cancer Network : JNCCN* 11: 78-98.
134. Byers, L. A., and C. M. Rudin. 2015. Small cell lung cancer: where do we go from here? *Cancer* 121: 664-672.
135. Toyooka, S., T. Tsuda, and A. F. Gazdar. 2003. The TP53 gene, tobacco exposure, and lung cancer. *Hum Mutat* 21: 229-239.
136. George, J., J. S. Lim, S. J. Jang, Y. Cun, L. Ozretic, G. Kong, F. Leenders, X. Lu, L. Fernandez-Cuesta, G. Bosco, C. Muller, I. Dahmen, N. S. Jahchan, K. S. Park, D. Yang, A. N. Karnezis, D. Vaka, A. Torres, M. S. Wang, J. O. Korbil, R. Menon, S. M. Chun, D. Kim, M. Wilkerson, N. Hayes, D. Engelmann, B. Putzer, M. Bos, S. Michels, I. Vlastic, D. Seidel, B. Pinther, P. Schaub, C. Becker, J. Altmuller, J. Yokota, T. Kohno, R. Iwakawa, K. Tsuta, M. Noguchi, T. Muley, H. Hoffmann, P. A. Schnabel, I. Petersen, Y. Chen, A. Soltermann, V. Tischler, C. M. Choi, Y. H. Kim, P. P. Massion, Y. Zou, D. Jovanovic, M. Kontic, G. M. Wright, P. A. Russell, B. Solomon, I. Koch, M. Lindner, L. A. Muscarella, A. la Torre, J. K. Field, M. Jakopovic, J. Knezevic, E. Castanos-Velez, L. Roz, U. Pastorino, O. T. Brustugun, M. Lund-Iversen, E. Thunnissen, J. Kohler, M. Schuler, J. Botling, M. Sandelin, M. Sanchez-Cespedes, H. B. Salvesen, V. Achter, U. Lang, M. Bogus, P. M. Schneider, T. Zander, S. Ansen, M. Hallek, J. Wolf, M. Vingron, Y. Yatabe, W. D. Travis, P. Nurnberg, C. Reinhardt, S. Perner, L. Heukamp, R. Buttner, S. A. Haas, E. Brambilla, M. Peifer, J.

- Sage, and R. K. Thomas. 2015. Comprehensive genomic profiles of small cell lung cancer. *Nature* 524: 47-53.
137. Rudin, C. M., S. Durinck, E. W. Stawiski, J. T. Poirier, Z. Modrusan, D. S. Shames, E. A. Bergbower, Y. Guan, J. Shin, J. Guillory, C. S. Rivers, C. K. Foo, D. Bhatt, J. Stinson, F. Gnad, P. M. Haverty, R. Gentleman, S. Chaudhuri, V. Janakiraman, B. S. Jaiswal, C. Parikh, W. Yuan, Z. Zhang, H. Koeppen, T. D. Wu, H. M. Stern, R. L. Yauch, K. E. Huffman, D. D. Paskulin, P. B. Illei, M. Varella-Garcia, A. F. Gazdar, F. J. de Sauvage, R. Bourgon, J. D. Minna, M. V. Brock, and S. Seshagiri. 2012. Comprehensive genomic analysis identifies SOX2 as a frequently amplified gene in small-cell lung cancer. *Nature genetics* 44: 1111-1116.
138. Kiefer, P. E., G. Bepler, M. Kubasch, and K. Havemann. 1987. Amplification and expression of protooncogenes in human small cell lung cancer cell lines. *Cancer research* 47: 6236-6242.
139. Krystal, G., M. Birrer, J. Way, M. Nau, E. Sausville, C. Thompson, J. Minna, and J. Battey. 1988. Multiple mechanisms for transcriptional regulation of the myc gene family in small-cell lung cancer. *Molecular and cellular biology* 8: 3373-3381.
140. Umemura, S., S. Mimaki, H. Makinoshima, S. Tada, G. Ishii, H. Ohmatsu, S. Niho, K. Yoh, S. Matsumoto, A. Takahashi, M. Morise, Y. Nakamura, A. Ochiai, K. Nagai, R. Iwakawa, T. Kohno, J. Yokota, Y. Ohe, H. Esumi, K. Tsuchihara, and K. Goto. 2014. Therapeutic priority of the

- PI3K/AKT/mTOR pathway in small cell lung cancers as revealed by a comprehensive genomic analysis. *J Thorac Oncol* 9: 1324-1331.
141. Ross, J. S., K. Wang, O. R. Elkadi, A. Tarasen, L. Foulke, C. E. Sheehan, G. A. Otto, G. Palmer, R. Yelensky, D. Lipson, J. Chmielecki, S. M. Ali, J. Elvin, D. Morosini, V. A. Miller, and P. J. Stephens. 2014. Next-generation sequencing reveals frequent consistent genomic alterations in small cell undifferentiated lung cancer. *Journal of clinical pathology* 67: 772-776.
142. Byers, L. A., J. Wang, M. B. Nilsson, J. Fujimoto, P. Saintigny, J. Yordy, U. Giri, M. Peyton, Y. H. Fan, L. Diao, F. Masrourpour, L. Shen, W. Liu, B. Duchemann, P. Tumula, V. Bhardwaj, J. Welsh, S. Weber, B. S. Glisson, N. Kalhor, Wistuba, II, L. Girard, S. M. Lippman, G. B. Mills, K. R. Coombes, J. N. Weinstein, J. D. Minna, and J. V. Heymach. 2012. Proteomic profiling identifies dysregulated pathways in small cell lung cancer and novel therapeutic targets including PARP1. *Cancer discovery* 2: 798-811.
143. Coe, B. P., K. L. Thu, S. Aviel-Ronen, E. A. Vucic, A. F. Gazdar, S. Lam, M. S. Tsao, and W. L. Lam. 2013. Genomic deregulation of the E2F/Rb pathway leads to activation of the oncogene EZH2 in small cell lung cancer. *PloS one* 8: e71670.
144. Hubaux, R., K. L. Thu, B. P. Coe, C. MacAulay, S. Lam, and W. L. Lam. 2013. EZH2 promotes E2F-driven SCLC tumorigenesis through modulation of apoptosis and cell-cycle regulation. *J Thorac Oncol* 8: 1102-1106.

145. Poirier, J. T., E. E. Gardner, N. Connis, A. L. Moreira, E. de Stanchina, C. L. Hann, and C. M. Rudin. 2015. DNA methylation in small cell lung cancer defines distinct disease subtypes and correlates with high expression of EZH2. *Oncogene*.
146. Murai, F., D. Koinuma, A. Shinozaki-Ushiku, M. Fukayama, K. Miyaozono, and S. Ehata. 2015. EZH2 promotes progression of small cell lung cancer by suppressing the TGF- β -Smad-ASCL1 pathway. *Cell Discovery* 1: 15026.
147. Gardner, E. E., B. H. Lok, V. E. Schneeberger, P. Desmeules, L. A. Miles, P. K. Arnold, A. Ni, I. Khodos, E. de Stanchina, T. Nguyen, J. Sage, J. E. Campbell, S. Ribich, N. Rekhtman, A. Dowlati, P. P. Massion, C. M. Rudin, and J. T. Poirier. 2017. Chemosensitive Relapse in Small Cell Lung Cancer Proceeds through an EZH2-SLFN11 Axis. *Cancer cell* 31: 286-299.
148. Dooley, A. L., M. M. Winslow, D. Y. Chiang, S. Banerji, N. Stransky, T. L. Dayton, E. L. Snyder, S. Senna, C. A. Whittaker, R. T. Bronson, D. Crowley, J. Barretina, L. Garraway, M. Meyerson, and T. Jacks. 2011. Nuclear factor I/B is an oncogene in small cell lung cancer. *Genes & development* 25: 1470-1475.
149. Denny, S. K., D. Yang, C. H. Chuang, J. J. Brady, J. S. Lim, B. M. Gruner, S. H. Chiou, A. N. Schep, J. Baral, C. Hamard, M. Antoine, M. Wislez, C. S. Kong, A. J. Connolly, K. S. Park, J. Sage, W. J. Greenleaf, and M. M.

- Winslow. 2016. Nfib Promotes Metastasis through a Widespread Increase in Chromatin Accessibility. *Cell* 166: 328-342.
150. Semenova, E. A., M. C. Kwon, K. Monkhorst, J. Y. Song, R. Bhaskaran, O. Krijgsman, T. Kuilman, D. Peters, W. A. Buikhuisen, E. F. Smit, C. Pritchard, M. Cozijnsen, J. van der Vliet, J. Zevenhoven, J. P. Lambooij, N. Proost, E. van Montfort, A. Velds, I. J. Huijbers, and A. Berns. 2016. Transcription Factor NFIB Is a Driver of Small Cell Lung Cancer Progression in Mice and Marks Metastatic Disease in Patients. *Cell reports* 16: 631-643.
151. Fiorentino, F. P., E. Tokgun, S. Sole-Sanchez, S. Giampaolo, O. Tokgun, T. Jauset, T. Kohno, M. Perucho, L. Soucek, and J. Yokota. 2016. Growth suppression by MYC inhibition in small cell lung cancer cells with TP53 and RB1 inactivation. *Oncotarget*.
152. Augustyn, A., M. Borromeo, T. Wang, J. Fujimoto, C. Shao, P. D. Dospoy, V. Lee, C. Tan, J. P. Sullivan, J. E. Larsen, L. Girard, C. Behrens, Wistuba, II, Y. Xie, M. H. Cobb, A. F. Gazdar, J. E. Johnson, and J. D. Minna. 2014. ASCL1 is a lineage oncogene providing therapeutic targets for high-grade neuroendocrine lung cancers. *Proceedings of the National Academy of Sciences of the United States of America* 111: 14788-14793.
153. Christensen, C. L., N. Kwiatkowski, B. J. Abraham, J. Carretero, F. Al-Shahrour, T. Zhang, E. Chipumuro, G. S. Herter-Sprie, E. A. Akbay, A. Altabef, J. Zhang, T. Shimamura, M. Capelletti, J. B. Reibel, J. D. Cavanaugh, P. Gao, Y. Liu, S. R. Michaelsen, H. S. Poulsen, A. R. Aref,

- D. A. Barbie, J. E. Bradner, R. E. George, N. S. Gray, R. A. Young, and K. K. Wong. 2014. Targeting transcriptional addictions in small cell lung cancer with a covalent CDK7 inhibitor. *Cancer cell* 26: 909-922.
154. Loven, J., H. A. Hoke, C. Y. Lin, A. Lau, D. A. Orlando, C. R. Vakoc, J. E. Bradner, T. I. Lee, and R. A. Young. 2013. Selective inhibition of tumor oncogenes by disruption of super-enhancers. *Cell* 153: 320-334.
155. Pott, S., and J. D. Lieb. 2015. What are super-enhancers? *Nature genetics* 47: 8-12.
156. Kato, F., F. P. Fiorentino, A. Alibes, M. Perucho, M. Sanchez-Cespedes, T. Kohno, and J. Yokota. 2016. MYCL is a target of a BET bromodomain inhibitor, JQ1, on growth suppression efficacy in small cell lung cancer cells. *Oncotarget*.
157. Jahchan, N. S., J. S. Lim, B. Bola, K. Morris, G. Seitz, K. Q. Tran, L. Xu, F. Trapani, C. J. Morrow, S. Cristea, G. L. Coles, D. Yang, D. Vaka, M. S. Kareta, J. George, P. K. Mazur, T. Nguyen, W. C. Anderson, S. J. Dylla, F. Blackhall, M. Peifer, C. Dive, and J. Sage. 2016. Identification and Targeting of Long-Term Tumor-Propagating Cells in Small Cell Lung Cancer. *Cell reports* 16: 644-656.
158. Pleasance, E. D., P. J. Stephens, S. O'Meara, D. J. McBride, A. Meynert, D. Jones, M. L. Lin, D. Beare, K. W. Lau, C. Greenman, I. Varela, S. Nik-Zainal, H. R. Davies, G. R. Ordonez, L. J. Mudie, C. Latimer, S. Edkins, L. Stebbings, L. Chen, M. Jia, C. Leroy, J. Marshall, A. Menzies, A. Butler, J. W. Teague, J. Mangion, Y. A. Sun, S. F. McLaughlin, H. E. Peckham, E.

- F. Tsung, G. L. Costa, C. C. Lee, J. D. Minna, A. Gazdar, E. Birney, M. D. Rhodes, K. J. McKernan, M. R. Stratton, P. A. Futreal, and P. J. Campbell. 2010. A small-cell lung cancer genome with complex signatures of tobacco exposure. *Nature* 463: 184-190.
159. Teves, S. S., L. An, A. S. Hansen, L. Xie, X. Darzacq, and R. Tjian. 2016. A dynamic mode of mitotic bookmarking by transcription factors. *eLife* 5.
160. Li, Y., H. Wen, Y. Xi, K. Tanaka, H. Wang, D. Peng, Y. Ren, Q. Jin, S. Y. Dent, W. Li, H. Li, and X. Shi. 2014. AF9 YEATS domain links histone acetylation to DOT1L-mediated H3K79 methylation. *Cell* 159: 558-571.
161. Wan, L., H. Wen, Y. Li, J. Lyu, Y. Xi, T. Hoshii, J. K. Joseph, X. Wang, Y. E. Loh, M. A. Erb, A. L. Souza, J. E. Bradner, L. Shen, W. Li, H. Li, C. D. Allis, S. A. Armstrong, and X. Shi. 2017. ENL links histone acetylation to oncogenic gene expression in acute myeloid leukaemia. *Nature* 543: 265-269.
162. Egan, B., C. C. Yuan, M. L. Craske, P. Labhart, G. D. Guler, D. Arnott, T. M. Maile, J. Busby, C. Henry, T. K. Kelly, C. A. Tindell, S. Jhunjunwala, F. Zhao, C. Hatton, B. M. Bryant, M. Classon, and P. Trojer. 2016. An Alternative Approach to ChIP-Seq Normalization Enables Detection of Genome-Wide Changes in Histone H3 Lysine 27 Trimethylation upon EZH2 Inhibition. *PloS one* 11: e0166438.
163. Torres, I. O., K. M. Kuchenbecker, C. I. Nnadi, R. J. Fletterick, M. J. Kelly, and D. G. Fujimori. 2015. Histone demethylase KDM5A is regulated by its

- reader domain through a positive-feedback mechanism. *Nat Commun* 6: 6204.
164. Lan, F., R. E. Collins, R. De Cegli, R. Alpatov, J. R. Horton, X. Shi, O. Gozani, X. Cheng, and Y. Shi. 2007. Recognition of unmethylated histone H3 lysine 4 links BHC80 to LSD1-mediated gene repression. *Nature* 448: 718-722.
165. Manning, E. T., T. Ikehara, T. Ito, J. T. Kadonaga, and W. L. Kraus. 2001. p300 forms a stable, template-committed complex with chromatin: role for the bromodomain. *Molecular and cellular biology* 21: 3876-3887.
166. Hilton, I. B., A. M. D'Ippolito, C. M. Vockley, P. I. Thakore, G. E. Crawford, T. E. Reddy, and C. A. Gersbach. 2015. Epigenome editing by a CRISPR-Cas9-based acetyltransferase activates genes from promoters and enhancers. *Nature biotechnology* 33: 510-517.
167. Rada-Iglesias, A., R. Bajpai, T. Swigut, S. A. Brugmann, R. A. Flynn, and J. Wysocka. 2011. A unique chromatin signature uncovers early developmental enhancers in humans. *Nature* 470: 279-283.
168. Buecker, C., and J. Wysocka. 2012. Enhancers as information integration hubs in development: lessons from genomics. *Trends in genetics : TIG* 28: 276-284.
169. Zentner, G. E., P. J. Tesar, and P. C. Scacheri. 2011. Epigenetic signatures distinguish multiple classes of enhancers with distinct cellular functions. *Genome research* 21: 1273-1283.

170. Musselman, C. A., M. E. Lalonde, J. Cote, and T. G. Kutateladze. 2012. Perceiving the epigenetic landscape through histone readers. *Nature structural & molecular biology* 19: 1218-1227.
171. Andrews, F. H., B. D. Strahl, and T. G. Kutateladze. 2016. Insights into newly discovered marks and readers of epigenetic information. *Nature chemical biology* 12: 662-668.
172. Taverna, S. D., H. Li, A. J. Ruthenburg, C. D. Allis, and D. J. Patel. 2007. How chromatin-binding modules interpret histone modifications: lessons from professional pocket pickers. *Nature structural & molecular biology* 14: 1025-1040.
173. An, W., and R. G. Roeder. 2003. Direct association of p300 with unmodified H3 and H4 N termini modulates p300-dependent acetylation and transcription of nucleosomal templates. *The Journal of biological chemistry* 278: 1504-1510.
174. Augert, A., and D. MacPherson. 2014. Treating transcriptional addiction in small cell lung cancer. *Cancer cell* 26: 783-784.
175. Jahchan, N. S., J. T. Dudley, P. K. Mazur, N. Flores, D. Yang, A. Palmerton, A. F. Zmoos, D. Vaka, K. Q. Tran, M. Zhou, K. Krasinska, J. W. Riess, J. W. Neal, P. Khatri, K. S. Park, A. J. Butte, and J. Sage. 2013. A drug repositioning approach identifies tricyclic antidepressants as inhibitors of small cell lung cancer and other neuroendocrine tumors. *Cancer discovery* 3: 1364-1377.

176. Schaffer, B. E., K. S. Park, G. Yiu, J. F. Conklin, C. Lin, D. L. Burkhardt, A. N. Karnezis, E. A. Sweet-Cordero, and J. Sage. 2010. Loss of p130 accelerates tumor development in a mouse model for human small-cell lung carcinoma. *Cancer research* 70: 3877-3883.
177. Kim, D. W., N. Wu, Y. C. Kim, P. F. Cheng, R. Basom, D. Kim, C. T. Dunn, A. Y. Lee, K. Kim, C. S. Lee, A. Singh, A. F. Gazdar, C. R. Harris, R. N. Eisenman, K. S. Park, and D. MacPherson. 2016. Genetic requirement for Mycl and efficacy of RNA Pol I inhibition in mouse models of small cell lung cancer. *Genes & development* 30: 1289-1299.
178. Zhang, W., L. Girard, Y. A. Zhang, T. Haruki, M. Papari-Zareei, V. Stastny, H. K. Ghayee, K. Pacak, T. G. Oliver, J. D. Minna, and A. F. Gazdar. 2018. Small cell lung cancer tumors and preclinical models display heterogeneity of neuroendocrine phenotypes. *Transl Lung Cancer Res* 7: 32-49.
179. Borromeo, M. D., T. K. Savage, R. K. Kollipara, M. He, A. Augustyn, J. K. Osborne, L. Girard, J. D. Minna, A. F. Gazdar, M. H. Cobb, and J. E. Johnson. 2016. ASCL1 and NEUROD1 Reveal Heterogeneity in Pulmonary Neuroendocrine Tumors and Regulate Distinct Genetic Programs. *Cell reports* 16: 1259-1272.
180. Mollaoglu, G., M. R. Guthrie, S. Bohm, J. Bragelmann, I. Can, P. M. Ballieu, A. Marx, J. George, C. Heinen, M. D. Chalisehar, H. Cheng, A. S. Ireland, K. E. Denning, A. Mukhopadhyay, J. M. Vahrenkamp, K. C. Berrett, T. L. Mosbrugger, J. Wang, J. L. Kohan, M. E. Salama, B. L. Witt,

- M. Peifer, R. K. Thomas, J. Gertz, J. E. Johnson, A. F. Gazdar, R. J. Wechsler-Reya, M. L. Sos, and T. G. Oliver. 2016. MYC Drives Progression of Small Cell Lung Cancer to a Variant Neuroendocrine Subtype with Vulnerability to Aurora Kinase Inhibition. *Cancer cell*.
181. Kaur, G., R. A. Reinhart, A. Monks, D. Evans, J. Morris, E. Polley, and B. A. Teicher. 2016. Bromodomain and hedgehog pathway targets in small cell lung cancer. *Cancer Lett* 371: 225-239.
182. van Meerbeeck, J. P., D. A. Fennell, and D. K. De Ruyscher. 2011. Small-cell lung cancer. *Lancet* 378: 1741-1755.
183. Kim, D. W., K. C. Kim, K. B. Kim, C. T. Dunn, and K. S. Park. 2018. Transcriptional deregulation underlying the pathogenesis of small cell lung cancer. *Transl Lung Cancer Res* 7: 4-20.
184. Jia, D., A. Augert, D. W. Kim, E. Eastwood, N. Wu, A. H. Ibrahim, K. B. Kim, C. T. Dunn, S. P. S. Pillai, A. F. Gazdar, H. Bolouri, K. S. Park, and D. MacPherson. 2018. Crebbp Loss Drives Small Cell Lung Cancer and Increases Sensitivity to HDAC Inhibition. *Cancer discovery* 8: 1422-1437.
185. Ramos, Y. F., M. S. Hestand, M. Verlaan, E. Krabbendam, Y. Ariyurek, M. van Galen, H. van Dam, G. J. van Ommen, J. T. den Dunnen, A. Zantema, and P. A. t Hoen. 2010. Genome-wide assessment of differential roles for p300 and CBP in transcription regulation. *Nucleic acids research* 38: 5396-5408.
186. Tate, J. G., S. Bamford, H. C. Jubb, Z. Sondka, D. M. Beare, N. Bindal, H. Boutselakis, C. G. Cole, C. Creatore, E. Dawson, P. Fish, B. Harsha, C.

- Hathaway, S. C. Jupe, C. Y. Kok, K. Noble, L. Ponting, C. C. Ramshaw, C. E. Rye, H. E. Speedy, R. Stefancsik, S. L. Thompson, S. Wang, S. Ward, P. J. Campbell, and S. A. Forbes. 2018. COSMIC: the Catalogue Of Somatic Mutations In Cancer. *Nucleic acids research*.
187. Zhou, X., M. N. Edmonson, M. R. Wilkinson, A. Patel, G. Wu, Y. Liu, Y. Li, Z. Zhang, M. C. Rusch, M. Parker, J. Becksfort, J. R. Downing, and J. Zhang. 2016. Exploring genomic alteration in pediatric cancer using ProteinPaint. *Nature genetics* 48: 4-6.

Vita

Yongming Xue was born in Jinan, China on July 16, 1988, the son of Ying Xu and Bin Xue. After completing his education at Shandong Experimental High School, Jinan, China in 2007, he entered China Agricultural University (CAU) in Beijing, China. He received the degree of Bachelor of Sciences with a major in biological sciences from CAU in July 2011. For the next three years, he worked as a graduate research assistant and lab technician in Chinese Academy of Sciences in Beijing, China. In August of 2014 he entered The University of Texas MD Anderson Cancer Center UTHealth Graduate School of Biomedical Sciences.

Permanent address:

5731 Gulfton Street, APT 2704,

Houston, Texas 77030